PARTICLE ACCELERATION AT THE SUN AND IN THE HELIOSPHERE

DONALD V. REAMES
NASA/ Goddard Space Flight Center, Greenbelt, MD 20771, U.S.A.;
E-mail: Reames@lheavx.gsfc.nasa.gov

(Accepted 16 February 1999)

Abstract. Energetic particles are accelerated in rich profusion at sites throughout the heliosphere. They come from solar flares in the low corona, from shock waves driven outward by coronal mass ejections (CMEs), from planetary magnetospheres and bow shocks. They come from corotating interaction regions (CIRs) produced by high-speed streams in the solar wind, and from the heliospheric termination shock at the outer edge of the heliospheric cavity. We sample many populations near Earth, but can distinguish them readily by their element and isotope abundances, ionization states, energy spectra, angular distributions and time behavior. Remote spacecraft have probed the spatial distributions of the particles and examined new sources *in situ*. Most acceleration sources can be 'seen' *only* by direct observation of the particles; few photons are produced at these sites. Wave-particle interactions are an essential feature in acceleration sources and, for shock acceleration, new evidence of energetic-proton-generated waves has come from abundance variations and from local cross-field scattering. Element abundances often tell us the physics of the source plasma itself, prior to acceleration. By comparing different populations, we learn more about the sources, and about the physics of acceleration and transport, than we can possibly learn from one source alone.

Table of Contents

1. Introduction
2. SEP Events and the Solar Flare Myth
   - 2.1. Demise of the Flare Myth
   - 2.2. Comparing Gradual and Impulsive SEP Events
3. Gradual SEP Events
   - 3.1. Shock Acceleration and Transport
   - 3.2. Longitude Structure
   - 3.3. Invariant Spectra
   - 3.4. Defining the Ejecta
   - 3.5. Abundance Variations
     - 3.5.1. Event-Averaged Abundances
     - 3.5.2. Time Variations
   - 3.6. High-Energy Spectra and Abundances

Space Science Reviews **90:** 413–491, 1999.

4. Impulsive SEP Events
   4.1. Photons from Flares
   4.2. Associations
   4.3. Abundances
   4.4. Theory
5. CIR-Associated Events
   5.1. The Spatial Distribution of Particles
   5.2. Cross-Field Particle Transport
   5.3. Energetic Ions at High Latitudes
   5.4. Abundances
6. The Anomalous Cosmic Rays
7. Planetary Sources of Energetic Particles
   7.1. Planetary Bow Shocks
   7.2. Trapped Radiation
8. Acceleration and Transport
   8.1. Transport
   8.2. Acceleration and Plasma Physics
9. Abundances
10. Summary and Conclusions

1. Introduction

One cannot help but marvel at the rich variety we have found in the populations of energetic particles in the heliosphere. Wherever we look, it seems, processes exist that can accelerate electrons and ions of the local plasma to energies of $\sim$1 $-$1000 MeV, sometimes more. These particles often propagate to us over great distances, carrying information in their energy spectra, ionization states, and abundances of elements and isotopes, on the properties of their source plasma and on the physical mechanisms of their selection and acceleration.

These particle populations tell us much about the nature, location and composition of the sources and about the physics of particle acceleration. Solar energetic particles (SEPs) are now understood to come from two different sources. The SEPs from solar flares have 1000-fold enhancements in ^{3}He/^{4}He and enhanced heavy ions because of resonant wave-particle interactions in the flare site; the ions are highly stripped of orbital electrons by the hot environment. However, the most intense SEP events, with particles of the highest energies, are produced by acceleration at collisionless shock waves driven by CMEs; on average, these particles directly reflect the abundances and temperature of ambient, unheated, coronal material. Behind the CMEs, bidirectionally streaming particles and particles from new flares or CMEs probe the topology of the magnetic fields. Corotating interaction regions (CIRs) form where high-speed solar wind streams overtake low-speed solar

wind emitted earlier in the solar rotation. Particles are accelerated at shock waves formed by CIRs at low solar latitudes, but they can appear high above the solar poles by migration of the solar magnetic fields that guide them. The 'anomalous cosmic-ray' (ACR) component is accelerated at the heliospheric termination shock. When interstellar neutral atoms enter the heliosphere, they are photoionized and 'picked-up' by the solar wind, then convected out to the shock where acceleration takes place. The pickup of interstellar neutrals was predicted to explain ACR observations long before most of the elements involved were directly observed in the solar wind. Nowadays, we even observe ACRs that have become trapped in the Earth's magnetosphere to form a radiation belt. This belt lies alongside the proton belt produced by the decay of neutrons expelled from nuclear reactions between energetic cosmic rays and atmospheric nuclei.

Yet, with the exception of γ-rays from flares, this entire complex of heliospheric sources of energetic ions is virtually invisible via photons. For most of the particle populations, ion acceleration takes place in low-density regions where interactions are rare and measurable intensities of photons are simply not produced. Nearly all of our information on the properties of energetic ion populations, and on their very existence, comes from the ions themselves. If the heliosphere provides a message for astrophysics generally, it is that most of the energetic-particle sources in the distant universe may be hidden from our view.

In this paper, we review observations of the energetic particles, especially ions from $\sim$1 MeV amu^{-1} to 1 GeV amu^{-1}, accelerated in the heliosphere, and our current understanding of those observations. We focus heavily on SEP events. These events provide the richest variety of source conditions and a complete complement of measurements. However, we pay special attention to the particles accelerated in similar ways at many different sites. Insights into shock acceleration, particle transport, and unusual source abundances can come from the comparative study of the same physical processes in many different environments.

We will find that a common thread in recent studies of particle acceleration is the importance of the plasma physics of resonant wave-particle interactions. This is true not only for the unique wave modes that produce 'ion-conics' in the auroral zone or enhance ^{3}He from impulsive solar flares. Active wave generation by streaming particles is also an essential feature of shock acceleration. The numerous low-energy particles generate resonant waves that effectively trap these particles near the shock, greatly increasing the rate of acceleration and producing rigidity-dependent modulation of the escaping ions. With increasing proton intensities, increasing modulation is seen in spectral and abundance variations with time. Such waves may also produce local cross-field scattering now observed near CIR shocks when proton intensities are high.

Another important thread is that element abundances often provide a unique signature of their own origin or reveal plasma properties, such as the temperature, that are otherwise inaccessible for remote sources. Abundances can also disclose processes involved in the production of the source plasma itself, espe-

cially ion-neutral fractionation in response to electromagnetic fields. This fractionation is seen for several of the particle populations as different dependence of the abundances on the first ionization potential (FIP) of the elements; it is a common phenomenon. The power of abundance measurements becomes clear when we compare a dozen different energetic-particle populations.

2. SEP Events and the Solar Flare Myth

High-energy particles from the Sun were first observed (Forbush, 1946) as sudden increases in intensity in ground-level ion chambers during the large solar events of February and March 1942. Since this was long before the discovery of coronal mass ejections (CMEs), it was natural to assume that the energetic particles came from the solar flares that often accompany large CMEs. Thus was born the 'flare myth' (Gosling, 1993) that dominated thought in the SEP community for over 40 years. If the particles are accelerated in a flare, it is reasonable to assume they are injected at a point source in space and time. Thus, all properties of SEP events observed during the next few decades were explained in terms of transport from a point source, rather than as characteristics of the acceleration and of the source itself. These properties included intensity-time profiles, the longitude distributions of the particles, and all variations of abundances with time. By forcing us to ignore any variations of the source in space or time, the flare myth has had a profoundly negative effect on nearly all aspects of SEP studies for many years. The change in this picture, illustrated by the cartoon in Figure 2.1, has provided an awakening in understanding the physical mechanisms of particle acceleration in SEP events.

The earliest clear evidence that two distinct processes of particle acceleration contribute to SEP events came from radio observations (Wild et al., 1963). The emission frequency in radio bursts is related to the local plasma frequency, which varies as the square root of the electron density. Thus, the fast frequency drift of type III bursts was ascribed to 10–100 keV electrons streaming out of the corona at $\sim$0.1 c from an impulsive flare through plasma of decreasing density. On the other hand, type II bursts had a much slower drift rate that corresponded to local electron acceleration at a $\sim$1000 km s^{-1} shock wave moving out through the corona. Wild et al. (1963) suggested that electrons were primarily accelerated in the impulsive phase of an event that produced the type III bursts, while proton acceleration occurred later at the expanding shock wave. This is remarkably close to our current understanding, but it was largely ignored by those who rushed to calculate diffusive transport from point-source flares.

2.1. DEMISE OF THE FLARE MYTH

The fall of the flare myth began after the discovery of CMEs when Kahler et al. (1978, 1984, 1987a) found a high correlation (96%) between large SEP 'proton

Source of Solar Energetic Particles

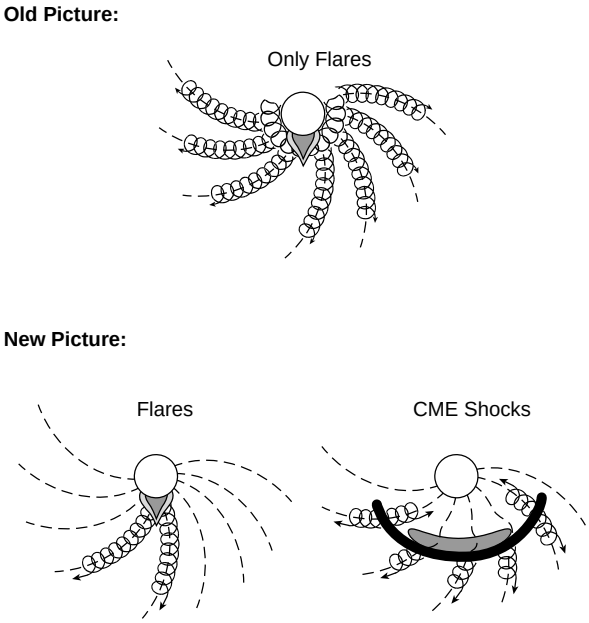

Figure 2.1. A paradigm shift.

events' and CMEs. Then, Cliver et al. (1983) studied proton events associated with flares with 'weak impulsive phases', as determined by hard X-rays. The flare myth, as espoused by Lin and Hudson (1976), stated that high intensities of hard X-rays were required for events that produce significant proton intensities. The proton events with weak impulsive phases seemed to suggest that X-ray flares were irrelevant. Even the largest SEP events were correlated with CMEs, not flares.

Meanwhile, the evidence for two types of events grew. Pallavicini et al. (1977) distinguished impulsive and long-duration (gradual) soft X-ray events; the latter were associated with CMEs (Sheeley et al., 1975). Kahler (1992) has reviewed such differences between flares and CMEs. The connection between these two phenomena and energetic particles in space was made when Cane et al. (1986) found that SEPs associated with the two classes of X-ray events had different proton/electron ratios. The terms 'gradual' and 'impulsive' have stuck, even though time scales, especially X-ray time scales, poorly resolve those acceleration mechanisms we wish to distinguish.

A different line of evidence came from particle abundances. In 1970, Hsieh and Simpson (1970) had discovered some small SEP events with greatly enhanced abundances of the rare isotope ^{3}He. These ^{3}He-rich events were subsequently found to have $\sim$1000-fold enhancements in ^{3}He/^{4}He and $\sim$10-fold enhancements in Fe/O

relative to coronal abundances (see, e.g., Reames et al., 1994, and references therein). The average abundances in large SEP events were known to reflect coronal abundances (e.g., Meyer, 1985a). Abundance variations were often explained in terms of rigidity-dependent transport from a flare, but it was impossible to explain the huge enhancement in ^{3}He/^{4}He in this way. It became clear that two different physical mechanisms of acceleration were required. ^{3}He-rich events were explained in terms of resonant wave-particle interactions in the source plasma (Fisk, 1978; Temerin and Roth, 1992). Reames and Stone (1986, see also Reames et al., 1988) made the connection between ^{3}He-rich events, type-III radio bursts, and impulsive X-ray events. Subsequently Reames (1988) found a bimodal distribution of Fe/O with clearly distinct contributions from impulsive (^{3}He-rich) and gradual SEP events (see review by Reames, 1990b).

A compelling line of evidence for the different origin of impulsive and gradual SEP events comes from measurements of the ionization states of the energetic ions. Ionization states were well resolved in measurements by Luhn et al. (1984, 1987). In gradual events, none of the elements above He were fully ionized and the charge state of Fe was found to be 14 ± 1, on average. This indicated source material with an electron temperature of $\sim$2 MK (2×10^6 K), a typical temperature of the ambient corona. In contrast, in ^{3}He-rich events, all elements up through Si were fully ionized and the ionization state of Fe, $Q_{\rm Fe} = 20.5 \pm 1.2$ on average, typical of flare-heated material with a temperature of $\sim$10 MK. More-recent measurements of $Q_{\rm Fe}$ in gradual events using a variety of instruments to cover the region from 0.3 to 600 MeV amu^{-1} are all in the range $Q_{\rm Fe} \sim 11-15$ (Tylka et al., 1995; Leske et al., 1995; Mason et al., 1995). High-energy Fe would be rapidly stripped of additional electrons at coronal densities where flares occur. This Fe must have been accelerated high in the corona, at $>$2 solar radii where low-density material is traversed by a collisionless shock wave.

2.2. Comparing gradual and impulsive SEP events

Various aspects of gradual and impulsive SEP events have been compared and described in a variety of review articles (Reames, 1990b, 1993, 1995b, 1997; Kahler, 1992, 1994; Gosling, 1993; Cliver, 1996). In this section, we document several aspects of this comparison that provide a background for subsequent discussions.

Figure 2.2 compares the intensity-time profiles of protons and electrons in gradual and impulsive events on the same scale. The events chosen are particularly appropriate because they are 'pure' events. The gradual event of 1981 December 5, shown in Figure 2.2(a), is a well-known erupting-filament event (Kahler et al., 1986) in which a filament erupts from the Sun as part of a CME with no accompanying flare. In fact, the event does not occur in an active region. The ^{3}He-rich events on 1982 August 13 and 14, shown in Figure 2.2(b), are associated with impulsive flares on the Sun (Reames et al., 1988) that have no evidence of accompanying CMEs or of type IV radio bursts that are associated with CMEs. Differences in

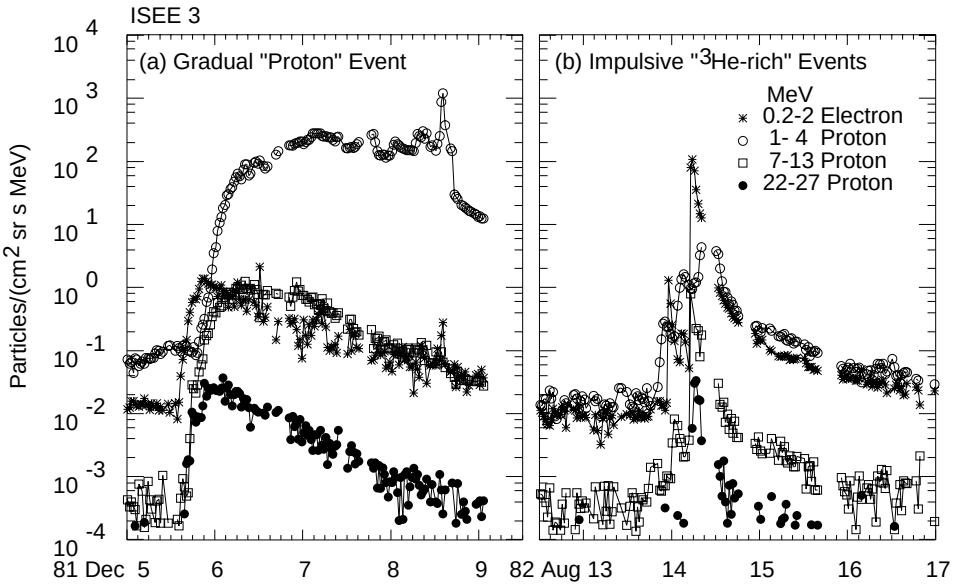

Figure 2.2. Intensity-time profiles of electrons and protons in 'pure' (a) gradual and (b) impulsive SEP events. The gradual event is a disappearing-filament event with a CME but no impulsive flare. The impulsive events come from a series of flares with no CMEs.

the time scales of gradual and impulsive particle events are clear in the figure. The gradual event is dominated by protons; near 1 MeV, the protons reach a small peak near the time of shock passage. In contrast, electrons dominate the impulsive events in Figure 2.2. Peak electron intensities in the impulsive events in the figure exceed that in the gradual event. The extended intensity-time profiles of gradual events come from the continuous particle acceleration; the duration of the time profiles of the impulsive events is determined by scattering of the particles as they traverse interplanetary space. The terms 'gradual' and 'impulsive' originally came from the time scales of the associated X-ray events, but they now more accurately distinguish the time scales of the SEP events themselves at a few MeV.

Figure 2.3 compares distributions of the 'source longitude' of the associated flare for gradual and impulsive events. The distribution for gradual events is nearly uniform across the face of the Sun. In fact, many gradual events come from behind the limbs; these events have been omitted because their source longitudes are ill determined. Unfortunately, it is not presently possible to directly determine the source longitude of a CME, so we must use the longitude of the associated flare. Fortunately, most fast CMEs that produce gradual SEP events do have associated flares, although they are as likely to occur near the footpoints of the ejected loops as near the center. Thus, longitudes quoted for gradual events are no more accurate than $\sim \pm 20°$.

The impulsive events are distributed about the longitude of best magnetic connection to the observer. Much of the spread in the longitude distribution comes

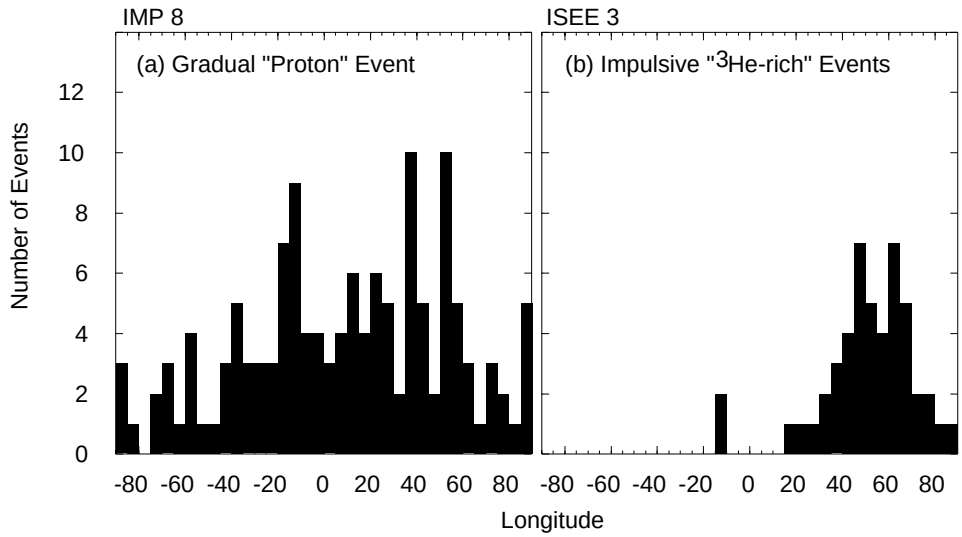

Figure 2.3. Histograms of the solar source longitude distributions of observed (a) gradual and (b) impulsive SEP events.

from changes in connection longitude resulting from variations in solar wind speed. The remaining variation probably comes from the random walk of the magnetic field lines that provides particle paths connecting a small region on the Sun to a distribution of longitudes at 1 AU (e.g., Jokipii and Parker, 1968; Parker, 1987). This comparison shows that the broad longitude distribution in the gradual events does not come from cross-field transport, which would presumably be present for impulsive events as well. The broad distribution of the gradual events strongly suggests the presence of a shock wave that can easily propagate across field lines and accelerate particles as it goes.

Figure 2.4 shows a comparison of abundances at $\sim$5 MeV amu^{-1} in gradual and impulsive events (see Reames et al., 1994). The two populations are rather well resolved and the event-to-event variations have a different behavior. However, we will see in Section 3.5.2 that large values of Fe/O do occur in gradual events, especially for short intervals of time. Usually, variations of different elements tend to be correlated in gradual events and uncorrelated in impulsive events, as we will discuss later.

We might prefer to compare ^{3}He/^{4}He in the two classes of events. ^{3}He/^{4}He$\sim$1 is typical in impulsive events, but ^{3}He/^{4}He$<$1% in gradual events is difficult to measure and not available for a large sample of events. There are substantial fluctuations of ^{3}He/^{4}He in the solar wind but values rarely exceed 1% (Coplan et al., 1984; Bodmer et al., 1995). Recent work (Zurbuchen et al., 1998) suggests that resonant wave-particle mechanisms operate in the corona to enhance ^{3}He/^{4}He in the solar wind, much as they do in impulsive SEP events, but to a much smaller extent. In addition, one might expect acceleration-dependent variations in gradual events

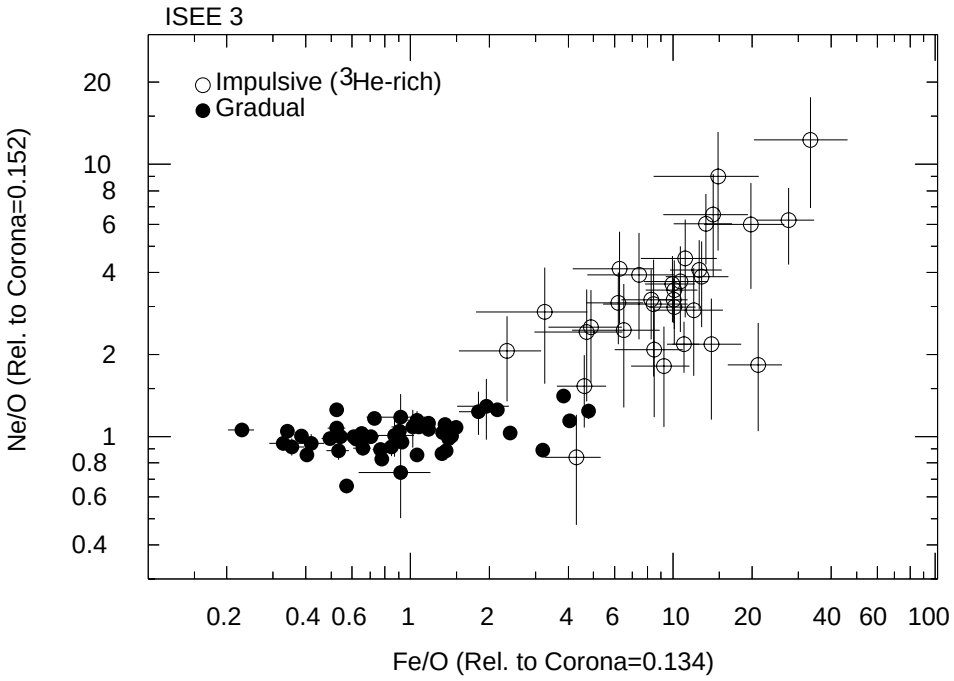

Figure 2.4. Plot of abundance ratios Ne/O *versus* Fe/O for gradual and impulsive events. Each point represents abundances averaged over one SEP event.

by factors as large as ∼5 arising from the different charge-to-mass ratio, *Q/A*, of the isotopes. Therefore, it is prudent to take '^{3}He-rich' to mean ^{3}He/^{4}He>10% if we wish to use this ratio alone to distinguish the physical mechanism that takes place in impulsive solar flares.

Ionization-state measurements for energetic Fe in gradual and impulsive events are summarized in Table 2.1. The measurements in gradual events cover a broad range of energies and involve several different measurement techniques. These ions did not come from flare-heated plasma. Above ∼20 MeV amu^{-1} Fe would be rapidly stripped of additional electrons if it were accelerated in the dense (∼10^{10} cm^{-3}) regions of the low corona where flares occur. The most energetic ions must be accelerated from material at low temperature and density corresponding to ∼2 MK corona above ∼2 solar radii. Plotting the source injection intensity vs CME height for protons accelerated to energies up to 21 GeV, Kahler (1994) concluded that maximum acceleration occurs when the shock is above 5 solar radii. This conclusion is in agreement with the requirements imposed by the ionization-state measurements of the energetic Fe.

To understand the distribution of ionization states of the energetic particles in gradual events we must first examine the ionization states of ions from various regions of the corona and the solar wind (e.g., Feldman et al., 1981; Gloeckler et al., 1999). As coronal material expands to form the solar wind, it cools, and

TABLE 2.1
Mean ionization states of energetic Fe in SEP events

MeV amu^{-1}	Q_{Fe}	Events	Reference
Large gradual events			
0.3–2	14.1 ± 0.2	12	Luhn et al. 1987
0.5–5	11.0 ± 0.2	2	Mason et al. 1995
15–70	15.2 ± 0.7	2	Leske et al. 1995
200–600	14.1 ± 1.4	3	Tylka et al. 1995
Impulsive-flare (^{3}He-rich) events			
0.3–2	20.5 ± 1.2	$\sim$26	Luhn et al. 1987

electrons may be captured to reduce average ionization states until the plasma becomes collisionless. Since electron capture and loss cross sections vary with species, the 'freezing-in' temperature actually depends upon the element and ionization state, and the process occurs throughout a region from $\sim$1.5 to 5 solar radii (e.g., Hundhausen et al., 1968). A recent study (Hefti et al., 1998; Gloeckler et al., 1999) found a complex distribution of Fe ions ranging from Fe^{+3} to Fe^{+16} inside an expanding CME. As the plasma expanded from a coronal temperature of $\sim$3 MK, Fe^{+16} ions, with a stable shell of 10 electrons, froze early while ions in lower charge states continued to evolve.

There have been recent reports of events with energy dependence in the ionization states of Fe for the large events of 1992 November 2 (Oetlicker et al., 1997) and 1997 November 6 (Mazur et al., 1999; Möbius et al., 1999). Q_{Fe} varies from $\sim$11 to 16 over the range from 0.2 to 70 MeV amu^{-1}, with most of the increase coming near 1 MeV amu^{-1} in the November 6 event. This may suggest that ions at higher energies are sampled from the corona close to the Sun while those at lower energies continue to be sampled farther out into the solar wind. There is good evidence that the low-energy part of the spectrum derives directly from the solar wind near shocks (e.g., Gosling et al., 1981). Alternatively, energetic particles that spend $\sim$1 day trapped behind a shock sampling the densities at several solar radii might tend to come to the equilibrium charge state appropriate for their velocity through the material. Fe ions of 0.1–1 MeV amu^{-1} would pick up electrons and come to an equilibrium charge like that of the solar-wind Fe while Fe above 10 MeV amu^{-1} might be further ionized. Each of the events with energy-dependent ionization states is the second in a series of events so it is difficult to determine when and where the particles were accelerated in these cases.

Boberg et al. (1996) noted that the ionization states of the SEPs are similar to those of the solar wind found in the sheath region ahead of the CME, somewhat

higher than elsewhere in the solar wind. Perhaps the shock preferentially accelerates hotter plasma from coronal active regions nearer the base of each flux tube near the Sun where the shock is likely to be the strongest.

A complete discussion of the relationship between flares and CMEs is beyond the scope of this paper (see, e.g., Kahler, 1992; Webb, 1995). However, we must distinguish these sources to understand SEP events. Circulation of plasma in and below the photosphere causes distortion and tangling of the coronal fields. Magnetic energy released from the reconnection of these fields probably powers flares and triggers the release of CMEs. In flares, this energy and the accelerated particles are largely contained by magnetic loops, resulting in hot plasma that cools by radiative emission. In CMEs, energy appears as kinetic energy of the CME; 10^{16} g ejected at 1000 km s^{-1} in a moderately large event account for $\sim 10^{32}$ ergs (e.g., Webb and Howard, 1994). It is clear that flares and CMEs can occur separately. In fact, most flares are not accompanied by a CME. The confusion occurs for the largest events where flares and CMEs occur together. Kahler (1982) coined the term 'big-flare syndrome'. In big events, there is a major reorganization of coronal fields leading to many different phenomena in great profusion. However, the mere fact that two phenomena occur together in many big events does not necessarily mean that they are causally related to each other.

It was once accepted that two types of shocks could be formed in solar events. Coronal shocks were short-lived blast-wave shocks induced by flares and confined to the solar corona while interplanetary shocks were driven by CMEs. A gap in the radio data from $\sim$2 to 20 MHz separated the ground-based metric measurements of coronal shocks from the space-borne kilometric measurements of interplanetary shocks. While shocks are common in the heliosphere and relatively easy to form, we suspect that this historical division is yet another holdover of the flare myth. Cliver et al. (1999) recently found that only 5% of the 2500 hard X-ray flares they studied had associated metric type II bursts. Of the largest 360 of these flares, only 24% had coronal shocks, yet 65% of the events with metric type II bursts were observed to have associated CMEs. Unless there is new evidence to the contrary, we must assume that the coronal shock is just an early phase of the CME-driven interplanetary shock in most cases. In fact, we think it likely that all shocks and shock-like phenomena in the corona, such as Moreton waves (Athay and Moreton, 1961; see recent observations of these waves in the EUV by Thompson, 1999) are a consequence of the eruption of a CME. Gradual SEP events are clearly correlated with CMEs, not with flares (Kahler et al., 1978, 1984, 1987a). If flare-associated shocks did exist, one might expect the energetic particles from them to have intensity-time profiles like those from an impulsive flare because of the short acceleration time. However, all events with such profiles have the abundance enhancements of ^{3}He-rich events; large ^{3}He enhancements cannot be produced by a shock, although Fe-enhancements can.

Our purpose in distinguishing gradual and impulsive SEP events is to permit separate study of the two physical mechanisms of particle acceleration involved. Of

course, there are also 'hybrid' cases where both mechanisms appear to contribute (Reames, 1990a; Cliver, 1996). In these events, one mechanism operates in the flare while the other operates independently at the CME-driven shock. However, one population or the other seems to dominate in a surprisingly large fraction of the events, and we shall see that the presence of Fe enhancements early in an event need *not* indicate a flare-associated component. The best evidence of a gradual (impulsive) event is the presence (absence) of a fast CME. It is probably less important to categorize every event than to collect sufficiently large samples of relatively 'pure' events to study the acceleration physics of each mechanism. Understanding each individual mechanism is sufficiently challenging by itself that we can safely postpone our concern about those few ambiguous events that occur in complex conditions and are difficult to categorize.

3. Gradual SEP Events

Kahler et al., (1986, 1987a) found a high correlation between SEP events and CMEs. However, that correlation alone does not tell us that SEP acceleration occurs at the CME-driven shock and *not* at the reconnection region behind the CME, for example. Often, of course, particle intensities peak at the time of shock passage, even at energies of $\sim$500 MeV, as we shall see. However, a more interesting case is provided by the large CME of 1997 January 6–10. A halo CME was launched from the Sun on January 6 near central meridian. The CME with an extremely well-defined magnetic cloud reached Earth on January 10 causing a severe geomagnetic storm (see, e.g., Fox et al., 1998; Goodrich et al., 1998) that was even reported in the popular press in major cities. However, *no* interplanetary protons of 1 MeV or above were observed. The shock transit speed of 385–490 km s^{-1} (Webb et al., 1998) barely exceeded the speed of the ambient solar wind. Only when shock transit speeds exceed 500 km s^{-1} do SEP events become likely, while speeds $>$750 km s^{-1} always produce SEP events (Reames et al., 1997c). Only the fastest $\sim$1–2% of CMEs cause particle acceleration. Large slow CMEs and magnetic clouds, even with the likelihood of substantial magnetic reconnection at the Sun, do *not* produce SEPs. Fast CME-driven shocks do.

3.1. Shock acceleration and transport

Particle acceleration by collisionless shock waves has been the subject of considerable theoretical interest for many years (see reviews by Jones and Ellison, 1991; Lee, 1997). However, there are only three available sites for *in situ* observations of both shocks and accelerated particles: the planetary bow shocks, CIRs, and interplanetary traveling shocks. With speeds up to 2000 km s^{-1}, interplanetary traveling shocks can be the most effective and energetic of the three, sometimes accelerating particles to GeV energies. All of the interplanetary traveling shocks that are capable

of producing type II radio bursts and accelerating particles of interest appear to be produced by CMEs (Cane et al., 1987). Near the Sun, CME and shock speeds sometimes can reach ~2000 km s^{-1} (Sheeley et al., 1985; Kahler, 1994) although speeds may decline as much as a factor of 2 by the time the shock reaches 1 AU. Shock compression ratios, $r = u_1/u_2$, the ratio of the upstream and downstream plasma speeds in the shock rest frame, vary from about 1.4 to 3.9 (e.g., Sheeley et al., 1985). In the standard equilibrium shock-acceleration theory the power-law spectral index, -β, of momentum in the accelerated-particle distribution function is given by $\beta = 3r/(r-1)$. Nonrelativistically, this results in a differential intensity spectrum vs energy with a spectral index of $-(r+1)/2(r-1)$ (Jones and Ellison, 1991).

Particles are accelerated when they are scattered back and forth across the shock by magnetic turbulence in the upstream and downstream region. When the magnetic field is quasi-parallel to the shock normal, particles gain an increment of velocity from the converging flow of scattering centers each time they traverse the shock. When the magnetic field is quasi-perpendicular to the shock normal, particles can gain energy by drifting in the $\mathbf{V}_{\text{shock}} \times \mathbf{B}$ electric field at the shock (e.g., Decker and Vlahos, 1986; see discussion in Jones and Ellison, 1991). This can increase the maximum attainable energy and decrease the acceleration time (Jokipii, 1987). However, multiple traversals are still required for acceleration to MeV energies. Clearly, a requirement for acceleration is that particles scattered in the downstream region should be able to overtake and re-cross the shock. This places a limit on the minimum speed of particle injection, which depends upon the relative speeds of the particle and the shock parallel to the magnetic field. To avoid the complexities of pitch-angle scattering most theorists choose to inject an isotropic 'seed-population' of particles with speeds much greater than the shock speed. However, this seed population is not required by the physics; shocks can and do accelerate particles directly from the tail of the thermal distribution of the local plasma (e.g., Gosling et al., 1981; Jones and Ellison, 1991). Of course, shocks will also accelerate particles from any other superthermal populations that happen to be present. For interplanetary shocks, different parts of the shock surface encounter a given magnetic flux tube at different times, first in the corona and continuing far out into interplanetary space. Particles accelerated early in this process can effectively serve as the seed population for later times.

For weak shocks or at early times, the ambient magnetic turbulence must suffice for particle scattering. This limits the accelerated proton spectrum to energies below about an MeV. However, as the shock strengthens and particle intensities increase, wave generation or amplification by accelerated particles streaming away from the shock can become adequate to increase the scattering and, hence, the acceleration rate. Wave amplification is a well-known process in plasma physics (Stix, 1962; Melrose, 1980). In quasi-linear theory, particles of magnetic rigidity P resonate with Alfvén waves of wave number k so that $k = B/\mu P$, where B is the magnetic field strength and μ is the cosine of the particle pitch angle. In

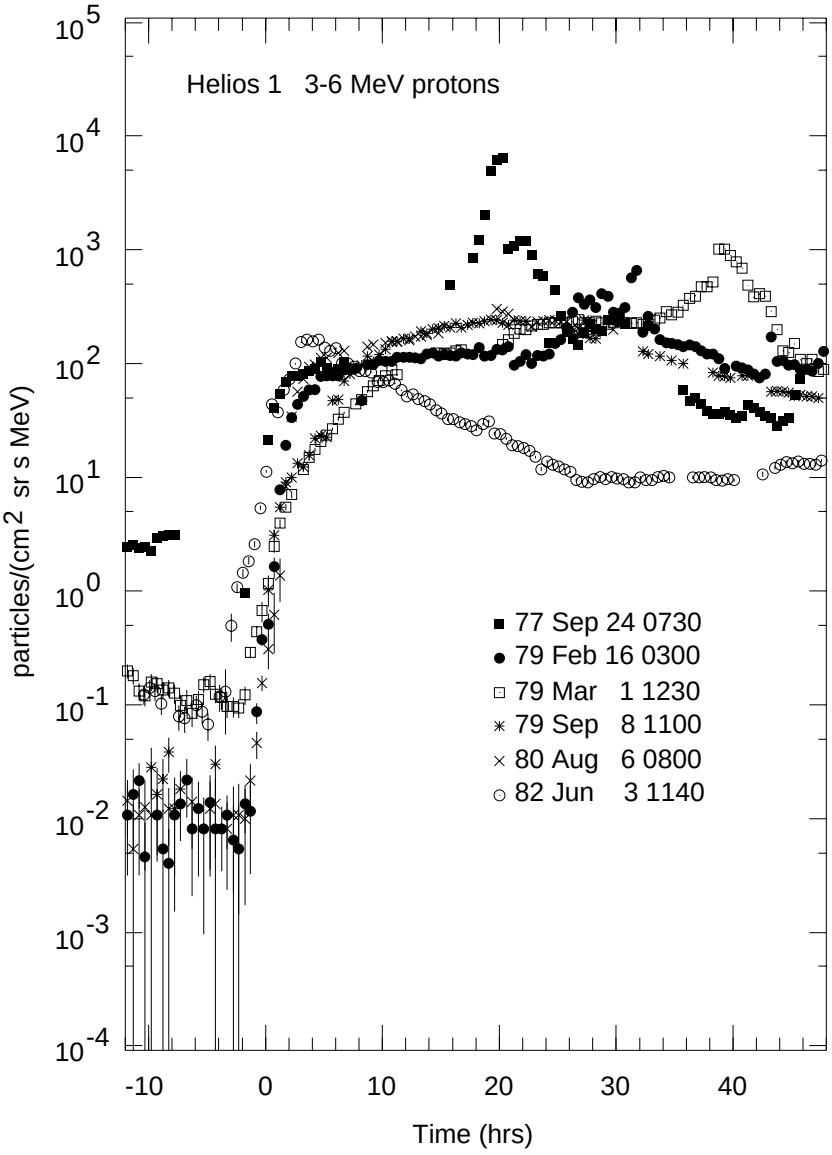

Figure 3.1. Superposed intensity-time profiles for 6 events observed by *Helios I* showing the similar streaming-limited intensities early in these events.

general, particle energy can be transferred to waves or absorbed from them in a nonlinear and time-dependent way. Self-excited waves are an essential feature of shock acceleration that allows rapid particle acceleration to high energies. However, waves generated as particles stream outward can be absorbed if those particles subsequently scatter and stream inward.

When intensities of resonant waves become large, scattering limits the intensities of particles that can stream away. Evidence of streaming-limited particle intensities early in large SEP events was first observed by Reames (1990a) as shown by the superposition of intensity-time profiles shown in Figure 3.1. Early in the events, when the shock is near the Sun, proton intensities at a few MeV can not rise above $\sim$200 (cm^2 sr s MeV)$^{-1}$ at Earth. Of course, intensities can rise much higher in the peaks that occur near the time of shock passage when we observe particles trapped near the shock by the waves. Ng and Reames (1994) did extensive numerical modeling of the time-dependent radial transport of the particles and the amplification and damping of waves, confirming the observed limit. Reames and Ng (1998) performed a more complete statistical comparison of the theory with large SEP events during the last two solar cycles and examined the radial gradient and energy dependence of the streaming limit. In very large events with strong shocks, protons up to $\sim$500 MeV can have flat intensity-time profiles with intensity peaks at the shock, as shown in Figure 3.2. The profiles of 100–500 MeV protons in Figure 3.2 look quite similar to the profiles of 3–6 MeV protons shown in Figure 3.1. For historical reasons, the intensity peaks near the shock are referred to as 'energetic storm particle' (ESP) events in the literature.

Strong shocks that continue to accelerate 500 MeV protons out to 1 AU, as shown in Figure 3.2, are rare. In fact, the 1989 October event was the largest of that solar cycle. However, it is important to note that when shocks are sufficiently strong, 500 MeV protons can behave just as 5 MeV protons do in the numerous small events that we study so often. If we can understand the behavior of 5 MeV protons in the common events, we have hope of predicting the behavior of the 500 MeV protons in the rare large events.

The particles seen in an ESP event are trapped near the shock by self-generated waves. The first self-consistent theory of shock acceleration that included waves was that of Bell (1978) based upon earlier ideas of cosmic-ray containment within the Galaxy by self-generated waves (see Wenzel, 1974). Lee (1983) applied this quasi-linear theory (QLT) to interplanetary shocks in the presence of a wave-intensity background. He found the equilibrium distribution and the spectra of both particles and waves and their spatial distribution as a function of distance from the shock, i.e., he described the structure of an ESP event. However, the solution was obtained for a planar shock in a uniform magnetic field, so effects of a radially diverging magnetic geometry were not included. In Lee's theory, the spectral index of generated waves at the shock depends upon the proton spectral index and hence upon the compression ratio r. For modest shocks with $r = 2$, this wave spectrum is flat, i.e., independent of k. Thus, it exceeds the background spectrum, usually taken to be a Kolmogorov spectrum of index $-\frac{5}{3}$, at high k. This predicted relationship between particle and wave spectra at shocks has been confirmed experimentally (Viñas et al., 1984; Kennel et al., 1986; Tsurutani and Gonzalez, 1987; Tan et al., 1989).

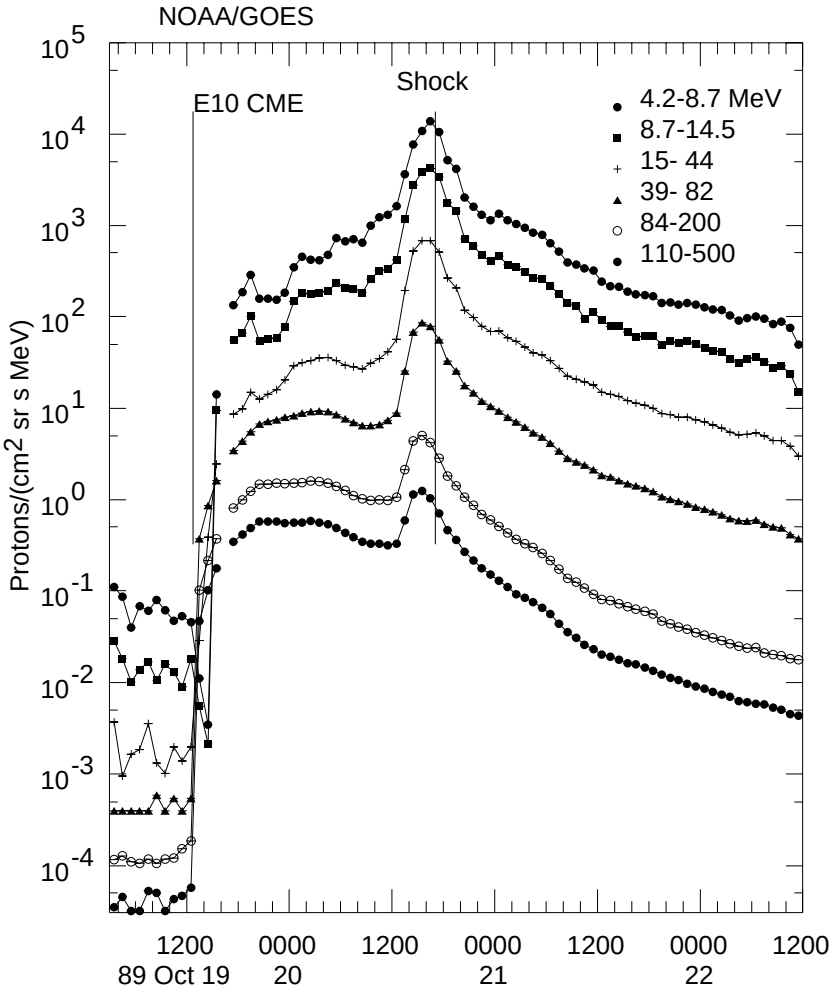

Figure 3.2. Intensity-time profiles at different energies for the large 1989 October 19 event show flat time profiles with intensity peaks near the time of shock passage even at very high energies at 1 AU. Compare Figure 3.1.

In the limit of low background wave intensity, i.e., the Bell limit of Lee theory, the distribution function $f_s(p, z)$ for particles of species s, momentum p, and rigidity $P = pc/Qe$, at a distance z from the shock is given by

$$f_s(p, z) = f_s(p, 0)\left[1 + \frac{\alpha_{\mathrm{H}}(P) f_{\mathrm{H}}(P, 0) V}{K_{\mathrm{H}}(P)} z\right]^{-A/Q} . \tag{3.1}$$

The species subscript, $s = H$ for protons.

This can be considered as the spectrum at the shock at $z = 0$ times a modulation factor that depends on rigidity, P, since protons of the same rigidity as the particles of interest generate the waves. The spectrum at the shock is given by

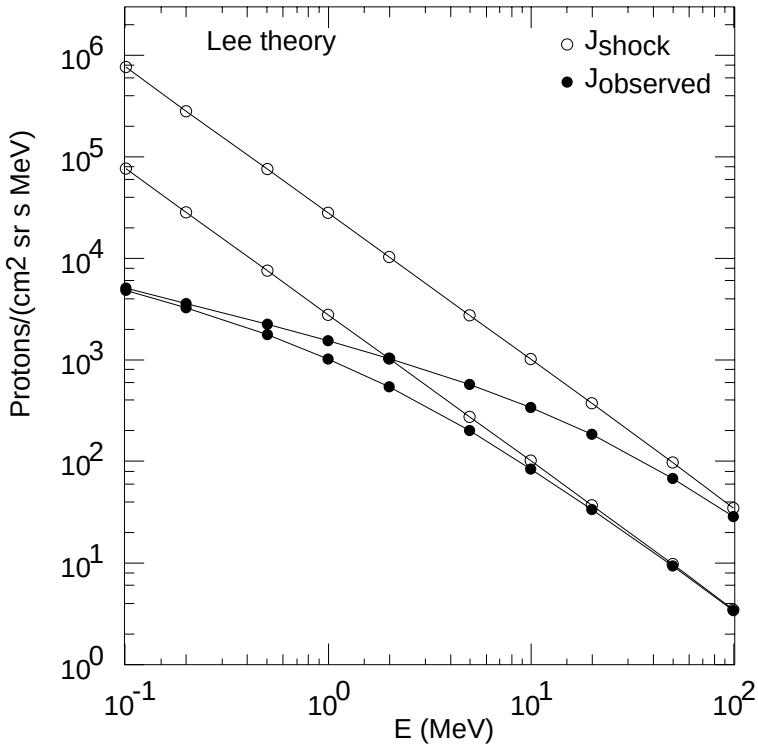

Figure 3.3. Spectrum at a distance from a shock shows a 'broken' power-law form compared with the power-law form at the shock, according to Lee theory. When the intensity at the shock increases, the intensity observed at low energy remains fixed.

$$f_s(p,0) = \beta \frac{N_s}{4\pi V p_{os}^3} \left(\frac{p}{p_{os}}\right)^{-\beta} , \tag{3.2}$$

where N_s particles cm^{-2} s^{-1} of species s are injected at momentum p_{os}, and V is the shock speed relative to the upstream plasma. The quantities $\alpha_{\rm H}$ and $K_{\rm H}$ parameterize wave growth and particle scattering, respectively, in Lee (1983) theory. They may be combined into a scale-height factor $z_{\rm H} = K_{\rm H}[\alpha_{\rm H} f_{\rm H}(P,0)V]^{-1}$ that also has a power law dependence on rigidity given by

$$z_{\rm H}(P) = \frac{(\beta-2)}{6\pi^2} \frac{m_{\rm H} c}{e^2} \frac{\Omega_{\rm H}}{N_{\rm H}} \frac{V}{V_{\rm A}} \left(\frac{P}{P_{oH}}\right)^{\beta-3} . \tag{3.3}$$

The spectrum of protons a distance z from the shock has the form of a 'broken' power law, as shown in Figure 3.3. When the intensity at the shock is increased, as shown in Figure 3.3, the observed intensity at z remains constant at low energy. No more low-energy protons can escape; they are trapped near the shock by resonant waves. This is the equivalent of the 'streaming limit' for Lee theory. However, the modulation factor in this theory is raised to the A/Q power for other species. This

creates a suppression of the low-energy spectra that is much stronger for particles with high A/Q than for protons. We will see that this strong A/Q dependence is not observed. Of course, it should not be surprising that an equilibrium theory in a rectilinear geometry does not fully explain the dynamic evolution that must occur in the acceleration at an interplanetary shock. However, Lee theory is the only theory available that specifically considers shock acceleration of ions in the presence of self-generated waves.

Lee (1983) also estimated the maximum energy of accelerated particles. Ironically, however, in this classic paper on wave growth, he considers only background turbulence in this estimate and obtains a very low value (however, see Lee, 1997). The phenomenon of resonance broadening, an extension to QLT caused by low-frequency intensity fluctuations in B, can cause waves generated by low-energy protons to scatter protons of higher energy more efficiently (Ng and Reames, 1995). This allows efficient trapping near the shock to propagate to higher energies than otherwise possible. This process, which was studied to understand particle scattering near $\mu = 0$, has not yet been quantitatively applied to shock acceleration.

Lee theory includes neither a diverging magnetic field nor a finite time scale, so it describes an 'ESP' profile of infinite extent. At some distance from the shock, intensities of protons of a given energy will fall to a level where they are unable to generate enough waves to disrupt the streaming in the time available. From this point outward, particles can stream freely away, scattered only by the background waves.

The flat intensity-time profiles, like those in Figures 3.1 and 3.2, are the mark of constant acceleration of particles of that energy. Suppose a shock accelerates a constant fraction of the particles from the seed population to a given energy. If both the seed population and the energetic ions have the same radial divergence as a function of distance R, then an observer at 1 AU will see a constant intensity. It would not matter whether (a) the acceleration occurred near the Sun and the energetic particles diverged radially or (b) the seed particles diverged radially and were then accelerated locally. However, the maximum *value* of this plateau intensity is determined by the streaming limit. When a shock weakens appreciably with time or the observer is magnetically connected to a weaker part of the shock, intensities decrease with time.

3.2. LONGITUDE STRUCTURE

The spiral pattern of the interplanetary field (Parker, 1963) causes an asymmetry in the intensity-time profiles of SEP events from eastern and western longitudes on the Sun. These longitude-dependent profiles were first systematically documented by Cane et al. (1988) who studied profiles of 235 proton events with intensities above 10^{-2} (cm^2 sr s MeV)$^{-1}$ accumulated over $\sim$20 years. When these events were organized by solar longitude, typical profiles behaved as shown in Figure 3.4 relative to the expanding shock (Reames, 1995b, 1997). Of course, CMEs and the

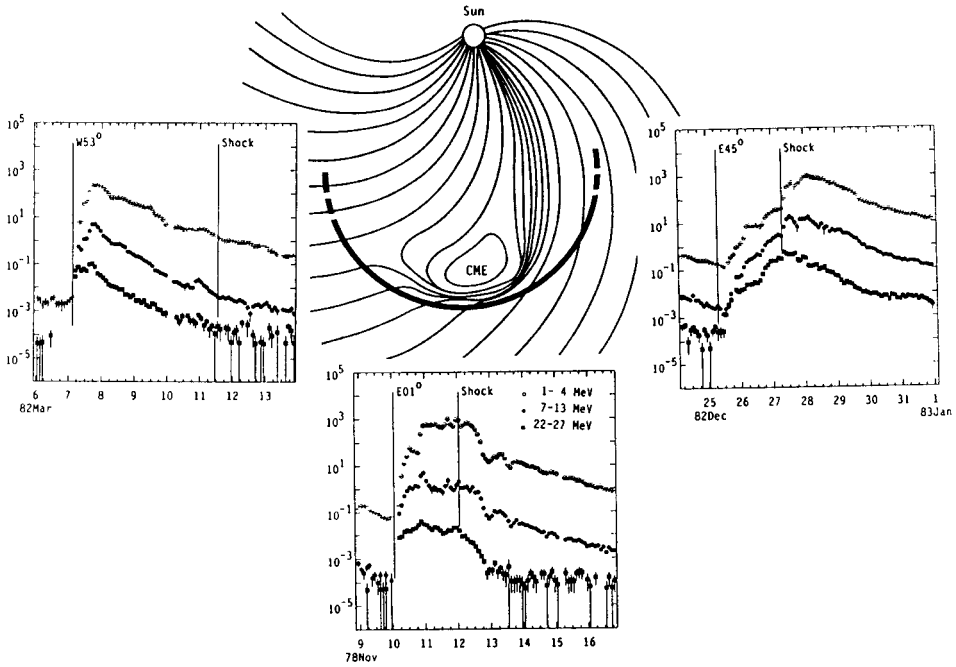

Figure 3.4. Typical intensity-time profiles are shown for 3 events viewed from different solar longitudes relative to the CME and shock.

shock surface can be irregular in shape. However, we assume that the strongest acceleration occurs near the central 'nose' of the shock, where the shock is strongest and the speed is likely to be highest, and declines around on the flanks.

On the eastern flank of the shock, an observer sees a CME erupt from western solar longitudes, like the sample event shown at W53 in Figure 3.4. The observer was well connected to the nose of the shock early, when the shock was near the Sun, but when this shock reaches 1 AU he is 53° around from the nose on the eastern flank of the shock. Thus, he moves onto flux tubes that connect him to a weaker and weaker source, as a function of time, and intensities decline. This decrease simply results from the magnetic geometry even if the speed and compression ratio at all parts of the shock remain constant with time. An observer's magnetic connection point to the shock surface swings eastward with time.

The centrally located observer (E01 in Figure 3.4) may see a slow initial rise since he is connected to the western flank of the shock early in the event. However, for a CME with wide longitude extent, he will see the flat time profile that corresponds to nearly constant acceleration. Just behind the shock, intensities drop by an order of magnitude or more as the observer crosses into the CME itself where many of the field lines may still have both legs connected to the Sun.

The final intensity-time profile in Figure 3.4 is for an observer on the western flank of the shock. He sees a source longitude of E45 in the example. Here, in-

tensities may begin to rise slightly as the shock encounters the base of his field line in the corona, far around to the west of the source. Intensities increase as his connection point swings eastward toward the nose of the shock. However, peak intensities only occur after the observer passes through the shock, 45° to the west of the nose, and he finally arrives on field lines that connect him to the intense nose of the shock *from behind*.

In the foregoing, we have examined multiple events from a single spacecraft. However, in some cases it is possible to observe a single event from multiple spacecraft spaced around it at different heliolongitudes. Such an example is shown in Figure 3.5; the spacecraft locations are shown in the inset (Reames et al., 1997c). The nose of the CME (shown as E58 in the inset) passes slightly to the west of Helios 1. Thus, that spacecraft sees the flat time profile with a peak at the shock as we would expect for an event near central meridian. Helios 2 and IMP 8, farther to the west, see an increasingly slow rise. Since intensities at both spacecraft peak after shock passage, we would infer that this CME has a relatively narrow longitude span. That is, the shock is not very strong at the longitudes where these spacecraft cross it. In other events, the shock itself is seen to extend as much as 110° around from the nose of the shock at 1 AU. This and other examples of detailed multi-spacecraft observations of events can be found in Reames et al. (1996) and Reames et al. (1997).

Attempts have been made to model the spatial evolution of a shock and the SEP event produced by it (e.g., Heras et al., 1994, 1995). These models involve calculations of the space-time evolution of the shock itself and calculations of the transport of the energetic particles from the connection point to the observer through ambient interplanetary turbulence. Using the observed intensities, one can then infer the accelerated particle intensities at the shock.

Far out in the heliosphere, CMEs and shocks from different events merge, as faster events overtake slower ones, to form merged interaction regions (Burlaga et al., 1984, 1985). At 30–50 AU, there is evidence that these shocks begin to accelerate interstellar pickup ions (see Section 6.) such as O^+, since C/O decreases to values of ∼0.2 (Maclennan et al., 1996). Inside ∼5 AU, C/O $\simeq$ 0.5 at these shocks.

3.3. INVARIANT SPECTRA

Figure 3.5 also shows a phenomenon described by McKibben (1972) long ago. Late in these large SEP events, nearly identical intensities are frequently seen at spacecraft separated widely in longitude. For the event shown in Figure 3.5, the intensities all join on March 5, within a factor of ∼2. By that time the shock has expanded beyond the spacecraft to a distance of perhaps ∼2 AU. These intensities then decline gradually for a time of several days with an e-folding time scale that ranges from 8–30 hours in different events (Reames et al., 1997c). Reames et al. (1996) discussed this decay in terms of trapping of particles in CME loops or quasi-

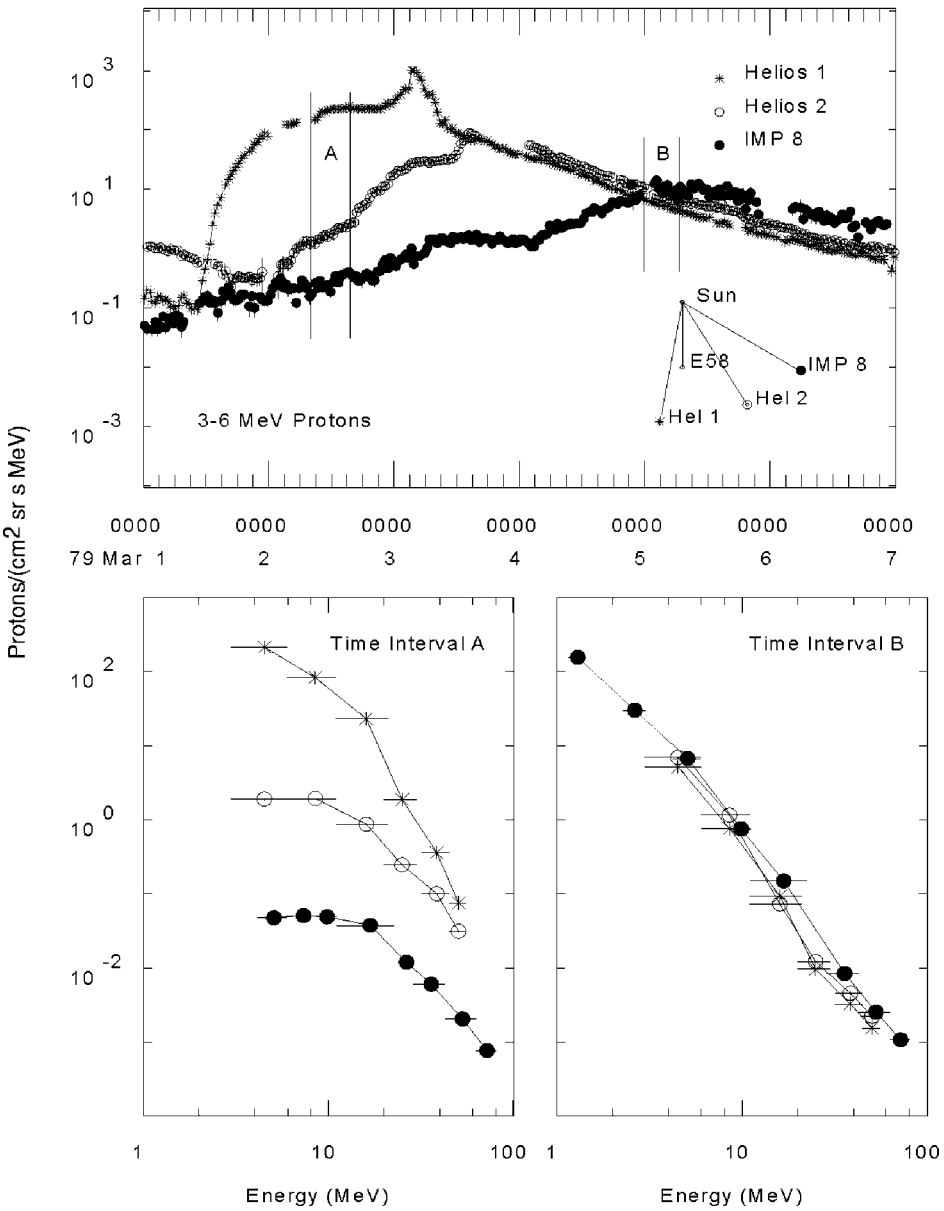

Figure 3.5. Multi-spacecraft examination of the intensity-time profiles viewed from 3 longitudes with the spacecraft configuration indicated by the inset. Spectra at the times indicated at A and B are shown in the lower panels. Spatial invariance of the spectra seen at B contrasts with the diverse spectra seen at A.

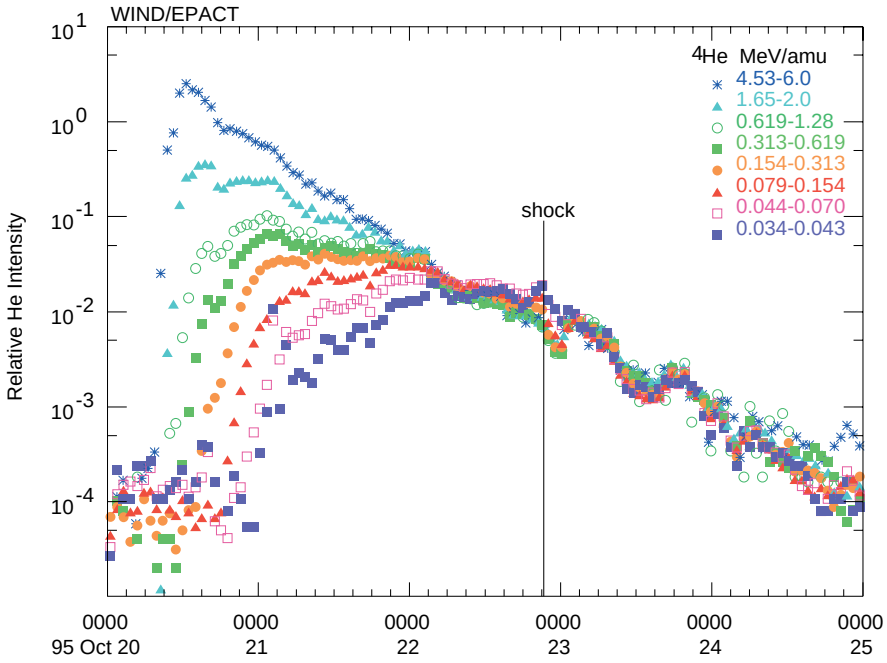

Figure 3.6. Intensity-time profiles of He at different energies are normalized at one point after shock passage in this W55 event. The spectrum is invariant in shape for all times that the same normalization is maintainted.

trapping of particles behind the shock. In the latter case, particles are strongly scattered at the shock and mirror in the converging fields near the Sun. In this environment, particle intensities slowly decline as the 'bottle' in which they are trapped expands. Since the particles do work on the expanding bottle, they lose energy. This adiabatic deceleration preserves the shape of the particle spectra. Time scales for this process can be estimated theoretically (Reames et al., 1996) and are in agreement with those that are observed (Reames et al., 1997c).

Figure 3.5 contrasts the evolving, spatially diverse, energy spectra early in the event with the invariant spectra late in the event. In this event, the same invariant spectra are seen over a longitude interval of about 60°; in other cases this interval extends to 160° or more (Reames et al., 1997c).

If we wish to examine the invariance of the spectral shape at a single spacecraft as a function of time, we can normalize the intensities of particles of different energies at a single time, as in Figure 3.6 (Reames et al., 1997b). If all the intensities continue to track each other as time progresses, then the invariant spectral shape has been maintained. Using this technique, we can study the invariance independently of the actual spectral shape. In Figure 3.6, He ions from 30 keV amu^{-1} to 6 MeV amu^{-1} maintain an invariant spectrum for an interval of almost 3 days. With the exception of a short period near shock passage, the intensities all track, following

each bump and wiggle of the time profile. For this W55 event, we are on the eastern flank of the shock, which is quite weak in this local region. Many other examples of this representation of spectral invariance are shown by Reames et al. (1997c).

However beautifully the event in Figure 3.6 displays spectral invariance, it does not fit the explanation we have given for the phenomenon. Here, the invariance begins well *ahead* of the shock. These particles cannot be trapped in bottles formed by the shock or by closed loops behind it. In this case and several others like it, the bottle seems to have been ejected by the Sun *prior* to onset of the shock that accelerated the particles. However, as we consider this possibility further, it does not seem so surprising. The Sun ejects 2.5 CMEs/day at solar maximum (Webb and Howard, 1994). If we consider one steradian as a characteristic size, this rate is ∼0.2 CMEs/day in one steradian. Now, most of these CMEs are ejected at speeds near that of the solar wind; ∼98% of them do not form shocks that are fast enough to accelerate SEPs. However, they do carry 'closed' magnetic flux ropes or loops into space, where 'closed' means that both footpoints of the loops go directly back to intercept the Sun. These loops may slowly reconnect with open field lines by some mechanism (e.g., McComas et al., 1994; Gosling et al., 1995c), but CMEs and closed magnetic flux ropes are often still observed out to ∼5 AU (e.g., Gosling et al., 1995a; Osherovich and Burlaga, 1997).

Therefore, near solar maximum, we might expect partially closed loop systems from old CMEs to be spaced at intervals of about 1 AU as we move radially out through a steradian of solid angle. With the corresponding numbers for solar minimum, old loops will be spaced every ∼10 AU in radius. An injection of particles from a new fast CME-driven shock near the Sun will fill these old CME loops with particles when the lowest-energy particles have had time to fully explore the extent of the loop. Typically on a time scale of about 1−2 days. For a western source, as our connection point swings to the weak flank of the shock, we may encounter an old loop and see invariant spectra well before the shock arrives. For this weak region of the shock, effects of acceleration are minimal and particle evolution is controlled by expansion of the bottle and by leakage from it.

Spectral invariance is seen in many events (Reames et al., 1997c). We can determine the spatial extent of the invariant region by estimating the location of the spacecraft with respect to the CME and shock at the time invariance is seen. We find that invariant spectra are seen in a region where magnetic field lines either connect to the eastern flank of the shock or are contained inside the magnetic cloud or the CME. This is roughly to the left of the darkened field line in Figure 3.7. Of course, the existence of invariant spectra in the region ahead of the shock will depend upon the presence of loops from old CMEs in this region. In general, the eastern flank of the shock is a benign, slowly evolving region where the quasi-parallel shock ('ESP' event) moves outward in a self-similar pattern. In contrast, on the western flank, stronger and stronger regions of the quasi-perpendicular shock ('shock spike') overtake a given flux tube to produce rapid change and large spatial gradients.

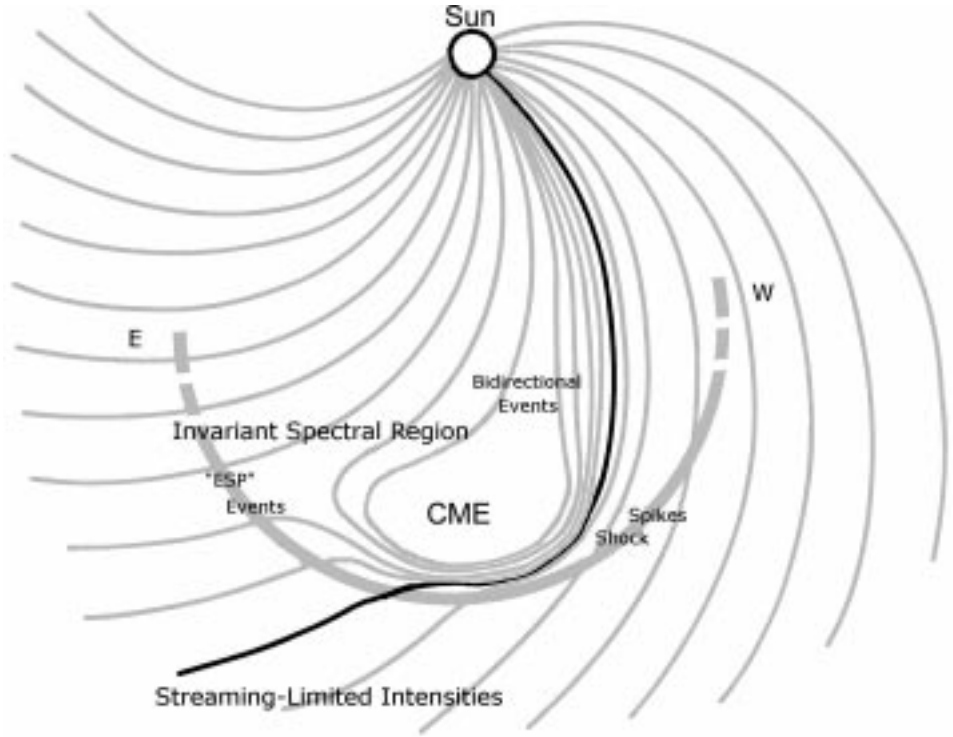

Figure 3.7. A map is shown of the location of various SEP population and phenomena with respect to the CME and shock. The observation of these phenomena at a particular energy will depend upon the width and speed of the CME, the strength of the shock, and the path of the spacecraft through the expanding structure.

3.4. DEFINING THE EJECTA

It is often not possible to make a one-for-one association between CMEs leaving the Sun and ejecta arriving near Earth. Magnetic clouds (Zhang and Burlaga, 1988) and their force-free flux-rope topology can be identified with ejected coronal fields, but they are clearly observed in only a few events. Electrons of 100 eV to 1 keV streaming out from the hot tail of the coronal thermal distribution become bidirectional if both ends of a field line intercept the corona (e.g., Gosling et al., 1987). These bidirectional electrons are a diagnostic of closed magnetic loops, but these electrons sometimes come from other sources. The presence of cool plasma or unusual abundances or charge states can also signal CME ejecta. However, these measures do not always agree and no single parameter gives an unambiguous identification.

Energetic ions can also help to outline the ejecta or map the field lines in it. Bidirectionally streaming protons near ∼10 MeV have been observed for many years (e.g., Rao et al., 1967; Palmer et al., 1978). More recently, large numbers of bidirectional events have been identified and compared with other observational

signatures of interplanetary CMEs (Marsden et al., 1987; Richardson and Reames, 1993). Unlike the superthermal electrons, these ions are not emitted in the corona and the abundances and spectra indicate that they leak into the CME from the shock-accelerated population outside. Ion intensities inside the CMEs are typically 1–10% as large as those outside. Partial reconnection of the internal fields to those that thread the shock (e.g., McComas et al., 1994; Gosling et al., 1995c) may explain the presence of the ions inside. The bidirectionality may be a direct consequence of the field geometry. If a magnetic flux tube is pinched together near the ends and bows out in the middle, particles injected near one end will be focused where the field expands. They will then mirror at the other end only to be focused to stream in the opposite direction as they re-cross the middle.

At times, when an observer is inside a CME, there can be new particles injected onto those field lines from impulsive flares or new gradual events at the Sun. Such observations were used by Kahler and Reames (1991) to confirm that at least one end of the field lines in CMEs at 1 AU was still connected to the Sun; CMEs were not detached plasmoids. Larson et al., (1997) used the streaming electrons of 1–100 keV that produce type III radio bursts to determine field topology inside a CME. In general, they were able to use the velocity dispersion to determine field-line lengths from 1.2 to 3 AU, compatible with the expectations of a helical flux-rope model. However, in detail, neighboring field regions showed a complex pattern of field lines that are connected and disconnected to the source at the Sun, perhaps as suggested by Gosling et al. (1995c; see also Kahler, 1997).

High-energy particles, such as galactic cosmic rays (GCRs), also probe CMEs since they are partially excluded by the closed field structure. Actually, the study of these 'Forbush decreases' in GCR intensities led Forbush (1946) to observe the associated increases from SEPs. Richardson (1997) has reviewed recent work on these decreases that can occur both at the shock and within the CME. Cane et al. (1996) have compiled an extensive list of decreases and used it to study the mean longitude extent of CME ejecta.

3.5. Abundance variations

Abundances of the elements C through Si in an SEP event were first measured on sounding rockets in the large 1960 September 3 SEP event by Fichtel and Guss (1961). These measurements were extended to elements up through Fe as other events were observed using the same techniques during the 1960s (Bertsch et al., 1969). Measurements on spacecraft improved during the next decades and the review by Meyer (1985a) showed that SEP abundances differed from those in the photosphere for two reasons: (1) There were event-to-event variations that became larger for heavier ions. Meyer showed that these variations were strongly correlated with the charge-to-mass ratio, Q/A, of the ions. (2) The underlying averaged abundances showed a step-like dependence on the first ionization potential (FIP) of the ion. Since the ions became highly ionized at coronal temperatures

prior to acceleration, Meyer recognized that the FIP-dependence must be a property of coronal abundances, not of the acceleration. An ion-neutral fractionation must occur during transport of material from the cool photosphere, where high-FIP elements are neutral, to the hot corona (see Section 9). He found that the determination of coronal abundances from SEPs agreed with other techniques and greatly extended the number of elements measured.

To measure element abundances, we compare elements at the same velocity or energy/nucleon because, to first order, this comparison has been shown to reproduce the abundances of the source plasma. SEP abundances have significant advantages in comparison with other sources of information on coronal abundances. Surprisingly, perhaps, they provide abundances for the largest sample of elements available (Reames, 1995a, 1998). Atomic line spectra provide abundances on a limited sample of coronal elements that are ionized to states that emit lines in a given spectral region (e.g., McKenzie and Feldman, 1992; Schmelz, 1993; Meyer, 1996). Such measurements are extremely sensitive to temperature variations along the observer's line-of-sight through the corona. Ionization states and line emission intensities change dramatically with temperature. Gamma-ray lines, produced by nuclear reactions in flares are highly insensitive to temperature and are beginning to produce useful samples of abundances (Ramaty et al., 1996a, b; Share and Murphy, 1995). The high- and low-speed solar wind also provides a measure of coronal abundances for a growing sample of elements (e.g., Geiss et al., 1995).

3.5.1. *Event-Averaged Abundances*

The FIP dependence of abundances and their variations from event to event have been described at length in recent reviews (Reames, 1995a, 1998) so the details will not be presented here. The underlying FIP dependence of SEP abundances will be considered together with that of other particle populations in Section 9.

Following the work of Meyer (1985a), Brenneman and Stone (1985) plotted abundance enhancements of the elements from C through Ni vs Q/A for 10 SEP events and actually fit this dependence as a power law. They also determined the average abundances for a large number of elements. However, since they used photospheric abundances with an error in the Fe abundance, they concluded that a systematic correction was necessary to map the averaged SEP abundances to coronal abundances. Using recent photospheric abundances (Grevesse, Noels, and Sauval 1996) it seems that average SEP abundances in the MeV region require no such correction. Furthermore, while the event-averaged abundances of C through Ni do correlate well with Q/A, the abundances of H and He do not (Reames, 1995a, 1998). The generality of empirical power-law fits to enhancement vs Q/A seems limited. Figure 3.8 shows abundances, relative to coronal, vs Q/A for many elements, including H and He, in several events. The events shown in the figure were chosen because ionization states Q were measured for each element during each of these events by Luhn et al., (1985). However, power-law behavior will not

be restored to the events in Figure 3.8 by small changes in Q, and the Q/A value for H is immutable.

All of the abundance measurements we have considered above were obtained by comparing ions of the same velocity or energy/nucleon near 5 MeV amu^{-1}. However, SEP abundances are known to vary with energy. At a different energy, one can expect to find a different dependence on Q/A. Mazur et al., (1992) studied the energy dependence of abundances and found that the abundances approached coronal values with minimal event-to-event variation at low energies near $\sim$1 MeV amu^{-1}. At high energies $>$10 MeV amu^{-1} they showed an increasing divergence. At energies above $\sim$100 MeV amu^{-1} a new domain of variations may begin and Fe/O ratios seem to increase in several of the largest events observed during the last $\sim$20 years (Tylka et al., 1997). We will consider these high-energy abundances further in Section 3.6.

Isotopic abundance measurements (Williams et al., 1998) provide additional species for the study of Q/A-dependent effects. In this case, it is likely that isotopes of a given element have the same Q, so the differences in Q/A, though small, are well defined even in the absence of charge measurements. It is important to realize that ^{3}He/^{4}He is also affected by Q/A-dependent acceleration. We should not mistake the modest enhancements in ^{3}He/^{4}He in gradual events as evidence of material from impulsive flares. If the acceleration source is not independently known, only values of ^{3}He/^{4}He > 0.1 provide convincing evidence of resonant processes in impulsive flares.

Recently, Cohen et al. (1999) have attempted to *determine* Q for Fe by assuming that the enhancements of all species fit a single power law, a behavior that is not at all obvious from the data in Figure 3.8. We will see in the next section that the abundance variations actually result from rigidity-dependent suppression of the spectra of particles escaping the shock. There is no reason to believe that a power law should describe the complex behavior shown in Figure 3.8.

Plots of abundance variations as a function of Q/A are rather phenomenological and are of limited value in understanding the underlying physics. In addition, event-averaged data can only hint at the complex dynamic behavior of an evolving CME-driven shock. To progress we must examine variations with time.

3.5.2. *Time Variations*

A new generation of larger-geometry instruments launched on the Wind and ACE spacecraft in the last few years has allowed us to measure the time variations of abundances within an event with greatly increased detail. The number and variety of these events is increasing with the new solar cycle. All elements from H through Fe have been observed to participate in these variations.

Figure 3.9 shows the remarkable systematic variations of abundances during the event of 1998 April 20 (Tylka et al., 1999). With the exception of H/He, the abundance variations are actually correlated with the Q/A of the ions at each step in time. Although they have been poorly studied because of limited instrument

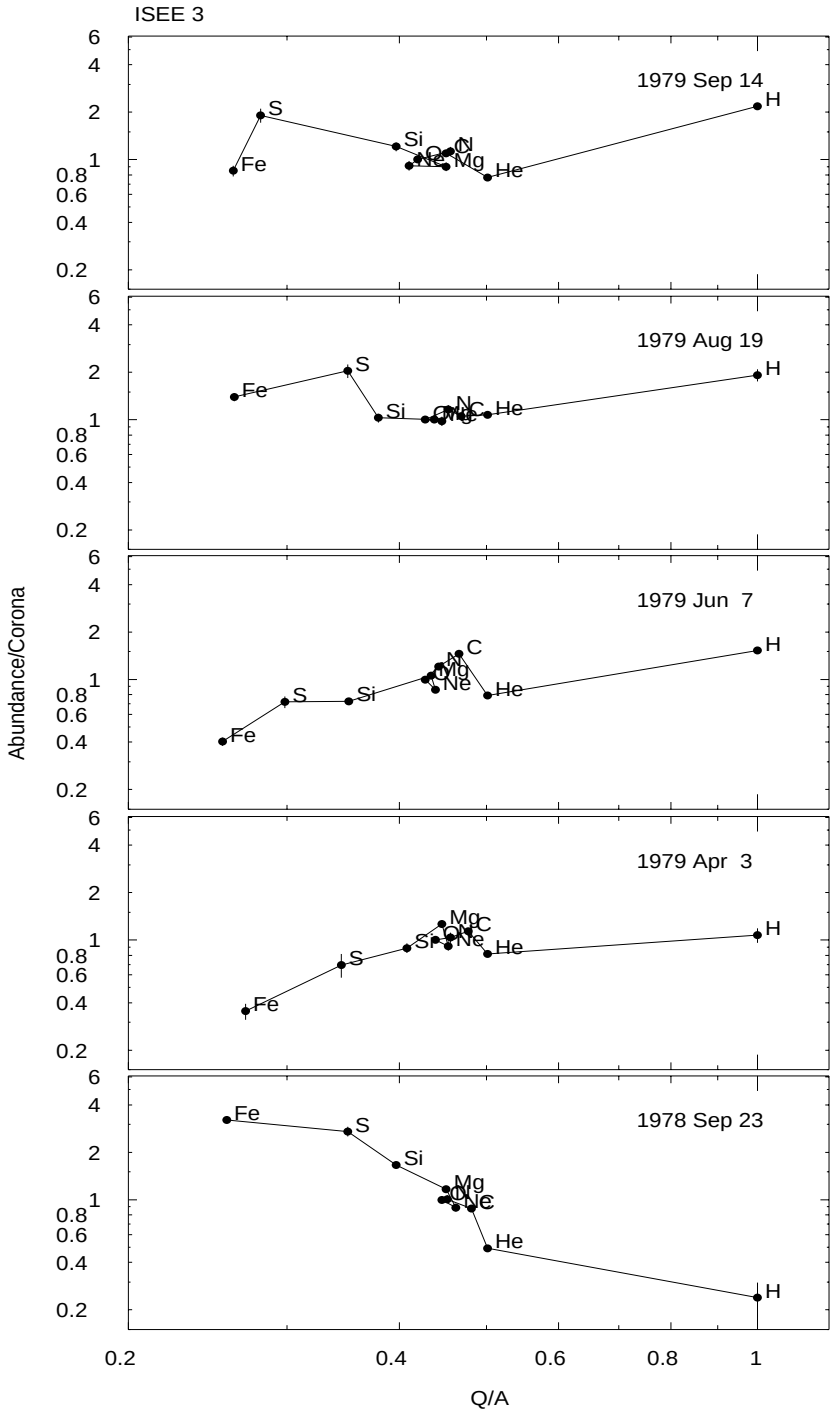

Figure 3.8. Event-averaged element abundances, normalized at O, reltive to the corresponding coronal abundance, for 5 SEP events are shown as a function of Q/A. The average values of Q measured (Luhn et al.,1985) for each element in each event are used. Variations for the elements C−Fe are correlated but power-law fits vs Q/A seem poorly justified.

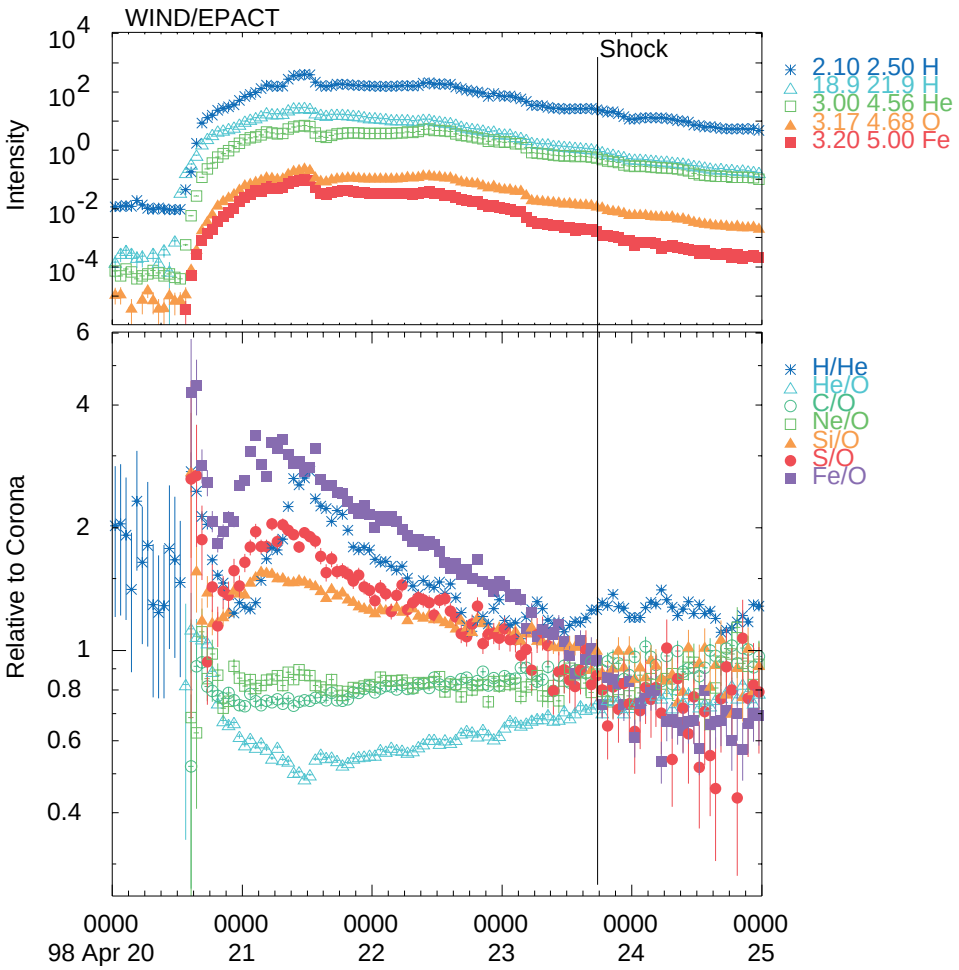

Figure 3.9. Systematic abundance variations (relative to coronal abundances) for several elements at ~3 MeV amu^{-1} in the 1998 April 20 event are shown in the lower panel and typical intensity-time profiles in the upper panel.

sensitivity, variations similar to those shown in Figure 3.9 have actually been seen in other events during the last two solar cycles (e.g., Reames 1990a).

Time variations in events were once considered to arise from random fluctuations in the coronal source material as a function of longitude (Mason et al., 1984). These abundance fluctuations were presumably sampled randomly as the shock crossed different flux tubes. The smoothly varying abundances seen in Figure 3.9 are clearly incompatible with this sort of model. The observed variations must be a property of the physics of shock acceleration, not of the source material. However, Mason et al. (1984) did show that the abundance variations with longitude that

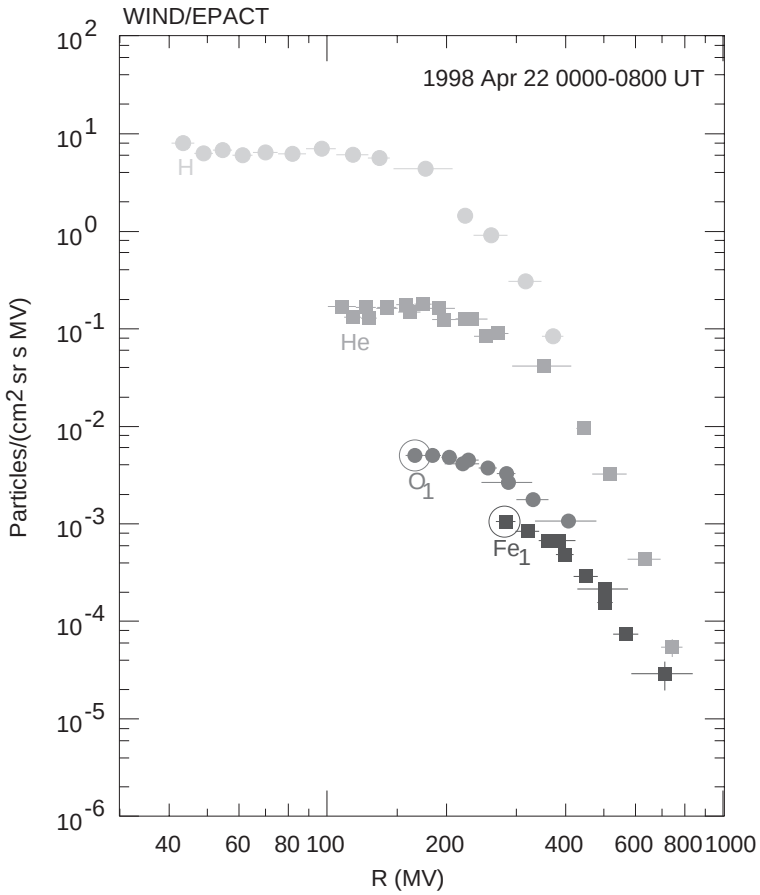

Figure 3.10. Differential rigidity spectra of H, He, O, and Fe for the period 00:00–08:00 UT on 1998 April 22. At low rigidity, the ions must pass through proton-generated waves to escape the shock, resulting in flat spectra. Points labeled Fe_1 and O_1 have the same velocity or energy/nucleon and increase Fe/O (in Figure 3.9) because O_1 is suppressed more than Fe_1.

would be expected from coronal-diffusion models of the flare-myth era were not observed.

We can gain a qualitative understanding of the abundance variations by looking at the *rigidity* spectra of H, He, O, and Fe shown in Figure 3.10. Differences between the observed proton spectrum and a power-law spectrum at high energies tell us about wave generation at the shock. Thus, the flattened proton spectrum is both a signature of and proxy for wave generation as described by Lee (1983) and shown in Figure 3.3. Other ions such as O and Fe must propagate through the waves generated by protons of the same magnetic rigidity. The circled points shown as O_1 and Fe_1 in Figure 3.10 have the same velocity or energy/nucleon; they were used to generate the Fe/O ratio shown in Figure 3.9. However, the point O_1 is at a rigidity that is heavily suppressed by waves while Fe_1 is out in the power-

law region where wave suppression is minimal. *Hence, Fe/O increases because O is suppressed more than Fe by the waves, not because Fe is enhanced.* The time variation of the abundances occurs as the wave growth increases and then decreases as the shock strength waxes and wanes on the observer's field line. During the same period, the H/He ratio increases because the low-rigidity part of the spectrum actually rises slightly, affecting H more than He at a given velocity.

Note that our understanding of the abundance variations suggests that the rigidity spectra are similar for all species emerging from the shock, as can be seen for the spectra of H and He in Figure 3.10. This spectral behavior differs from expectations of the equilibrium theory of Lee (1983) where the modulation increases as A/Q. However, this equilibrium theory might not be expected to follow the dynamic evolution of these events in a radially diverging field. In a dynamic situation, wave growth falls rapidly below equilibrium as proton intensities decrease with distance from the shock, that is, when the time scale for wave growth becomes greater than the time since acceleration began.

Ng et al. (1999) have adapted the transport theory of Ng and Reames (1994) to model particle acceleration and transport from a moving shock. The acceleration is simulated crudely by injecting power-law spectra at the location of the moving shock. All particle species are injected with the same energy/nucleon spectrum and with coronal abundances, but wave generation is neglected for all species except protons, as in Lee's (1983) theory. However, the amplification and damping of waves are coupled to the transport and scattering of protons. Other species, nominally represented by He and O with $Q/A = 0.5$ and Fe with $Q/A = 0.25$, obey the equations of focused diffusive transport through the proton-generated waves that evolve dynamically in space and time.

Figure 3.11 shows results for time variations of He/H and of Fe/O at 3 different energies from a theoretical simulation by Ng et al. (1999). These results approximately compare with observations in the 1998 April 20 event that were shown in Figure 3.9. All ratios are taken for elements of the same velocity or energy/nucleon. The time-evolution of Fe/O in Figure 3.11 can be understood qualitatively in the following way. Early in the event, particles propagate through ambient interplanetary turbulence that is assumed to have a Kolmogorov wave spectrum. Although this scattering is small for all species (the scattering mean free path, $\lambda \sim 1$ AU), differing rigidities cause O to be scattered slightly more than Fe. Hence, the arrival of O is delayed and Fe/O begins at a high value. Fe/O decreases as O intensities begin to rise and the ratio reaches a minimum a few hours after event onset. At this time, proton-generated waves near the shock have become important and Fe/O again rises because O is more efficiently trapped near the shock than is Fe. Many hours later, Fe/O begins to fall as the shock expands and weakens and the trapping diminishes. At higher energies, the enhancement of Fe/O is smaller because of reduced wave generation by higher-rigidity protons.

The behavior of He/H in the shock simulations can be much more complex. Initially, one would expect He/H to behave just as Fe/O; the highest-rigidity species,

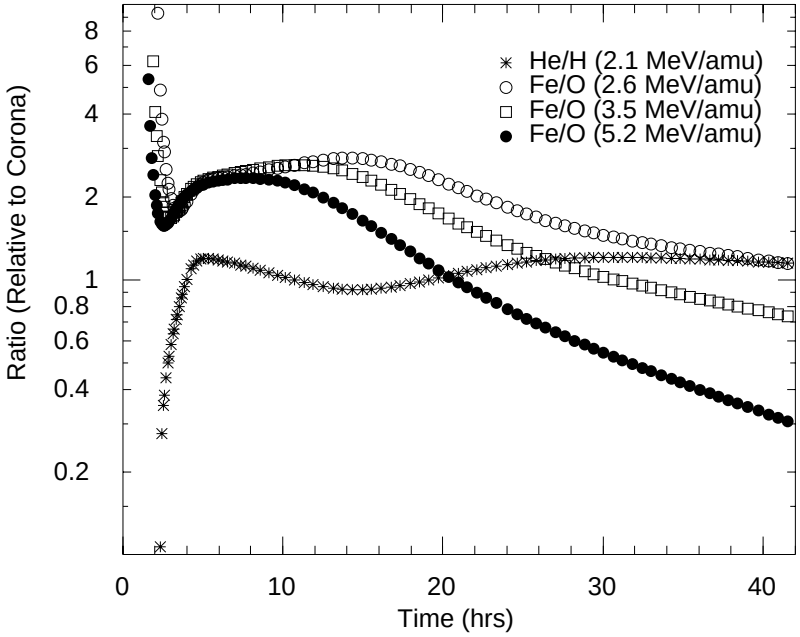

Figure 3.11. Theoretical time variations in Fe/O and H/He are derived in the shock simulation (Ng et al., 1999) including transport through proton-generated Alfvén waves. The event simulated is similar to that shown in Figure 3.9 and 3.10.

in the numerator of the ratio, should arrive earliest. However, the 2 MeV protons resonate with waves that they themselves must generate, while 2 MeV amu^{-1} He resonates with waves generated by *faster* protons that easily propagate out ahead of the He. Thus He/H can either rise or fall initially in response to the intensity and spectrum of the waves and the protons that generate them. Examples of both types of behavior can be found in observations in different events. Thus, *the lack of correlation between He/H and Fe/O in gradual SEP events* (Reames 1995a, 1998) *is actually strong evidence for the presence of self-generated waves.* Ambient Kolmogorov turbulence would produce *correlated* variations in these ratios (Ng et al., 1999).

In Figure 3.12 we show rather different behavior in an event near central meridian. Here the abundances such as Fe/O decrease from their coronal values early in the event and remain at low levels, with some variation, right through the time of passage through the shock, the ESP event, and the CME. We have already discussed the fact that proton-generated waves preferentially trap O near the shock while allowing Fe, of the same velocity, to escape. Thus, it is not surprising that we see *depressed* Fe/O near the shock. However, the detailed time behavior farther ahead of the shock, when we are magnetically connected to its quasi-perpendicular western flank, has not been simulated. Neither do the simulations allow the advancing shock to incorporate these particles with altered abundances and accelerate

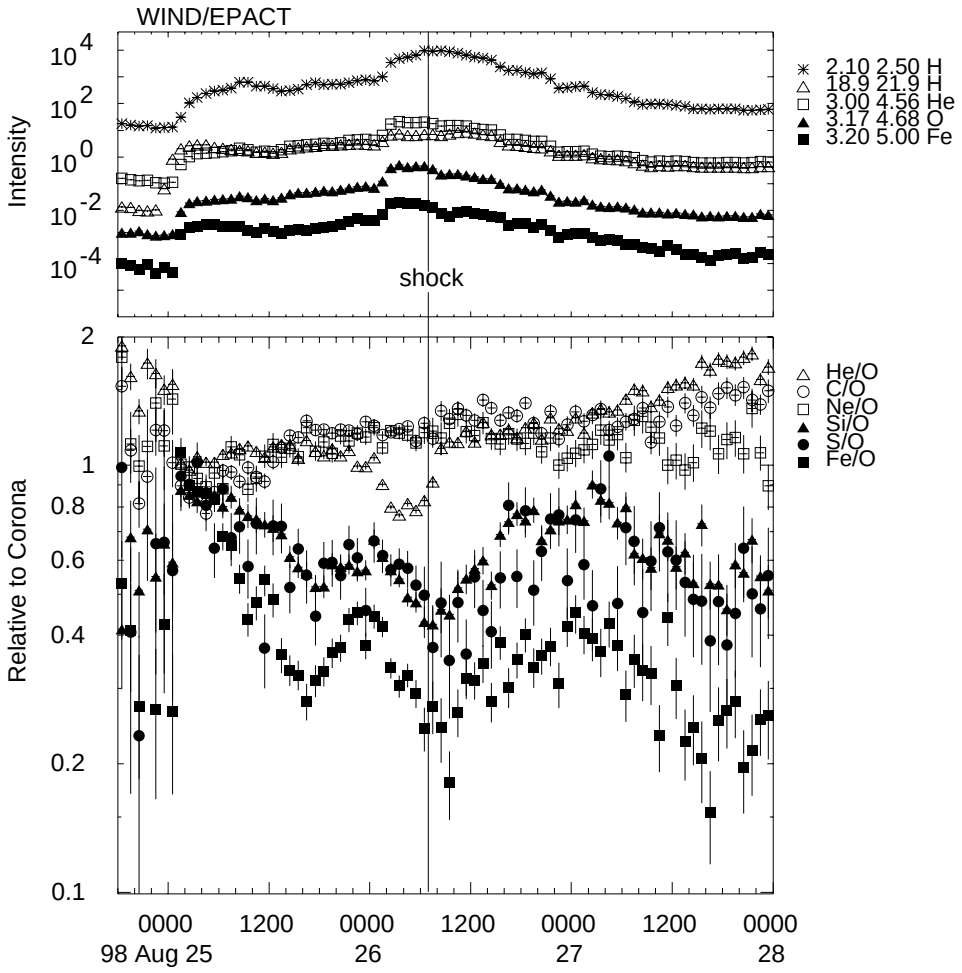

Figure 3.12. Abundance ratios, relative to coronal abundances, and intensity-time profiles are shown for the large event of 1998 August 25. Here, ratios such as Fe/O are suppressed even during passage of the shock and ESP event on August 26.

them to higher energy. This latter process could lead to the exaggerated abundance variations often seen at energies above $\sim$10 MeV amu^{-1} (Mazur et al., 1992).

Note that the two events we have considered, involving different source longitudes, have enhancements and suppressions of Fe/O. Western events tend to have enhancements while eastern events show suppression (Cane et al., 1991) when the proton intensities at the shock are sufficiently high for extensive wave growth. To first order, the effect of proton-generated waves is to differentially redistribute the elements in space; enhancements of ratios in one place imply corresponding depressions elsewhere. If we could average over all space and time, we would obtain coronal abundances. When we examine many events, on average, we do

find that the Q/A-dependencies are averaged away. We know that this happens by comparing the abundances of Fe with those of Mg or Si, averaged over ∼50 events. These elements have much different values of Q/A, but very similar values of FIP. The fact that the abundances of these species agree well on the FIP-effect plot (see Figure 9.1) means that the Q/A-dependencies have averaged away (Reames, 1995a, 1998).

We do not yet fully understand all abundance and spectral variations in detail, especially when early events disturb the interplanetary medium for events that follow. However, it is already clear that the abundances are a powerful probe of the structure and wave spectra at the shock. The shock seems to accelerate different species to the same spectra in velocity, but the escape of the ions through waves, largely generated by protons, depends upon their rigidity or Q/A. Hence, different species at a given velocity differentially probe the wave spectrum near the shock. These abundance variations are much easier to see than the spectral variations that they represent, since the latter are plotted on an intensity scale of several decades.

3.6. HIGH-ENERGY SPECTRA AND ABUNDANCES

The highest-energy particles from the largest SEP events are observed by neutron monitors and meson telescopes on Earth. The primary ions cause a cascade of secondary products as they interact with the atmosphere and the secondaries are observed in these 'ground-level' events (GLEs). Information on source abundances is lost to this technique. Because of the differences in techniques and venue, this research is often considered separately from that centered on spacecraft observations. However, this important energy region allows us to explore the limits of shock acceleration.

Kahler (1994) tied the highest energy particles to CMEs by studying the acceleration profiles of 1–21 GeV protons vs the height of the CME-driven shock. He found that for particles at the highest energy, peak acceleration occurred when the shock was at a distance of 5–10 solar radii. At these distances, densities are sufficiently low that Fe at the highest observed energies (600 MeV amu^{-1} or 33 GeV) is not stripped of electrons during acceleration (Tylka et al., 1995).

Using multiple neutron monitors with different geomagnetic cutoff rigidities and asymptotic look directions, it is possible, in principle, to measure the energy spectrum and anisotropy of the incoming protons (McCracken 1962). At energies near ∼1 GeV amu^{-1}, spectra have steepened considerably relative to those observed in the 10–100 MeV region, as shown in Figure 3.13 taken from the work of Lovell et al. (1998). Spectra in this region have been fit to the semi-empirical shock-acceleration model of Ellison and Ramaty (1985) but no further attempt has been made to connect the steepening to the physics of the shock.

At ∼0.1–1 GeV amu^{-1}, the highest energies where abundances have been measured, Tylka et al. (1997) observe interesting increases in Fe/O. These observations may suggest that the spectrum of O begins to roll off at a lower energy/nucleon

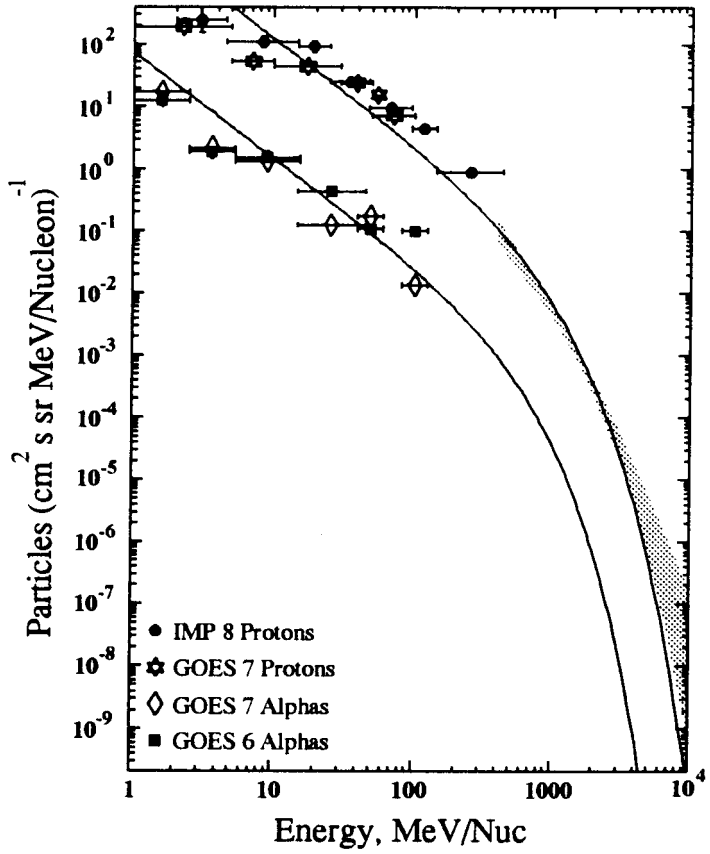

Figure 3.13. Energy spectra of H and He in the 1989 September 29 event including data points from IMP 8, GOES 6 and 7, and the neutron monitor spectrum (shaded region). Fitted curves are the shock theory of Ellison and Ramaty (1985). (Lovell et al., 1998).

than that of Fe. Here we have questions of particle containment and abundance variations around the 'knee' of the SEP spectrum near 1 GeV. Similar questions are often asked about the 'knee' of the GCR spectrum near 10^{15} eV. The requisite abundance measurements are substantially easier to make for the SEP case.

4. Impulsive SEP Events

The energetic particles from impulsive solar flares constitute one of the most fascinating particle populations we have observed. The unusual abundances in these events give us insight into the plasma physics of resonant wave-particle interactions in flares. The existence of these processes in flares was discovered *via* energetic particles in space and direct particle observations continue to provide the primary window available for studying them.

4.1. PHOTONS FROM FLARES

There is a long and rich history of the observation of flares beginning with their first detection by Carrington (1860). However, most of the photon emission from flares is either thermal emission from the heated plasma or, in the case of hard X-rays and radio bursts, is produced by non-thermal electrons. Only in recent years has it been possible to observe γ-rays and neutrons produced by nuclear reactions of accelerated ions in several events (see, e.g., Ramaty et al., 1979; Chupp, 1984; Evenson et al., 1990; Muraki et al., 1992; Yoshimori et al., 1994). The fast time scale of the earliest γ-ray-line observations showed that ions were indeed accelerated in impulsive flares and not only by shocks. The narrow γ-ray lines from excited nuclei of the ambient plasma provide information on coronal abundances and on energy spectra above $\sim$1 MeV (Ramaty et al., 1996a).

Cliver et al. (1989) made a careful comparison of SEP events and γ-ray-line flares during a 5-year period near solar maximum. They found a relatively poor correlation between γ-ray-line fluences and 10 MeV proton intensities, with the ratio of the two varying over 4 orders of magnitude. Even very large SEP events often lacked measurable γ-ray-line fluences, although the largest γ-ray-line events usually had an accompanying SEP event.

Ramaty et al. (1993) compared the electron-induced bremstrahlung with the proton-induced γ-ray lines in flares to derive the ratio of 0.5 MeV electrons to 10 MeV protons. They found a high ratio corresponding to the ratio for impulsive SEP events in interplanetary space. Since similar ratios were found for flares with widely varying time scales, they suggest that the same stochastic acceleration mechanism was operating in flare loops, if not in space. This finding was used to support the suggestion of Cliver (1996) that there are hybrid gradual events for which different acceleration mechanisms operate in different locations, i.e., in the flare loops and in interplanetary space. Ramaty et al. (1996b) found a comparable energy content in the protons and electrons accelerated on flare loops.

For one event, it was possible to deduce abundances from the broad γ-ray lines emitted from excited nuclei of the accelerated particles (Murphy et al., 1991). The abundances of the 'beam' showed the same pattern of enhancements of ^{3}He and heavy ions that were seen in the impulsive SEP measurements.

Very recently, Mandzhavidze et al. (1999) have analyzed measurements by Share and Murphy (1998) of γ-ray lines emitted exclusively by ^{3}He bombardment of He, O and Fe, especially the 0.937 MeV line from de-excitation of ^{18}F* produced *via* ^{16}O(^{3}He,p)^{18}F*. Comparing these lines with those produced by ^{4}He or by both ^{3}He and ^{4}He, they find that 7 of 20 flares show clearly enhanced ^{3}He/^{4}He > 0.1 and in some cases ^{3}He/^{4}He $\sim$1. ^{3}He/^{4}He cannot be directly measured in the remaining flares, but it is consistent with being $\geq$0.1 in all cases. This important work further confirms the strong association between ^{3}He-rich particle events and flares. However, the authors point out that the flare *duration* is actually not important. Evidently, any acceleration in flares on closed loops in the low corona can produce

^{3}He-rich events. This again supports Cliver's (1996) idea that all acceleration in flares in the corona produces ^{3}He-rich energetic particles. In gradual events, the shock, driven by the associated CME, accelerates so many particles out on open field lines that those few that escape the flare loops are overwhelmed.

4.2. ASSOCIATIONS

Improved instruments launched in 1978 August on the ISEE-3 spacecraft, with increased geometry and resolution near 1 MeV amu^{-1}, provided a flood of new measurements of ^{3}He-rich events. The new ISEE-3 measurements provided information on ionization states (e.g., Luhn et al., 1987), abundances (e.g., Mason et al., 1986) and energy spectra (e.g., Möbius et al., 1982). In addition, however, they also provided the statistics necessary for correlation with impulsive solar flares (see review by Reames, 1990b).

The earliest of these associations connected ^{3}He-rich events with the scatter-free nonrelativistic (10−100 keV) electron beams that generate type III radio bursts (Reames et al., 1985). Velocity dispersion, i.e., the particles arriving in inverse order of their velocities, was found to be consistent for the electrons and ions and could be used to determine the solar onset time of the particle acceleration within a few minutes. The associations with streaming electrons and with metric and kilometric type III bursts (Reames and Stone, 1986) provided the timing necessary for associations with Hα (Kahler et al., 1987b) and X-ray (Reames et al., 1988) flares. Radio mapping of the trajectories of the type III bursts provided further confirmation of the source identifications.

The fervent hope of these investigators was to pinpoint the sources of these unusual events. By correlating properties of the environment or flare plasma with ^{3}He/^{4}He, one sought the peculiar subset of flares that gave rise to these unusual isotopic enhancements. No such correlation was found. The truly surprising result was that there was *nothing* remarkable at all about the ^{3}He-rich flares and no strong correlations with any flare properties (e.g., Reames et al., 1988). The flares associated with ^{3}He-rich events seemed to span the distribution of flare properties with respect to temperature, size, and emission of hard and soft X-rays. *Particles from any flare could be ^{3}He-rich; perhaps all flares.* However, there was a weak inverse correlation of ^{3}He/^{4}He with X-ray and radio flux and a weak inverse correlation of Fe/O ratios with flare duration (Reames, 1990b).

Furthermore, when results were available on the rates of occurrence of ^{3}He-rich events, it seemed that they were not much less common than hard X-ray events, for example. Figure 4.1 shows ^{3}He/^{4}He ratios in individual events during a solar cycle in the upper panel and rate of occurrence in the lower panel, during a 14-year period. After 1983, the rates must be corrected for the poor tracking coverage of the spacecraft by the Deep Space Network, often only ∼2 hrs per day. Nevertheless, it is clear that the event rate decreases by a factor >50 during solar minimum. The occurrence rate of ^{3}He-rich events near solar maximum is ∼100

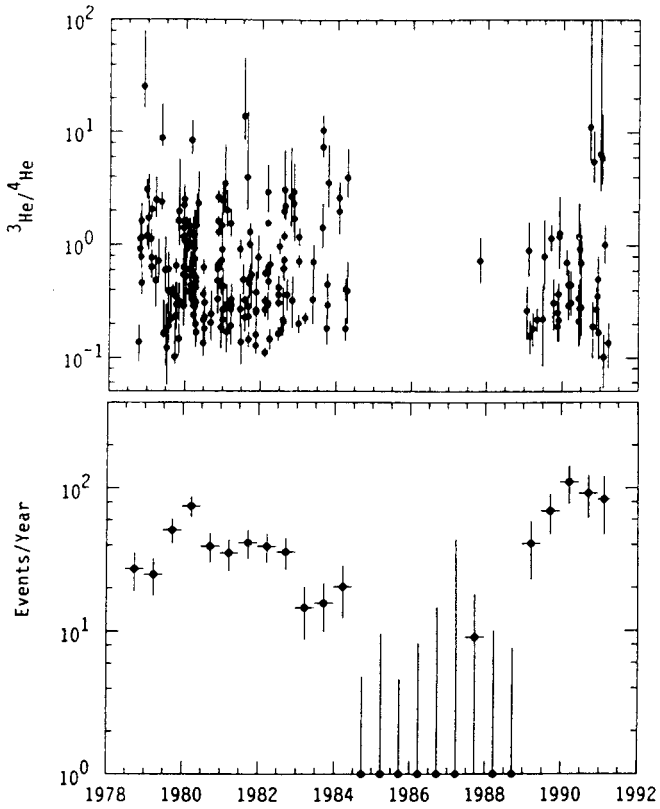

Figure 4.1. The upper panel shows ^{3}He/^{4}He ratios measured in individual impulsive events during a 14-year period. The lower panel shows the event occurrence rate corrected for spacecraft coverage that displays a strong solar-cycle effect.

yr^{-1}. However, if we recall that these events come from a solar longitude interval of $\sim$20° (Figure 2.3), then we see that the rate of event occurrence on the visible solar disk is $\sim$1000 yr^{-1}. It is this rate that we must compare with the rate of hard X-ray events, Hα flares, or metric type III bursts of $\sim$4000 yr^{-1}, $\sim$10 000 yr^{-1}, and $\sim$10 000 yr^{-1}, respectively (Reames, 1993; Reames et al., 1994). Allowing for events below the threshold of sensitivity of the ISEE-3 instruments, we find that ^{3}He-rich events are a ubiquitous phenomenon. Much smaller ^{3}He-rich events have now been seen, even at solar minimum, with instruments of higher sensitivity on the Wind spacecraft (Reames et al., 1997b).

An interesting estimate of the efficiency of acceleration of ^{3}He can also be made for these events (Reames, 1993). A moderately large event with ^{3}He/^{4}He $\sim$1 can produce a fluence of 10^5 ^{3}He ions cm^{-2} at 1 AU. Assuming they occupy a 20° cone, or $\sim$0.1 sr, this implies $\sim 2 \times 10^{30}$ ^{3}He ions accelerated to energies above $\sim$1 MeV amu^{-1} in the event. Using a flare of area (3000 km)^2, scale height of 10 000 km, density of 10^{10} H-atoms cm^{-3}, and ^{3}He/H $= 5 \times 10^{-5}$, we find there

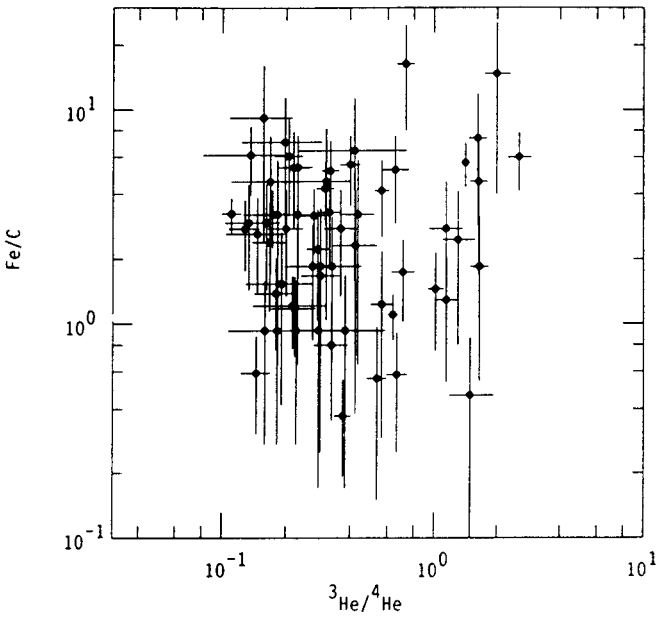

Figure 4.2. Scatter plot of the abundance ratios ^{3}He/^{4}He vs Fe/O in individual ^{3}He-rich events. The mean abundance ratios are enhanced in both cases but variations are not correlated.

are only $\sim 5 \times 10^{31}$ ^{3}He ions in the flare volume. Allowing for ^{3}He ions in the spectrum down to 100 keV amu^{-1} that have recently been seen (Reames et al., 1997b) this means that more than 10% of the ^{3}He in the flare volume is accelerated. The observed decrease in ^{3}He/^{4}He ratios in large events may actually result from depletion of ^{3}He in the flare volume.

These estimates also argue *against* the possibility of acceleration of ^{3}He in 'high coronal flares' where densities are only $\sim 10^8$ H-atoms cm^{-3} (Cliver and Kahler, 1991). There is not enough ^{3}He in the high corona. It is also difficult to ionize Fe to the observed charge state $Q_{\rm Fe} = 20.5 \pm 1.2$ at such low densities, as noted by Cliver and Kahler (1991).

4.3. ABUNDANCES

Soon after the discovery of ^{3}He-rich events, it was found that abundances of elements up to Fe were also unusual in these events (Hurford et al., 1975). Relative to C or O, the degree of enhancement seemed to increase with Z up to Fe, with Fe/O $\sim$10 times its value in the corona or in large gradual SEP events (see, e.g., Mason et al., 1986).

A fascinating feature of all of the abundances in ^{3}He-rich events is that event-to-event variations in the abundance of one species are almost completely uncorrelated with those in another species. This effect was shown by Mason et al. (1986) and explored further by Reames et al. (1994). Heavy element abundances,

TABLE 4.1
Abundance enhancements in impulsive events (relative to coronal)

^{4}He/C	0.85 ± 0.17	
N/C	1.52 ± 0.34	$\sim$1
O/C	1.10 ± 0.12	
Ne/C	3.51 ± 0.50	
Mg/C	2.35 ± 0.32	$\sim$2.8
Si/C	2.76 ± 0.38	
Fe/C	6.67 ± 0.80	$\sim$6.7

specifically Fe/C, are not correlated with ^{3}He/^{4}He, as is shown in Figure 4.2. This has been interpreted as evidence that different mechanisms or, at least, different wave modes are involved in the enhancements of ^{3}He and Fe, or that they are accelerated in different spatial regions. However, the same behavior can be seen for the impulsive events in the plot of Ne/O vs Fe/O shown in Figure 2.4 or in *any* other pair of element abundances (Reames et al., 1994). We can scarcely introduce a special acceleration model for each species.

Note that this uncorrelated behavior is remarkably different from behavior we have seen in gradual events where variations in Ne, Mg, Si, S, and Fe usually show systematic correlated behavior, even as a function of time within a single event. This is another distinction between gradual and impulsive events. Furthermore, abundances in impulsive events usually show no energy dependence.

It is useful to summarize the pattern of average abundance enhancements other than ^{3}He/^{4}He in impulsive events as shown in Table 4.1. Abundances in the table seem to fall into three groups, ^{4}He, C, N and O in the first group, Ne, Mg, and Si in the second, and Fe in the third. Reames et al. (1994) proposed that each group had a characteristic value of Q/A. Species in each group resonate with waves in a given frequency region, but that frequency, and the intensity of resonant waves, varies from one group to another. Reames, Meyer and von Rosenvinge (1994) plotted Q/A for different species vs plasma temperature, as in Figure 4.3, based upon ionization equilibrium calculations (Arnaud and Rothenflug, 1985; Arnaud and Raymond, 1992). They noticed that in the temperature range of 3–5 MK, elements in the first group, ^{4}He, C, N, and O, were fully ionized with $Q/A = 0.5$. Elements in the second group, Ne, Mg and Si, had a stable 2-electron configuration with $Q/A \approx 0.42$, and Fe had $Q/A \approx 0.28$. The abundance grouping seemed to be the signature of a 3–5 MK plasma.

Of course, this conclusion is in direct conflict with the measurements that all the elements up to Si are fully ionized, with $Q/A = 0.5$ (Luhn et al., 1985).

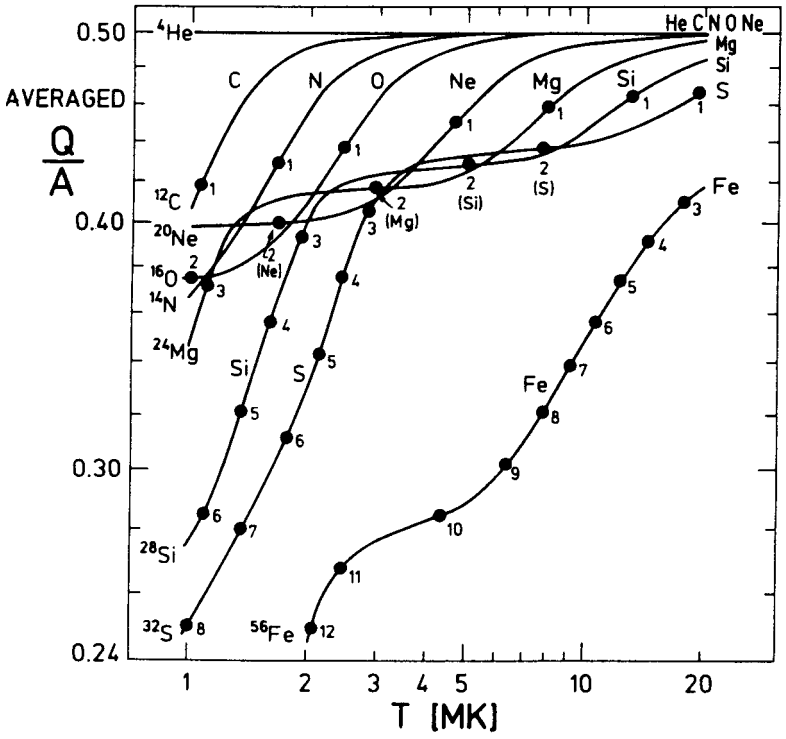

Figure 4.3. The charge-to-mass ratio, Q/A, for various elements as a function of temperature based upon theory of Arnaud and Rothenflug (1985) and Arnaud and Raymond (1992) as plotted by Reames et al. (1994).

However, if all the elements from ^{4}He through Si have $Q/A = 0.5$ then there is no known way to distinguish them with electromagnetic fields and generate the observed abundance enhancements. The abundances are in conflict with the ionization-state measurements. A resolution of this conflict is obtained if the ions are accelerated early in the flare from a 3–5 MK plasma and then ionized later as the plasma is heated. Thus, the acceleration time scale is shorter than the ionization time scale. Estimates of these time scales (Miller and Viñas, 1993) suggest that this sequence of events is quite reasonable. In fact, for acceleration time scales of seconds, thermal stripping would be extremely slow; ion stripping by electron beams might predominate. In either case, the abundances are completely independent of the charge states finally observed.

If we know the temperature and the equilibrium ionization states, we can plot the averaged enhancements relative to coronal abundances as a function of Q/A (Reames, 1995a). Such a plot is shown in Figure 4.4. The figure shows a relatively smooth dependence on Q/A. Since the gyrofrequencies of the ions are proportional to Q/A, we can interpret Figure 4.4 as the average resonant frequency spectrum

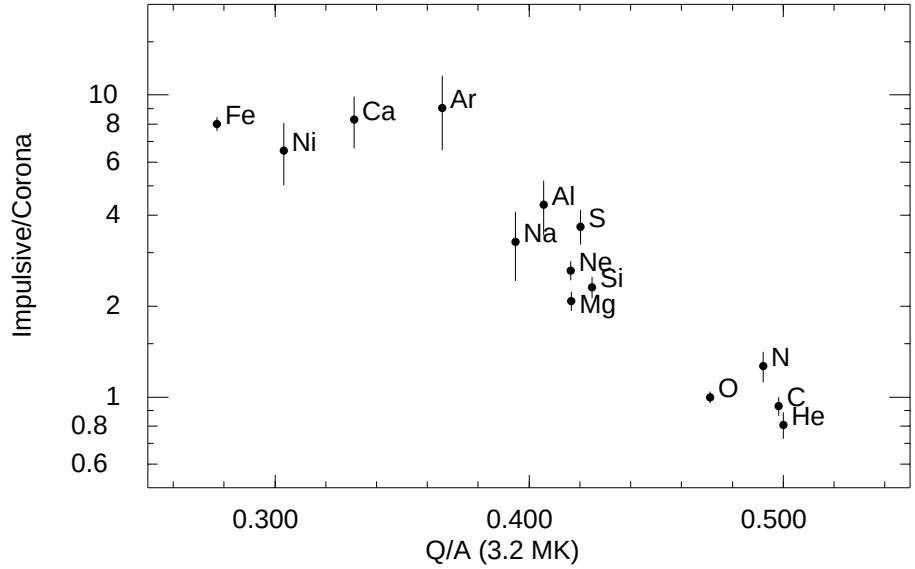

Figure 4.4. Average abundance enhancements in impulsive events, relative to coronal abundances, vs Q/A for a 3.2 MK thermal plasma.

seen by the ions during acceleration. Isotope measurements by Mason et al. (1994) are also consistent with the Q/A dependence shown in Figure 4.4.

4.4. THEORY

Typically, the value of ^{3}He/^{4}He $\sim$1 in these events, compared with $\sim 5 \times 10^{-4}$ in the solar atmosphere or solar wind (Coplan et al., 1984; Bodmer et al., 1995). Yet, despite large variations, H/^{4}He $\sim$20 in these events is not far from the coronal value (Reames, 1994). Since Q/A for ^{3}He lies between the values for H and ^{4}He, it is clear that this pattern of abundances is far beyond the scope of transport models from the flare-myth era. These models had to explain all abundance variations in terms of rigidity- or Q/A-dependent transport from a point-source flare. ^{3}He-rich events must involve acceleration physics that differs greatly from that in gradual SEP events.

The large enhancement of ^{3}He with its gyrofrequency, $\Omega_3 = \frac{2}{3}\,\Omega_{\rm H}$ uniquely situated between those of the dominant species, H and ^{4}He, led to suggestions of selective enhancement by resonant wave absorption in the source plasma. Fisk (1978) proposed the first viable mechanism for selective heating of ^{3}He by absorption of electrostatic ion cyclotron (ESIC) waves produced *above* the ^{4}He gyrofrequency. Here the waves could be resonantly absorbed, heating the rare ^{3}He ions without significant damping. These waves represent electrostatic oscillations of the electrons relative to ions, ^{4}He in this case, in a direction along the magnetic field. Their production requires an enhancement in the electron-ion temperature ratio, T_e/T_i,

and an enhancement in ^{4}He/H to produce ^{4}He- rather than H-cyclotron waves. Fisk suggested that Fe^{+17} would be enhanced by resonance with the same waves through the second harmonic of its gyrofrequency. The wave absorption only causes preferential heating of the ions, not acceleration. However, ions in the tail of the thermal distributions would then be available for stochastic acceleration, for example, to MeV energies (e.g., Möbius et al., 1982).

The narrow resonance of the Fisk (1978) theory made rather specific predictions about which charge states would be selected for each element and these predictions did not agree well with subsequent measurements (Luhn et al., 1987). Also, enhanced ^{4}He/H ratios in the source plasma were more plausible when ^{3}He-rich events were thought to be rare than when they seemed to occur in any solar flare. Recently, attempts have been made to extend ESIC-wave theory in the light of current observations of abundances and ionization states (Zhang, 1995; Zhang and Ohsawa, 1995; Toida and Ohsawa, 1997).

The strong association between ^{3}He-rich events and streaming 10-100 keV electrons (Reames et al., 1985) and type III radio bursts (Reames and Stone, 1986) has been exploited in the theory of Temerin and Roth (1992; Roth and Temerin, 1997). They noted an analogy with electron-beam generated waves that coupled to ions in the Earth's aurora to produce 'ion conics'. Here, downward streaming electrons generate oblique *electromagnetic* ion cyclotron (EMIC) waves that the ions absorbed near their mirror points to produce the conic pitch-angle distribution. In the aurora, electrons, ions and waves can all be observed simultaneously *in situ*. The clear presence of electron beams, shown by the presence of type III radio bursts, for example, suggested that a similar process might occur in solar flares. EMIC waves are produced *below* Ω_H where they can resonate directly with ^{3}He; there are no special requirements for large ^{4}He/H. Furthermore, this is a mechanism for acceleration of ions to MeV energies, not a heating mechanism, so no second process is required. As before, heavy ions can be accelerated as they interact with the waves through the second harmonic of their gyrofrequencies. Roth and Temerin (1997) used extensive plasma simulations to study the mechanism. Following the original work by Temerin and Roth (1992), Miller and Viñas (1993) examined other wave modes that might accompany the EMIC waves. They suggested that heavy ions might be accelerated by shear Alfvén waves produced at the same time. Litvinenko (1996) examined the effects on the observed energy spectra of Coulomb energy losses in the flare.

Large-scale restructuring of the solar magnetic fields during a solar flare might be expected to generate turbulence at long wavelength scales. Large-amplitude, long-wavelength Alfvén waves would then cascade to shorter length scales until they reached the dissipation range and were absorbed by ions of the thermal plasma. Miller and Roberts (1995) studied the stochastic acceleration of protons by cascading Alfvén waves in impulsive solar flares. Wave energy requirements of the model are modest and acceleration time scales are consistent with those obtained from γ-ray observations. As the waves cascade to higher frequency, they interact

with particles of lower energy. Near the end of the cascade, they first encounter ambient ions of the lowest gyrofrequency, namely Fe, and progress toward higher Q/A. Waves not absorbed by Fe, continue to cascade through resonance with Si, Mg, Ne, then O and C, to He and eventually H. Thus, Kolmogorov cascading can lead naturally to the progression of heavy element enhancements seen in impulsive flares (Miller and Reames, 1996).

Miller et al. (1996) and Miller (1997) applied cascading fast-mode waves to the stochastic acceleration of electrons in impulsive flares, providing a consistent model for electrons and ions, except for ^{3}He which is *not* selectively enhanced by cascading waves. An extensive review of the status of various theories of particle acceleration in impulsive flares has been published recently (Miller et al., 1997). Until very recently it was thought that electrons above $\sim$20 keV contained much more energy than protons above $\sim$1 MeV. Recently, however, it has become clear from γ-ray line measurements that the energy content in accelerated electrons and ions is comparable (Ramaty et al., 1996b), 10^{31}–10^{32} ergs in large flares. Proton spectra below $\sim$1 MeV cannot be deduced from measurements of γ-ray lines, but interplanetary spectra suggest that low-energy protons can contribute another factor of 5–10 to the energy content (Reames et al., 1997b).

Steinacker et al., (1997) examined the resonant wave absorption by a hot multi-ion plasma. The strong damping profile of ^{4}He, which they call the 'helium valley', can extend over a wide range of frequencies and affect the wave intensities available for many other species. In fact, ions may be 'enhanced' relative to ^{4}He simply because they lie farther from the bottom of the 'valley'. Of course, a more complete theory should consider wave generation and damping together.

5. CIR-Associated Events

The dipole component of the magnetic field of the Sun is drawn out radially by the solar wind and wound into the well-known Parker (1963) spiral at low latitudes by solar rotation. Between the approximately hemispheric regions of opposite polarity lies the equatorial current sheet (see, e.g., Hoeksema, 1995). The average solar wind speed is lower, $\sim$300 km s^{-1}, at low latitudes above regions of closed loops and coronal streamers, than in the high latitude 'coronal holes', where it can reach $\sim$800 km s^{-1}. The dipole axis is aligned with the rotation axis during solar minimum but tilts and eventually inverts during an 11-year solar cycle. This tilt, as well as more irregular variations, can bring high-speed solar wind from coronal holes down into the ecliptic. As the Sun rotates, high-speed solar wind is then emitted in the same direction as previously-emitted low-speed wind. When a high-speed stream overtakes the low-speed wind, an interaction occurs. The interaction strengthens as we follow this stream interface farther out from the Sun where more and more of the high-speed stream plows into the region. Since this entire pattern corotates with the Sun, it is called a corotating interaction region (CIR). CIRs are

relatively stable structures that can persist for many solar rotations depending, of course, upon the stability and topology of the high-speed stream. The pattern of alternating high- and low-speed streams and related alternation in the magnetic sector structure has been observed for many years (e.g., Belcher and Davis, 1971; Hundhausen, 1972; Burlaga, 1974).

A pair of shock waves form at the edges of CIRs, the forward shock propagates outward into the slow solar wind and the reverse shock propagates inward into the high-speed stream. Occasionally the shocks form at 1 AU but they strengthen with distance as the plane of the interface becomes less radial and more azimuthal. Radial evolution of CIRs was observed out to ∼5 AU on the Pioneer 10 and 11 spacecraft (e.g., Gosling et al., 1976; Hundhausen and Gosling, 1976). Observations showed that particles were accelerated to MeV energies at both shocks (McDonald et al., 1975; Barnes and Simpson, 1976). However, the reverse shock was found to have the highest intensities and hardest spectra, perhaps because of the higher particle injection speeds. Using the observations from the Helios and Pioneer spacecraft, intensities of the energetic particles from CIRs could be studied over a large radial span (Van Hollebeke et al., 1978; Mewaldt et al., 1978). Radial gradients of the MeV protons flowing sunward from the reverse shock through the high-speed stream were 350% AU^{-1} between 0.4 and 1 AU and 100% AU^{-1} from 1 to ∼4 AU.

5.1. THE SPATIAL DISTRIBUTION OF PARTICLES

Fisk and Lee (1980) presented a theory of particle acceleration and transport from a CIR that included the effects of adiabatic cooling of the particles in the expanding solar wind. Assuming the diffusion constant $\kappa = \kappa_0 v R$, depends only upon particle speed v and distance R, they found the distribution function f given by

$$f \propto \left(\frac{R}{R_S}\right)^{2\beta/(1-\beta)+V/(\kappa_0 v)} v^{-3/(1-\beta)} \exp\left(-\frac{6\kappa_0 \beta v}{V(1-\beta)^2}\right) , \tag{5.1}$$

where V is the upstream solar wind speed, R_S is the radial position of the shock, and β is the inverse of the shock compression ratio. The theory was found to be in good agreement with the observations of Gloeckler et al. (1979).

CIRs can appear throughout the solar cycle, but they are most easily studied near solar minimum when they persist for long periods without disruption from CMEs. After intense study of CIRs by a fleet of well positioned spacecraft during solar minimum of the mid 1970s, their study was much less common during the 1980s. However, Richardson et al. (1993) studied a large sample of events during this period, examining anisotropies, abundances, spectra, and spatial distributions using Helios 1, IMP-8, ISEE-3/ICE and Pioneer-Venus Orbiter spacecraft.

Observations during the 1990s were marked by the *Ulysses* mission that explored the high-latitude solar regions, which we discuss below, and a new generation of larger-geometry instrumentation with broad energy coverage on the Wind

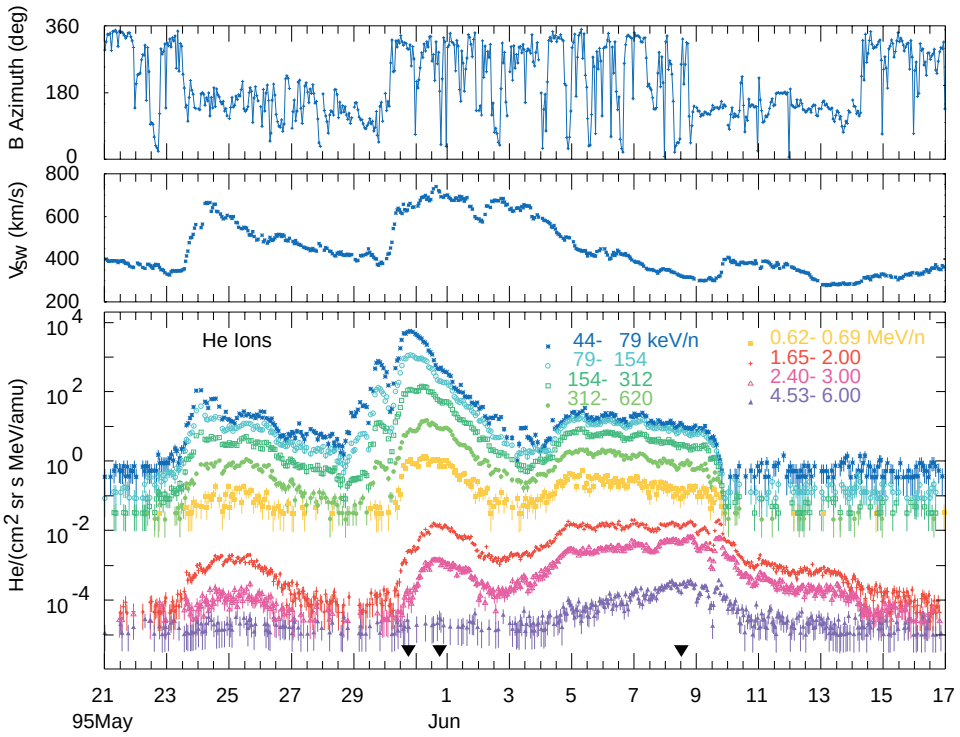

Figure 5.1. Intensity-time profiles for He ions are shown for a 27-day solar rotation in the lower panel, with magnetic azimuth and solar wind speed in the upper panels. A small particle event is associated with the CIR passage on May 24 and an extended event with the CIR on May 30.

spacecraft near Earth. Intensity-time profiles of He ions over a wide span of energy are shown in Figure 5.1 during a 27-day period observed by the Wind spacecraft in 1995 (Reames et al., 1997d). Upper panels in the figure show the magnetic azimuth angle to define the magnetic sector structure and the solar-wind speed that shows the onsets of high-speed streams on May 23 and 30, coincident with sector-boundary crossings. The particle event of May 28–June 14 seen in Figure 5.1 is remarkable because of its long duration, being visible over ∼225° of solar longitude. However, it does illustrate many properties common to CIR-associated events. The small peak in the low-energy ion intensities on May 29 represents ions from the forward shock flowing back to 1 AU, since both shocks form beyond 1 AU. When we cross the stream interface on May 30, we begin to see ions from the reverse shock. Early on, we are connected to the weak shock that is relatively close to us; we see steep spectra and the dominance of low-energy ions. Later, we see spectra harden as the shock strengthens and the low energy ions are affected by the transport over longer distances. Unlike SEP events, particles from the reverse CIR shock show *inverse* velocity dispersion (because of the increasing strength and distance of shock with time); the low energy ions are seen first.

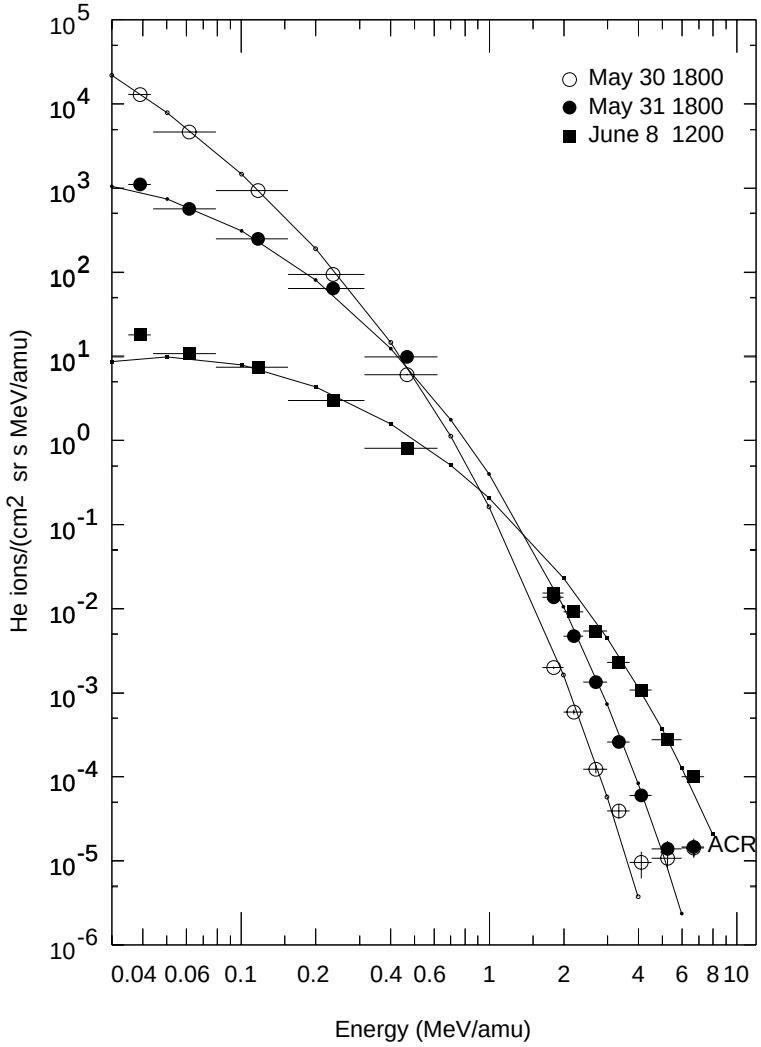

Figure 5.2. Energy spectra of He are shown for the times listed and marked in Figure 5.1. Curves through the spectra are fits from Fisk and Lee (1980) theory.

Energy spectra, at selected times during the 1995 May–June event, are shown in Figure 5.2. The spectra are shown for the times marked along the abscissa in Figure 5.1. Curves through the points in Figure 5.2 are obtained by adjusting the parameters of Equation 5.1 from the theory of Fisk and Lee (1980) using distances of $R_s = 1.2$, 2, and 4 AU at successive times. At the latest time, it is necessary to choose a very large shock compression ratio to obtain the fit (Reames et al., 1997d). This may be because the radial or rigidity dependences of the diffusion constant are not quite correct, or because proton-generated wave growth at the shock, that would flatten the spectra escaping the shock, has been neglected in the

theory. Nevertheless, theoretical fits, using equilibrium theory, seem more suitable for these quiescent CIR events than for the dynamic SEP events. Historically there has been some argument whether CIR spectra are exponential or power-law in character. With the large energy range in Figure 5.2, both the exponential and power-law factors in the Fisk-Lee theory contribute. However, a need for nonphysical shock-compression ratios and the excessive spectral rollover predicted at the lowest energies, suggest that the theory does need to be improved.

5.2. CROSS-FIELD PARTICLE TRANSPORT

In a recent study of particle angular distributions in CIR events on the Wind spacecraft near 1 AU, Dwyer et al., (1997a) found large values of the ratio of perpendicular to parallel diffusion constants, $\kappa_\perp/\kappa_\parallel$. Values of $\kappa_\perp/\kappa_\parallel = 1.47 \pm 0.07$, 0.13 ± 0.02, and 0.45 ± 0.02 occurred for several hours near peak intensity of the 80–154 keV amu^{-1} He ions in three large events, including the 1995 May 30 event we showed in Figure 5.1. The particles in the events with the largest $\kappa_\perp/\kappa_\parallel$ were found to be streaming sunward, away from the shock, independent of the magnetic field direction. The time variation of $\kappa_\perp/\kappa_\parallel$ that Dwyer et al. (1997a) found in the 1995 May 30 event is shown in Figure 5.3. Cross-field diffusion is high during the intensity maximum but is quite small at other times. Turbulence related to the interaction region, or Alfvén waves in the high-speed stream (Belcher and Davis, 1971), have been suggested as possible sources of the scattering.

However, it seems much more likely that the localized region of large $\kappa_\perp$ results from particle-generated waves restricted to those regions with high particle intensities. Such wave generation by energetic ions at CIRs has been overlooked previously in the literature. Peak proton intensities near 100 keV reach $\sim 2 \times 10^4$ (cm^2 sr s MeV)$^{-1}$ in the CIR events studied by Dwyer et al. (1997a) and are comparable with those at shock passage in moderately large ESP events. Values of $\kappa_\perp/\kappa_\parallel \sim 1$ may mean that wave activity is so intense that scattering is likely to occur within a single gyroperiod. The longer lifetime of the CIR shocks may also compensate for somewhat lower wave-growth rates. Several AU from the Sun, the CIR shocks are highly quasi-perpendicular. In this regime, self-generated waves could provide enough cross-field diffusion to keep low-energy ions from being swept downstream. Wave generation also produces flattened upstream spectra, relaxing the need for hard shock spectra to fit the energy spectra observed at late times (Reames et al., 1997d). That is, the spectra may be flattened at low energies by wave modulation (Lee, 1983) in addition to adiabatic deceleration (Fisk and Lee, 1980). Inclusion of proton-generated waves at the shock would decouple the turbulence involved in acceleration at the shock from that controlling transport over large radial distances, especially at low energies.

For comparison, Dwyer et al. (1997a) also examined a period during an SEP event and found no cross-field flow. However, intensities were lower during that period and it was not a time near shock passage.

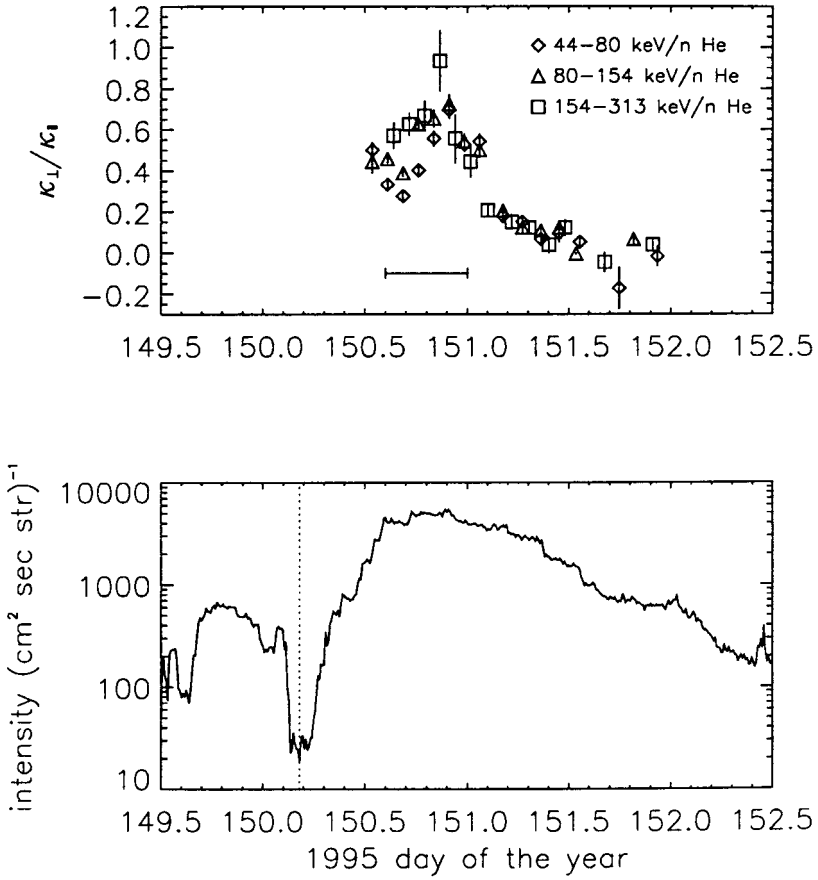

Figure 5.3. Variation of $\kappa_\perp/\kappa_\parallel$ and the 40–600 keV amu^{-1} He intensity with time during the 1995 May 30 CIR event shown in Figure 5.1. At peak intensity, the ions stream sunward away from the shock in the solar wind frame, almost independently of the magnetic field direction (after Dwyer et al., 1997a).

5.3. ENERGETIC IONS AT HIGH LATITUDES

A new perspective on CIRs was gained by the passage of the *Ulysses* spacecraft over the poles of the Sun. CIRs would be expected to disappear at high latitudes where the solar wind becomes uniformly fast. Gosling et al. (1995b) found that the forward shocks are not seen above 26° and reverse shocks disappear above 42° solar latitude, in agreement with a global tilted-dipole solar-wind model (e.g., Pizzo, 1991, 1994). However, the energetic particle observations (e.g., Simnett et al., 1995; Roelof et al., 1997) continued to show recurrent particle increases up to much higher latitudes.

Fisk (1996a) suggested a model for the behavior of the polar magnetic field geometry that would allow particles accelerated at lower latitudes to be seen on

field lines that had migrated to high latitude. The key lay in the model of solar rotation developed by Wang and Sheeley (1993). The polar coronal holes, from which the solar wind expands nonradially, rotate nearly rigidly and do not participate in the latitude-dependent differential rotation of the solar photospheric magnetic fields. Thus, a field line at low heliographic latitude can be carried out radially by the local solar wind to intercept a CIR. Meanwhile, the footpoint of that same field line rotates to high heliographic latitudes where the solar wind carries it to the high latitudes observed by Ulysses. This model allows high-latitude field lines to thread low-latitude CIRs. Zurbuchen et al. (1997) showed the time variations of the high-latitude magnetic field observed on Ulysses were in agreement with Fisk (1996) theory. A unique 20-day periodicity of the field, predicted by the theory, was also observed.

An alternative explanation of the high-latitude particles from CIRs was given by Kóta and Jokipii (1998). Using cross-field transport with $\kappa_\perp/\kappa_\parallel = 0.05$, they find results from their 3-dimensional anisotropic-diffusion model of the heliosphere that agree with the observations. Here the particle transport to high latitudes presumably comes from random walk of the magnetic field lines (Jokipii and Parker, 1968) rather than from systematic migration of those field lines found in the Fisk (1996) model. Jokipii et al. (1995) studied magnetic field fluctuations in the heliospheric polar regions (see also Smith et al., 1995) in order to estimate $\kappa_\perp$. However, in Section 8.1 we examine the long history of difficulty in relating measured magnetic field fluctuations to particle transport.

5.4. ABUNDANCES

Very early in their study, it became clear to observers that element abundances of energetic particles in CIR events were different from those in SEP events (McGuire et al., 1978; Hamilton et al., 1979; Scholer et al., 1979). In particular, both He/O and C/O were about a factor of 2 higher than in SEP events. H/He associated with the reverse shock was $\sim$15–20, somewhat lower than in SEP events, but the forward shock showed higher values. In the next decade, abundances were measured near 1 AU for a large sample of events and the abundance enhancements were plotted as a function of FIP for the first time (Reames et al., 1991; Richardson et al., 1993). Nearly all of the MeV ions measured at 1 AU are those accelerated from the high-speed stream at the distant reverse shock. Their abundances represent those of the high-speed stream and the coronal hole, in contrast to SEP abundances that are coronal in origin. The CIR abundances show a weaker dependence on FIP than SEP abundances, with low-FIP elements enhanced by only a factor of about 2 relative to high-FIP elements. In general, the abundances of energetic CIR and SEP ions correspond to those seen directly in the high- and low-speed solar wind (Geiss et al., 1995), respectively. In the solar wind, differences between high- and low-speed regions are clearly delineated by changes in Mg/O and Fe/O, which measure the amplitude of the FIP effect. The stream interface seems to form an effective

barrier to mixing of energetic particles from the high- and low-speed solar wind in the CIR (Intrilligator and Siscoe, 1994). We compare the FIP dependence of these averaged abundances in Section 9.

The higher abundances of H and especially He in the ions accelerated at the reverse shock may come from the preferential acceleration of interstellar pickup ions injected at higher speed where the shock is several AU from the Sun. These pickup ions will be discussed in the next section in connection with ACRs. However, pickup of interstellar H and He continues deep into the heliosphere where these pickup ions have been observed directly in the solar wind, even near 1 AU (Möbius et al., 1985; Gloeckler et al., 1993; Geiss et al., 1994). It is therefore quite likely that these ions are preferentially accelerated at the reverse shock because of their high injection speed compared with ions of the solar wind. Pickup H and He could provide as much as $\sim$50% of those species observed in the energetic particles. Evidently, pickup O does not contribute significantly since C/O is unusually high in ions from the reverse shock. Elements such as Mg, Si, and Fe are abundant in the energetic particles at CIRs but are insignificant as pickup ions.

One might expect event-to-event variations in abundances in CIR events similar to those seen in SEP events. However, systematic Q/A-dependent variations are less evident in CIRs, although the statistics are more limited (Richardson et al., 1993). One of the unique features of the CIR abundances is the C/O ratio. Richardson et al. (1993) observed that near 2 MeV amu^{-1} the ratio depends rather strongly on the speed of the high-speed stream. Recently, Mason et al. (1997) confirmed the variation in the C/O abundances at 150 keV amu^{-1}. The dependence of C/O on stream speed is shown in Figure 5.4. A similar dependence on stream speed was seen in He/O near 2 MeV amu^{-1} and in Ne/O near 150 keV amu^{-1}, suggesting an energy dependence in these ratios. Perhaps the dependence of these abundances on stream speed is actually a dependence on shock strength. However, it is important to note that some isotopic abundances in the solar wind itself are observed to depend upon the solar-wind speed (Kallenbach et al., 1998).

Geiss et al., (1995) have found an 'inner source' of C^+ pickup ions in the heliosphere within a few AU of the Sun. They believe that these ions come from evaporation of interstellar grains near the Sun. Because of their higher injection speed, pickup ions from this source would be preferentially accelerated at the CIR shocks. However, total pickup C^+/O^+ does not exceed 0.3 at any location, so it is difficult to see why this source would produce C/O $\sim$1 in the accelerated ions.

6. The Anomalous Cosmic Rays

Studies of the quiet-time spectra of ions in the region 10–50 MeV amu^{-1} (Garcia-Munoz et al., 1973, 1975; McDonald et al., 1974) found a population of particles with anomalous abundances and spectra. The ions had O/C $>$ 20 and He/O $\sim$1. The energy spectrum of the 'anomalous O' was steeper than that of the galactic

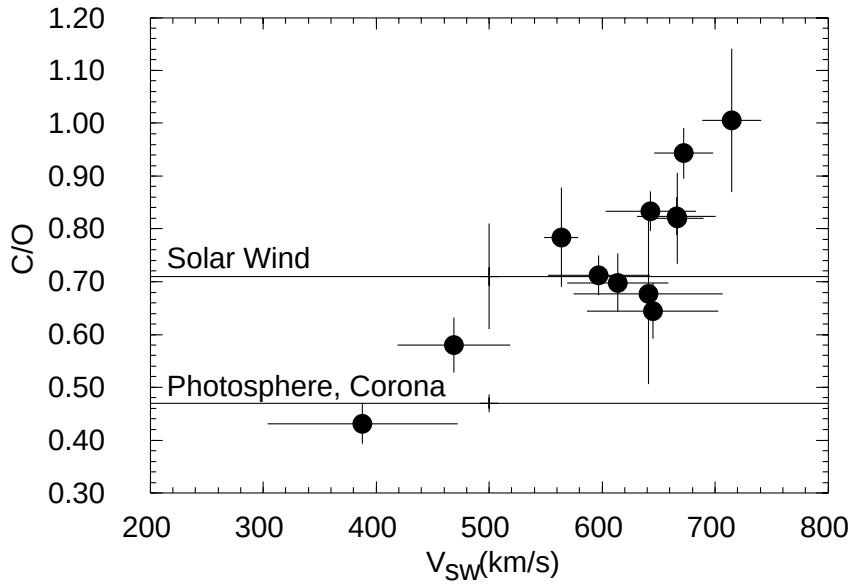

Figure 5.4. Dependence of the C/O abundance ratio for energetic ions on the maximum stream speed (data from Mason et al., 1997).

cosmic rays. The anomalous cosmic rays (ACRs), then thought to consist of He, N, O, and Ne, were observed to be modulated in phase with the GCRs during the solar cycle. In fact, they completely disappeared from view during solar maxima and their reappearance is still welcomed in each new decade (e.g., Hasebe et al., 1994; Fujii and McDonald, 1999).

Shortly after the discovery of ACRs, Fisk, Kozlovsky, and Ramaty (1974) proposed a model for their origin that explained the anomalous abundances. They suggested that in interstellar material, just outside the heliosphere, elements with FIP below that of H, at 13.6 eV, would be ionized while those of high FIP, like He, N, O, and Ne, would be neutral. This presumably occurs because interstellar H can absorb and remove all photons above 13.6 eV, but not those at lower energies. As the solar system moves through the interstellar medium, neutral atoms easily flow into the heliospheric cavity, but ions are effectively excluded by the magnetic fields. When the neutral atoms approach the Sun, they are photoionized and 'picked up' by the magnetic fields, which they suddenly 'feel'. Neutral H can also be ionized and picked up by charge exchange with H ions of the solar wind (see detailed models for H, e.g., Zank and Pauls, 1996). The distribution function of the pickup ions is flat out to twice the solar wind speed. The singly ionized pickup ions are convected out to the heliospheric termination shock where they are preferentially accelerated (Pesses et al., 1981; Fisk, 1996b; Lee, 1996). After acceleration, the ions are modulated as they propagate back, against the flow of the solar wind, to the inner heliosphere where they are observed.

In the solar wind, singly ionized pickup He^+ was first observed by Möbius et al. (1985) at 1 AU. Other pickup ions, such as H^+, N^+, O^+, and Ne^+ have been observed more recently (Gloeckler et al., 1993; Geiss et al., 1994) at larger heliocentric distances. These pickup ions were predicted from the ACR observations 20 years before they were actually observed. For the ACRs, O was first shown to be singly charged by Adams et al. (1991). In recent years the ionization states of the ACRs have been measured extensively on the SAMPEX spacecraft (see review by Klecker et al., 1995 and references therein). No sooner was it confirmed that most of the ACR ions were singly ionized, than a component of doubly ionized ACR ions was found at high energies (Mewaldt et al., 1996). These ions are presumably produced by stripping of the energetic ions during acceleration at the termination shock, providing an estimate of the acceleration time found to be a few years.

In Figure 6.1 we show low-energy quiet-time spectra at 1 AU for several elements measured during the 1996 solar minimum by Reames (1999; see also Hasebe et al., 1997; Reames et al., 1997; Takashima et al., 1997). Strict criteria have been imposed to eliminate any contribution to these spectra from SEP or CIR sources. With high-sensitivity measurements, we not only see the classical ACR elements, He, N, O, and Ne, but we also add the rarer high-FIP element Ar. In addition, however, we also begin to see increases in the low-FIP elements, especially S, but also Mg and Si. These measurements show flat spectra for C and Fe; Klecker et al. (1997) have found that all of the C at low energies is multiply charged. The low-energy component of species such as Fe might represent ambient solar wind ions, from the tail of the thermal distribution function, that are also accelerated at the termination shock. Elements such as Mg, Si, and S might represent low levels of interstellar neutrals, or, in the case of S, might be from volcanism on the Jovian moon Io.

A recent measurement of isotopic abundances in the ACRs (Leske et al., 1996) has shown them to be similar to solar system abundances, in particular $^{22}Ne/^{20}Ne \sim 0.1$. Since this is a measure of the abundances of the interstellar medium, it has greater significance for GCRs than for ACRs. The high value of this ratio in the GCR source, where $^{22}Ne/^{20}Ne \sim 0.4$, suggests that they cannot simply be accelerated from material like the local interstellar medium.

In the first model for shock-acceleration of the ACRs, Pesses et al. (1981) suggested that acceleration occurred primarily in the polar regions where the solar wind speed, and hence the speed of the quasi-parallel termination shock, are highest. More recently, Jokipii (1990) discussed shock-drift acceleration as particles are transported from equator to poles, or conversely, depending on the phase of the solar cycle. Once the particles drift through the maximum $\mathbf{V} \times \mathbf{B}$ potential at the shock, their energy spectrum steepens, but since the maximum energy depends upon charge, multiply ionized particles appear at the highest energies (Jokipii, 1996). Of course, the acceleration time increases with energy, leading to a higher probability of stripping.

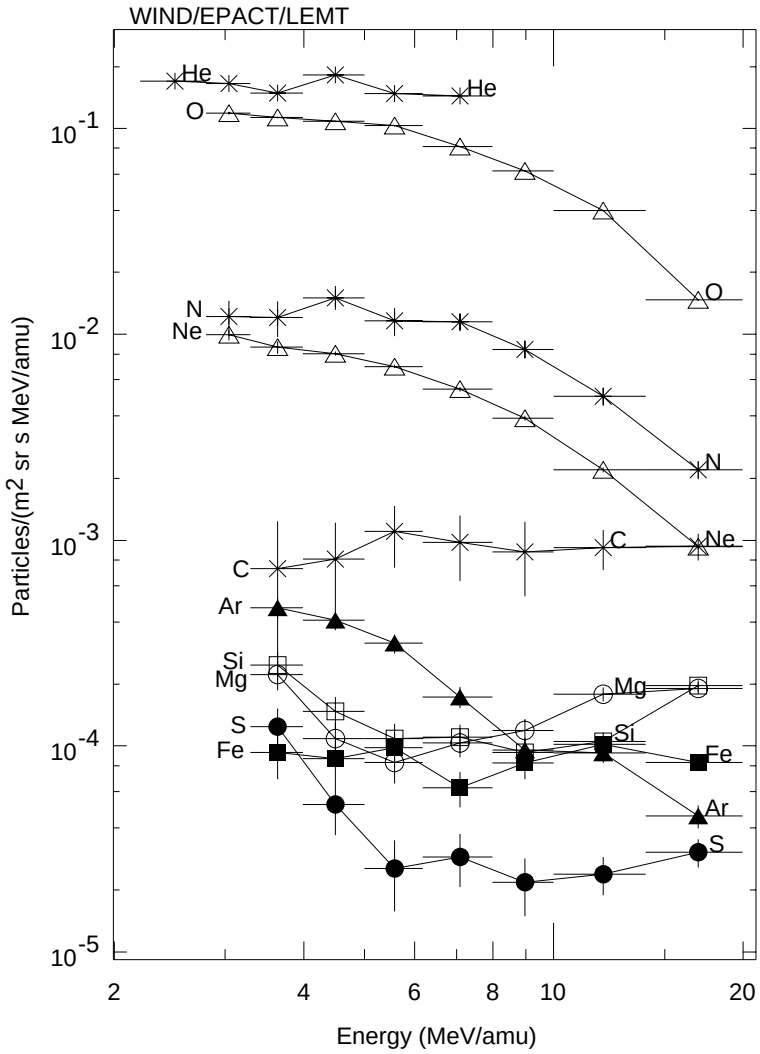

Figure 6.1. Quiet-time energy spectra of elements show low-energy increases due to ACRs for He, N, O, Ne, Mg, Si, S, and Ar, but no clear increase for C or Fe.

Giacalone et al. (1997) have suggested that ions accelerated at the termination shock to produce ACRs may be pre-accelerated at CIRs in the outer heliosphere. However, the element abundances in ACRs are drastically different from those measured at CIRs, especially C/O. In addition, low-FIP ions like Fe are suppressed by factor of ∼100, relative to O, in ACRs, but are FIP-enhanced at CIRs (see Section 9). *A priori*, it is possible that the relative acceleration of pickup ions at CIRs increases at large heliocentric distances. However, CIR shocks weaken and dissipate in the distant heliosphere and energetic-particle intensities soon decline

to the point that ion abundances can no longer be measured. Hence, there is no evidence of a component with altered abundances that is associated with CIRs.

An alternative approach has been taken by Ellison et al. (1999). These authors have performed Monte Carlo calculations of acceleration at the termination shock that are similar to those described for the Earth's bow shock and for interplanetary shocks. By assuming that the scattering mean free path, λ, is 5–10 times the particle gyroradius, the authors find they can easily accelerate pickup ions directly, without pre-acceleration, a problem for the competing models. While the authors treat λ as a free parameter, it is likely that the small values represent the presence of proton-generated waves. Such waves may also increase $\kappa_\perp/\kappa_\parallel$ to 0.1–0.2 or more near the shock, making it easier for ions to scatter back to the quasi-perpendicular shock from downstream.

Correctly accounting for solar modulation of the ACRs as they are transported inward from the termination shock and distinguishing the effects of acceleration and modulation is a difficult task. It is best to consider modulation of ACRs and GCRs together in a single model. However, a complete discussion of such models would be extensive and is beyond the scope of this paper (see Fisk, 1999; Moraal et al., 1999). While it is generally believed that drift along the neutral sheet can be a major route of access to the inner heliosphere, diffusive transport, both parallel and perpendicular to the field, is usually invoked for specific calculation of spectra and abundances. In fact, the rigidity dependence of the transport coefficients is usually chosen to fit the observations (e.g., Cummings and Stone, 1996) as was once done for SEP events. The rigidity dependence of the spectra at the shock and of the transport may only become independently resolved when spacecraft actually cross the termination shock. Even then, the variations over the entire shock surface may be difficult to determine.

7. Planetary Sources of Energetic Particles

Planets, and their interaction with the interplanetary medium, can be a rich source of energetic particles. In general, there are three distinct regions where energetic particles can be found. First, there are planetary bow shocks. Second, there are inner magnetospheres where particles can be stably trapped in well-defined radiation belts. Finally, there are the dynamic regions of the outer magnetospheres, magnetosheaths, and magnetotails that are buffeted by the external force of the varying solar wind and the magnetic structures it contains.

Generally, magnetospheric physics is well beyond the scope of this review, especially the dynamic outer regions where a comprehensive modeling of the magnetic evolution and plasma flows is required to understand the particle acceleration that occurs. However, it is appropriate to mention some of the magnetospheric populations of energetic particles, their abundances, and their origins. We will focus on planetary bow shocks, that are relevant to other shocks we have considered,

and on trapped radiation, where the particle origins are often as simple as they are surprising.

This is not to suggest that the polar and outer regions of the magnetosphere are irrelevant or less interesting, only that they are too extensive to cover here. In fact, we have already mentioned the 'ion conics' produced in the aurorae when EMIC waves generated by precipitating electron beams couple to accelerate ions near their mirror points (Roth and Temerin, 1997). This mechanism was the model for the process in impulsive flares that produces solar ^{3}He-rich events. If He isotopes were present in the auroral region, ^{3}He-rich events might have been seen there! This mechanism works in a region of high magnetic field and low plasma β, the ratio of magnetic to thermal energy (for a review of auroral acceleration see Shelly, 1995).

7.1. PLANETARY BOW SHOCKS

The Earth's bow shock provides a stable structure where energetic particles and the spectrum of their self-generated waves can be studied together with the properties of the shock (Gosling et al., 1979; Paschmann et al., 1981; Hoppe et al., 1981; Eichler, 1981; Lee, 1982, 1992; Scholer, 1992). Typically, as the solar wind flows into the shock, magnetic flux tubes at the nominal spiral direction first encounter a quasi-perpendicular shock on the dusk side of the Earth. They are then convected across to the quasi-parallel region on the dawn side. From particle angular distributions, it is possible to distinguish ions that have undergone a single reflection from the shock from those that have undergone multiple traversals resulting in acceleration (e.g., Paschmann et al., 1981). As the field line first contacts the shock, a reflected beam of ions is seen upstream of the quasi-perpendicular shock, streaming back along the magnetic field. Next, resonant waves generated by this beam are seen (Hoppe et al., 1981) and the distribution of back-streaming ions begins to broaden from interaction with the waves. Finally, a diffusive region occurs with a nearly isotropic distribution of particles extending to $\sim$100 keV (e.g., Paschmann et al., 1981) and a related complex pattern of wave packets (Hoppe et al., 1981).

Upstream waves have been observed in association with bow shocks at Venus, Earth, Jupiter, Saturn, Uranus, and Neptune (Moses et al., 1990; Russell et al., 1990; see also Lee, 1992). The dominant frequencies of these waves scale with $|\mathbf{B}|$ as expected for doppler-shifted waves generated by particles streaming at about $2V_{SW}$, as is the case at Earth. Upstream accelerated particles and waves have been observed together at Jupiter (Baker et al., 1984) and at Venus (Williams et al., 1991).

Acceleration at the Earth's bow shock was studied theoretically by Lee (1982). Wave generation by the particles was included in this model, as it was in the interplanetary shock model (Lee, 1983) discussed previously. The principal difference for the bow shock is the shorter acceleration time as field lines are rapidly convected past the shock with a time scale of $\sim$10 min. Monte Carlo simulations of the

particle acceleration have been preformed more recently (e.g., Ellison et al., 1990; Scholer, 1992). Ions that undergo 1, 2, 3, *etc*. traversals of the shock contribute to increasingly high energies in the spectrum. These simulations do not explicitly include wave generation. However, the use of a short scattering mean free path, λ, of only a few gyroradii, presumes the presence of significant wave growth. These small values of λ are required for acceleration of particles directly from the solar wind. Unfortunately, no spatial dependence is assumed for λ in the Monte Carlo calculations; one would expect small values of λ to exist only near the shock, as found by Lee (1982).

Energetic particles from the bow shock are seen as 'upstream events' by a spacecraft sunward of Earth. These are high-intensity bursts of particles in the 10 $-$100 keV amu^{-1} region that occur when the magnetic field is directed so as to intercept the bow shock. The occurrence of upstream events is more likely during high-speed solar-wind streams, when the shock speed is highest relative to the upstream solar wind. Ion abundances have recently been measured in these events and usually they are similar to the abundances in the high-speed solar wind (Mason et al., 1996). In one case, an upstream event occurred during a solar ^{3}He-rich event; the ions in the intense upstream event were also ^{3}He rich (Dwyer et al., 1997b). These new abundance observations should end the old controversy on whether the upstream ions are shock accelerated or leak from the magnetosphere as suggested earlier by Sarris et al. (1976), for example.

7.2. TRAPPED RADIATION

The inner Van Allan radiation belts around the Earth consists almost entirely of protons and electrons. These particles come from the cosmic ray albedo neutron decay (CRAND) source (Singer, 1958; Hess, 1959; Freden and White, 1960; Lenchek and Singer, 1963; Lingenfelter, 1963). Neutrons, produced in nuclear interactions of galactic cosmic rays with nuclei of the atmosphere, can be projected upward into the closed magnetic field region. These neutrons decay in magnetic regions where the protons and electrons can be stably trapped (e.g., Northrop, 1963). The spectrum of trapped protons typically decreases almost inversely with energy from $\sim$1 MeV to $\sim$1 GeV, being flattened somewhat at low energies by increased energy losses. A similar process also provides particles for the electron and proton radiation belts of planets such as Jupiter and Saturn, although, Saturn's rings provide an additional source of CRAND neutrons (e.g., Cooper, 1983; Schardt and McDonald, 1983). Absorption of particles by the rings and moons of Jupiter, Saturn, Uranus, and Neptune cuts swaths through their radiation belts (e.g., Van Allan et al., 1975; McDonald et al., 1980; Simpson et al., 1980; Stone et al., 1986, 1989; Krimigis et al., 1986, 1989).

When spacecraft entered the Jovian magnetosphere they found a region $\sim$5–20 R_J where the abundances of the elements at $\sim$1–10 MeV amu^{-1} were completely dominated by S and O (e.g., Gehrels et al., 1981; Gehrels and Stone, 1983).

The origin of these unusual abundances was traced to gasses, like the abundant SO_2, emitted into space from volcanoes on the Jovian moon Io. This gas is dissociated, ionized, and accelerated in the Jovian magnetosphere to produce the energetic particle population dominated by S and O. Here is another beautiful case where abundances of energetic particles contain the information needed to identity the particle source.

More recently, a new radiation belt has been found at Earth by Grigarov et al., (1991; see also Selesnick et al., 1995) that consists of the same high-FIP elements found in the ACRs. Existence of this radiation belt had been predicted by Blake and Friesen (1977). Singly ionized ACR ions have a high rigidity and can penetrate rather deeply into the magnetosphere. If these ions encounter the upper atmosphere, they may suffer atomic collisions that lead to their ionization in regions where they become stably trapped because of the sudden reduction in their A/Q and magnetic rigidity. Thus, a radiation belt of interstellar N, O and Ne coexists with the classical Van Allan proton and electron belts produced by the CRAND process.

It is also possible to form temporary radiation belts during large SEP events when the associated CME and shock strike the Earth (e.g., Blake et al., 1992). The large perturbation in the magnetosphere allows sudden trapping of SEP ions and electrons that have filled the outer magnetosphere (see Hudson et al., 1997, 1998). As the particles are transported to inner shells (e.g., $L = 2$) they are energized with conservation of their first adiabatic invariant (see, e.g., Northrop, 1963). These new radiation belts can last for a period of months. While observations in these belts have been confined to protons and electrons, it seems safe to predict that SEP-like abundances will actually be present.

8. Acceleration and Transport

It is appropriate to consider particle acceleration and transport together because history suggests that they are often difficult to distinguish in the observations. For example, spatial distributions of energetic ions can result from a spatially extended source or from transport from a compact source. With a single-point measurement, it is virtually impossible to distinguish spatial and temporal variations; comparing the full intensity-time profiles using multi-spacecraft observations has been essential in these cases.

8.1. TRANSPORT

Among the greatest harm done by the solar flare myth was the distortion of transport models to fit features caused by other mechanisms. Not only did we misidentify the sources but we also spoiled our view of particle transport in the inner heliosphere. The flare myth has now received attention in the community and the importance of acceleration at CME-driven shocks has gained acceptance. However,

the effects of the flare myth on transport are more insidious and the errors continue to live on.

The classic work of the previous era was the Palmer (1982) 'consensus' on diffusion constants, especially on the parallel scattering mean free path, $\lambda_\parallel$, in the inner solar system. The Palmer review compiled information from several sources, and prominently considered 'scatter-free electron events', namely, electrons from impulsive flares. However, most of the measurements were based upon gradual SEP events. An important finding of the consensus was that $\lambda_\parallel \sim 0.08-0.3$ AU, was independent of rigidity.

The long slow decay of gradual SEP events from western sources has continued to entice those who attempt to fit diffusion theory. From Figure 3.4, showing intensity-time profiles vs longitude, we might conclude that only about $\frac{1}{3}$ of gradual events, namely those at western longitudes, had decreasing time profiles, while $\frac{2}{3}$ had flat or rising time profiles. These profiles result from continuing effects of the shock late in the events. However, events with eastern and central sources were simply discarded because they were 'not diffusive'. At the same time, the very steep decays of the impulsive events (see Figure 2.2b) could not be fit by standard diffusion theory because the particles continued to stream and the pitch-angle distributions did not relax to first-order anisotropy. These particles do not scatter enough to obey the Fokker–Planck equation (Jokipii and Parker, 1970; Forman et al., 1986). Eastern and central events were too flat, impulsive events were too steep, but western gradual events were 'just right'. This extraordinarily biased selection of events continually reconfirmed the small values of $\lambda_\parallel$. Of course, the identical slow decay at all energies in western gradual events, like that shown in Figure 3.6, actually results from magnetic trapping, *not* from slow transport with *identical* values of $\lambda_\parallel$ over orders of magnitude in energy.

Ironically, while much of the community focused on diffusive models with strong scattering, Roelof and Krimigis (1973) explained their observations below 1 MeV in terms of scatter-free transport and long acceleration time scales. It would be over 20 years before it became clear that weak interplanetary scattering also applied at arbitrarily high energies. Strong scattering is limited to regions near intense sources where there are proton-generated waves.

However, one of the defining moments in the author's education about particle transport came when Mason et al. (1989) published the intensity-time profiles shown in Figure 8.1. Here, during the long slow decay from a gradual SEP event, one sees the fast profile of an impulsive (^{3}He-rich) SEP event. Surely, the interplanetary medium cannot distinguish particles of the same species from different events and scatter them differently. It seems much more likely that the time profile of the gradual event has little to do with transport, but reflects continued acceleration followed by filling of leaky magnetic structures, all with minimal scattering. Even when $\lambda_\parallel \sim 1$ AU, 1 MeV protons traveling $\sim$1 AU hr^{-1} will behave diffusively after they traverse several scattering mean free paths in several hours.

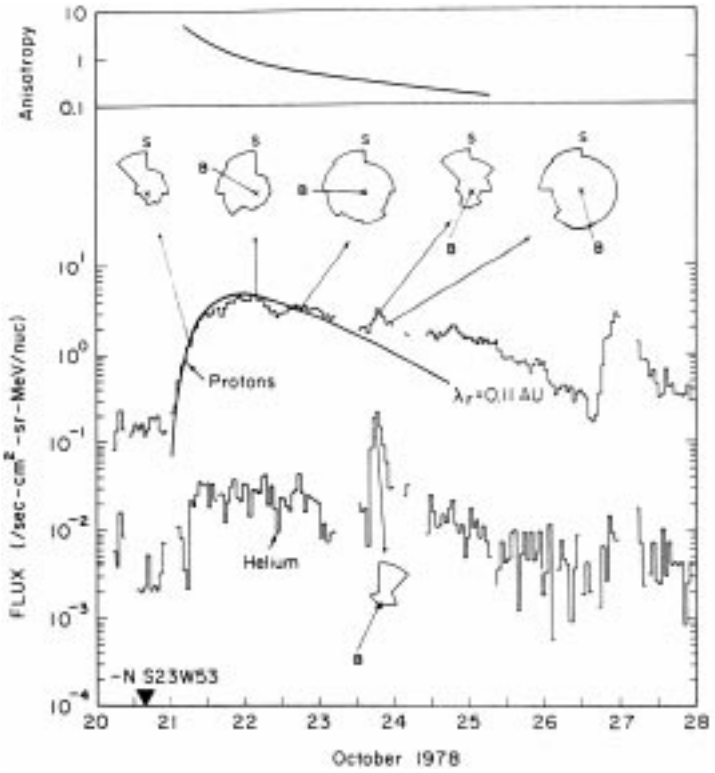

Figure 8.1. Particle anisotropies and intensities of 0.6–1.0 MeV amu^{-1} H and He vs time during a small gradual SEP event of 1978 October 20–25 and an impulsive ^{3}He-rich event on October 23. If the gradual decay is caused by scattering, how does the interplanetary medium know how to scatter the particles from the gradual event but not those from the impulsive event? (After Mason et al., 1989).

However, particles from a new impulsive injection will rapidly stream through the background distribution before they have time to scatter.

Impulsive SEP events provide the best information on the typical impulse response of the interplanetary medium (Earl, 1981, 1987; Mason et al., 1989). A fit for a typical event using the Boltzman equation to follow the particle transport in space, time, and pitch angle, is shown in Figure 8.2 (Mason et al., 1989). Such fits typically give $\lambda_\parallel \sim 0.5$ to 2 AU. New measurements of the interplanetary scattering mean free path have recently been made from observations of interstellar pickup ions (Gloeckler et al., 1995; Fisk et al., 1997; Möbius et al., 1998). These measurements give $\lambda_\parallel \sim 1$ AU at extremely low rigidities. Combining the electron and ion measurements from impulsive flares and the results from pickup ions, we find a rigidity-independent value of $\lambda_\parallel \sim 1$ AU from $\sim$1–100 MV. Again it is approximately constant, but at a new value that is about one order of magnitude larger than that found by Palmer (1982).

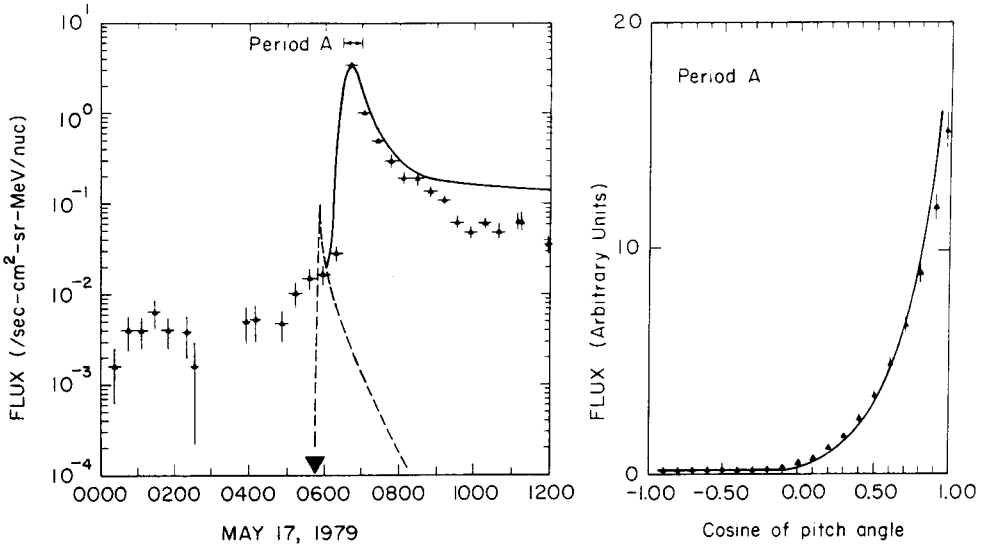

Figure 8.2. Fits to the intensity vs time and pitch angle distributions during an impulsive event are shown using the Boltzman equation (after Mason et al., 1989).

In principle, it is possible to derive the scattering parameters using QLT from direct observation of the spectrum of magnetic turbulence. However, it has been well known for many years (e.g., Fisk, 1979) that that process gives values of $\lambda_{\parallel} \sim 0.01$ AU, much smaller than the value of $\lambda_{\parallel}$ that the energetic particles see. When detailed comparisons are made with observations of impulsive events the discrepancy is striking (e.g., Tan and Mason, 1993). This is sometimes described as a 'failure' of QLT but it may be more correctly described as our inability to measure those fluctuations that affect a particle moving along the field. In part, it occurs because magnetometers on a single spacecraft cannot resolve spatial and temporal variations in the field. Tangential discontinuities or variations in $|\mathbf{B}|$ convected obliquely across the spacecraft contribute to the magnetic turbulence spectrum but are not seen by energetic particles. Tu and Marsch (1993; see also Matthaeus et al., 1990; Ghosh et al., 1998) described magnetic fluctuations as Alfvén waves plus convective spatial structures. Unfortunately, however, recent papers that treat the particle scattering in this environment theoretically (e.g., Bieber et al., 1994) are wedded to the old Palmer (1982) 'consensus' and still attempt to determine $\lambda_{\parallel}$ from gradual SEP events.

In fact, gradual SEP events are quite consistent with the assumption of $\lambda_{\parallel} \sim 1$ AU. Mason et al. (1991) re-fit intensity and anisotropy measurements in several events using $\lambda_{\parallel} = 0.8$ AU that were observed by spacecraft at different radial distances. For these events, one could adjust the injection profiles to fit the observed profiles at Helios at 0.6 AU, and then follow the evolution out to Voyager at 1.5 AU, for example. Those events had previously been fit with $\lambda_{\parallel} = 0.05–0.1$ (Beeck et al., 1987). It is possible to adjust the injection time profile to compensate for

changes of $\lambda_{\parallel}$ over a very wide range. One might expect anisotropy measurements to distinguish these different parameters, but in practice they do not. Observed particle anisotropies are most sensitive to *local* scattering conditions and not to conditions between the observer and the Sun.

Many of the effects we once attempted to explain in terms of interplanetary transport we now understand in terms of particle transport through self-generated waves near the shock. Only self-generated waves explain the transport properties that change rapidly with space, with time, and with proton intensity during an event. Systematic abundance variations and localized increases in $\kappa_{\perp}/\kappa_{\parallel}$ depend upon wave generation near shocks. In fact, $\kappa_{\perp}/\kappa_{\parallel} \sim 1$ may be taken as evidence that the scattering mean free path is comparable with the gyroradius near shocks. This would actually violate the assumptions of QLT locally.

Rigidity-dependent transport occurs because the resonant wave spectrum is derived from an intense, decreasing power-law proton spectrum. Most of the protons are at low rigidity so most of the resonant waves scatter low-rigidity protons and ions. Small gradual SEP events like that of 1995 October 20 (Reames et al., 1997a) show power-law spectra and minimal abundance variation while larger events like that of 1998 April 20 show the large spectral and abundance variations we have discussed. The rigidity dependence comes from proton-intensity-dependent waves generated locally near the shock, not from ambient waves distributed through the interplanetary medium. Otherwise, impulsive SEP events and pickup ions tell us that there is no evidence of rigidity dependence in the transport of $<$100 MV ions in the undisturbed interplanetary medium inside $\sim$5 AU.

Particle transport in the outer heliosphere seems to be a complex mixture of drift along neutral sheets and scattering along and across magnetic fields with the usual assumption that $\kappa_{\perp}/\kappa_{\parallel} \sim 0.1$. Need for a charge sign dependent transport is clear from comparisons of GCR electron/proton modulation. However, a complete discussion of modulation and transport models is beyond the scope of this paper (see Fisk, 1999; Moraal et al., 1999).

8.2. Acceleration and plasma physics

We can identify two primary acceleration mechanisms that dominate the particle populations we study:

(1) Stochastic acceleration, involving resonant wave-particle interactions that transfer energy from waves to particles. This occurs in regions of high magnetic field, low-β plasma with high Alfvén speeds, notably the terrestrial aurorae and solar flares.

(2) Shock acceleration that occurs in relatively high-β plasma, including planetary bow shocks, CME-driven shocks, CIR shocks, the heliospheric termination shock, and even supernova shocks.

Our view of both processes has changed radically. We once saw stochastic acceleration as the random transfer of energy to particles from an intense but sim-

ple power-law Alfvén-wave spectrum. We now believe that the spectrum must be complex with resonant peaks of EMIC waves generated by electrons and damped by ^{3}He. At high wave intensities, Kolmogorov cascading may also be important for coupling the energy of magnetic reconnection into the frequency region of efficient resonance with energetic particles.

We once saw shock acceleration in terms of particle scattering against ambient turbulence. We now see it as a dynamic process where wave generation by low-energy particles traps them near the shock, increasing the efficiency of their acceleration to higher energy, a process that repeats to GeV energies in the strongest shocks near the Sun. Yet, resonant wave generation depends upon the proton intensity, hence it modifies the spectra and abundances much more at low energies than at high. This altered appearance of an event at different energies has led to the mistaken idea that different acceleration mechanisms are operative, specifically, that the high-energy particles come from the flare. Motivations to revive the old flare myth are amazingly strong. Spectra in large gradual SEP events (e.g., Figures 3.10 and 3.13) show a steepening at high energies, not the flattening that would be expected from a new source. All of these particles come from the same source, but the spectra are flattened at low energies by the presence of self-generated waves (see Figure 3.3). Ionization state measurements (Tylka et al., 1995) and evidence of acceleration high in the corona (Kahler, 1994) confirm this.

Wave-induced cross-field diffusion of low-energy ions may help keep them from being systematically swept downstream in quasi-perpendicular shocks and distribute particles more uniformly along the surface of a quasi-parallel shock. There is evidently so much wave generation near some shocks that the scattering mean free path is comparable with the gyroradius and $\kappa_\perp/\kappa_\parallel \sim 1$, breaking assumptions of QLT locally. When wave intensities are so high, it may also be necessary to consider the effects of Kolmogorov cascading on the wave spectrum near shocks as well. Wave intensities and spectra vary in space and time in response to changes in the particle intensities and spectra, a tightly coupled nonlinear behavior. A realistic model of shock acceleration would include particle transport in pitch-angle, in space and in momentum, local wave generation and damping, and a realistic shock geometry and evolution. There is no such model at present.

We have yet to approach those issues related to multiple large SEP events that are closely spaced in time from a single region on the Sun. Particles accelerated at the shock from the second event may travel on closed loops ejected by the first event; they may also propagate through wave spectra that have been left behind. The new particles may begin to amplify these pre-existing waves. If no new event occurs, the old waves will be swept out by the solar wind or they may cascade to the dissipation range where they will be absorbed by the solar-wind plasma. Multi-event cross talk is nearly impossible to resolve experimentally without guidance from high-quality theoretical models. At present, we can only urge caution to those who might hastily interpret the unusual abundance enhancements in the 1997 November 6 or the 1998 May 2 CME events, for example, in terms of injection of

flare particles. Unlike the 1998 April 20 event that we discussed here (Figures 3.9, 3.10, and 3.11), those events occur in complex environments that have not been adequately modeled. Only by modeling each event in a series can we begin to describe the state of the interplanetary medium prior to each new onset.

For the shock acceleration that we have discussed, the term 'high energy' might be defined as the energy, E_0, where the particle spectrum steepens as wave growth rates become small and the acceleration times large. E_0 depends upon the proton intensities at the shock (see Figure 3.3) and, of course, it varies appreciably with time. The appearance of an event is much different at high energies than in the wave-dominated low-energy region. In the largest SEP events the break seems to occur at $\sim$1 GeV (see Figure 3.13), separating the ground-level events (GLEs) from the spacecraft observations. For smaller events, like the 1998 April 20 event (see Figure 3.10), $E_0 \sim 10-20$ MeV, and E_0 falls below 100 keV in the smallest SEP events. For the Earth's bow shock the wave dominated region only extends to $\sim$20 keV, controlled by the short acceleration time (e.g., Ellison et al., 1990). ACR spectra steepen above $\sim$10 MeV amu^{-1} (Cummings and Stone, 1996). However, in this case the spectral steepening is presently interpreted as the limit of shock-drift acceleration for singly ionized particles, rather than the limit of acceleration dominated by self-generated waves. It is often difficult to determine the cause of spectral steepening at high energies.

For the particle events associated with CME, CIR, and planetary bow shocks, each new event gives us another 'experiment' with different injection parameters, shock parameters and geometric configuration. To a limited extent, it is possible to observe those parameters and to study their effects. The ACRs and GCRs each provide only a single population of particles to study, albeit with an unusual 'seed' population in the former case.

9. Abundances

We have seen that element abundances are one of our most powerful tools to study the physics of particle acceleration and the nature of the plasma where they originate. In impulsive flares, they tell us the average accelerating wave spectrum as a function of gyrofrequency. In gradual SEP events, they probe the transparency of the proton-generated wave spectrum as a function of rigidity. However, in these and many other cases, an average background level of abundances exists that describes the source plasma and is important in its own right (e.g., Meyer, 1985a,b; 1993, 1996; Reames, 1995a, 1998). Those abundances often tell us the origin of the source plasma itself.

The high abundance of energetic S in the Jovian magnetosphere is a clue to an origin in the sulfurous gasses emitted from the volcanoes of Io. The nearly pure H abundance of the inner Van Allan radiation belts is a clue to their origin in neutron decay. The new ACR radiation belt has abundances like the ACRs, N, O and Ne

with no measurable C, Mg, Si or Fe. Low-FIP ions are suppressed in ACRs but enhanced in SEPs. The ^{3}He-rich abundance in the 'upstream' event that occurs during an impulsive SEP event tells us that these particles were re-accelerated by the bow shock; they did not leak from the magnetosphere. We might even mention the high abundances of Li, Be, and B in the GCRs that tell of fragmentation of heavier species during their $\sim 10^7$ year lifetime. When we examine all these particle populations together, the power of abundance measurements in identifying the sources becomes clear.

In Table 9.1 we summarize measurements of the element abundances of the major particle populations of the heliosphere. The table also includes the 'standard' abundances of Grevesse et al. (1996). The standard abundances represent photospheric and meteoritic abundances; they are the best estimate for the primitive Sun and the local region of the galaxy where it was formed. A newer table by Grevess and Sauval (1998) differs only slightly from the earlier one we have used. In Figure 9.1 we show plots of the abundance enhancements for each element relative to its standard abundance as a function of FIP. Plots are shown for gradual SEP, CIR, ACR and GCR components.

Once we average over the variations discussed in this paper, the gradual SEP events provide the most complete information we have on element abundances in the solar corona. It is not fortuitous that the variations have no systematic residual when we average over $\sim$50 SEP gradual events, it is a consequence of transport through proton-generated waves. As noted earlier, we can see evidence of this by comparing the abundances of Mg, Si, and Fe for gradual SEP events in Figure 9.1. These three elements have nearly the same value of FIP, yet Fe has a much different value of Q/A from the other two (see Figure 3.8). The fact that Fe falls between Mg and Si on the FIP enhancement strongly suggests that there are no residual Q/A-dependent effects, at least to an accuracy of about 10%.

The CIR abundances in Table 9.1 and Figure 9.1 are those measured in the region of a few MeV amu^{-1}, as are the SEP abundances. Presumably, these abundances represent the FIP-effect of the high-speed solar wind, i.e., of coronal holes, with the exceptions noted before of up to $\sim$50% contributions from pickup H, He, and possibly C. For the abundances of most elements at CIRs, event-to-event variations are more difficult to study and we are less sure that they have been removed in averaging over many events. The FIP-effect of the abundances of energetic particles at CIRs is different from that of the gradual SEPs. These abundance patterns parallel those in the high- and low-speed solar wind, respectively.

By presenting these abundances as a function of FIP we do not mean to exclude models that explain these abundances as a function of the ionization *time* rather than FIP (e.g., von Steiger and Geiss, 1989; Marsh et al., 1995). On the contrary, these models increase the quantitative understanding we have of the 'FIP effect'. These models follow ion flow from the chromosphere at a density of 10^{16} cm^{-3} and temperature of 10^4 K where H is mostly neutral out to the corona at 10^6 K and into the solar wind. Low-FIP ions are ionized at the beginning of the process and diffuse

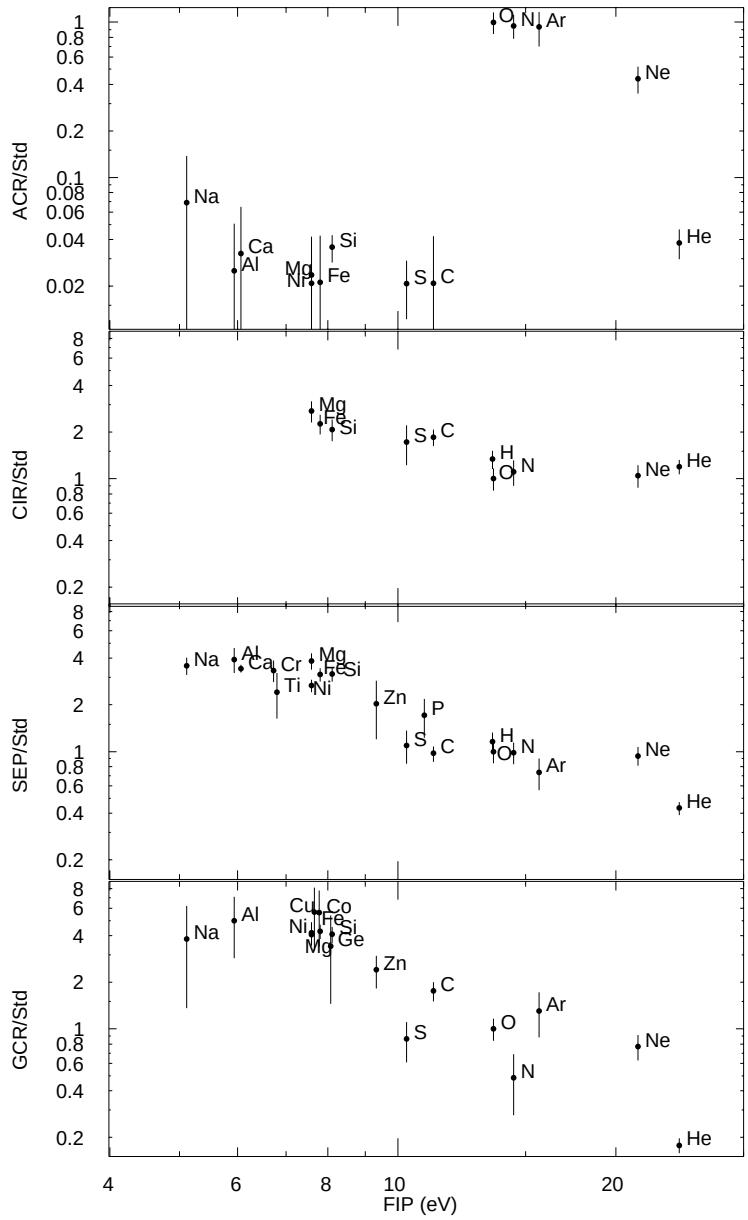

Figure 9.1. The abundances of elements are shown relative to corresponding 'standard' abundances as a function of FIP. Separate panels are shown for the gradual SEP, CIR, ACR, and GCR populations of energetic particle.

TABLE 9.1
Element abundances in energetic particle sources

	Z	FIP	Photosphere[1]	Gradual events[2] (SEP Corona)	CIR events[2] (Coronal Hole)	Impulsive flares[2]	Anomalous CR[3]	Galactic CR source[4]
H	1	13.53	1.35×10^6	$(1.57 \pm 0.22) \times 10^6$	$(1.81 \pm 0.24) \times 10^6$	$\sim 1 \times 10^6$	$\sim 1000 \pm 500$	$(1.74 \pm 0.43) \times 10^5$
He	2	24.46	$132\,000 \pm 11\,000$	57000 ± 3000	$159\,000 \pm 10\,000$	$46\,000 \pm 4000$	5000 ± 1000	$23\,500 \pm 1600$
C	6	11.22	479 ± 55	465 ± 9	890 ± 36	434 ± 30	<10	843 ± 67
N	7	14.48	126 ± 20	124 ± 3	140 ± 14	157 ± 18	120 ± 10	61 ± 24
O	8	13.55	1000 ± 161	1000 ± 10	1000 ± 37	1000 ± 45	1000 ± 10	1000 ± 40
F	9	17.34	0.05 ± 0.03	<0.1		<2	<2	<5
Ne	10	21.47	162 ± 22	152 ± 4	170 ± 16	400 ± 28	70 ± 10	125 ± 16
Na	11	5.12	2.9 ± 0.2	10.4 ± 1.1		34 ± 8	<0.2	11 ± 7
Mg	12	7.61	51 ± 6	196 ± 4	140 ± 14	408 ± 29	1.2 ± 0.3	207 ± 12
Al	13	5.96	4.0 ± 0.6	15.7 ± 1.6		68 ± 12	<0.1	20 ± 8
Si	14	8.12	48 ± 5	152 ± 4	100 ± 12	352 ± 27	1.7 ± 0.3	196 ± 12
P	15	10.9	0.38 ± 0.04	0.65 ± 0.17		4 ± 3	<0.1	<5
S	16	10.3	29 ± 7	31.8 ± 0.7	50 ± 8	117 ± 15	0.6 ± 0.2	25 ± 4
Cl	17	12.95	0.4 ± 0.3	0.24 ± 0.1		<2	<0.1	<3
Ar	18	15.68	4.5 ± 1.0	3.3 ± 0.2		30 ± 8	4.2 ± 0.5	5.9 ± 1.4
K	19	4.32	0.18 ± 0.05	0.55 ± 0.15		2 ± 2		<3.7
Ca	20	6.09	3.09 ± 0.14	10.6 ± 0.4		88 ± 13	<0.1	1.7 ± 3.5
Ti	22	6.81	0.14 ± 0.02	0.34 ± 0.1		<2	<0.1	<4.7
Cr	24	6.74	0.63 ± 0.04	2.1 ± 0.3		12 ± 5	<0.1	<5.7
Fe	26	7.83	42.7 ± 3.9	134 ± 4	97 ± 11	1078 ± 46	<0.9	182 ± 11
Ni	28	7.61	2.4 ± 0.05	6.4 ± 0.6		42 ± 9	<0.05	10 ± 1.7
Zn	30	9.36	0.054 ± 0.010	0.11 ± 0.04		6 ± 4	<0.05	0.13 ± 0.02

[1]Grevesse et al. (1996). [2]Reames (1995a, 1998). [3]Reames 1999. [4]Lund (1989).

upward along with H which is ionized by EUV photons from the hot corona. Ions are also drawn upward by the ambipolar electric field produced by differences in scale height of electrons and ions. The abundance of high-FIP elements depends upon the time required for them to be ionized and to join the upward flow.

In a recent paper, Schwadron et al. (1999) describe an alternative model for the FIP-effect that includes the effects of resonant wave-particle interactions that couple other ions to H^+. The presence of these interactions increases the pressure and scale-height of ions relative to the neutrals so the fractionation increases with height in the corona. This explains why the slow solar wind, coming from magnetic reconnection at the tops of previously closed loops in the streamer belt (Fisk et al., 1999), has a greater FIP fractionation than the fast solar wind that originates lower in the solar atmosphere. The model also provides the selective heating necessary to explain (Zurbuchen et al., 1998) the $^3He/^4He$ ratio that is $\sim$20% greater, on average, in the slow than in fast solar wind. Other fractionation models are reviewed by Hénoux (1995, 1998).

ACR abundances are not usually displayed as a function of FIP. However, it is extremely appropriate to do so because the large suppression of the low-FIP elements is indeed an ion-neutral separation caused by the magnetic fields of the outer heliosphere. Figure 9.1 shows ACR abundances at the termination shock corrected for modulation (Reames, 1999). Modulation affects H and He much more than the heavier ions. The high-FIP elements He and Ne are suppressed because they are less likely to be photoionized, than N or O. Fisk et al. (1974) list mean distances for photo-ionization of 0.5, 1.6, 4, and 3 AU for He, Ne, N, and O, respectively. H behaves differently because it can charge exchange with solar wind H; it does not experience the solar wind as a 'test particle' would (see, e.g., Zank and Pauls, 1996). Rucinski et al. (1996) have performed detailed calculations of the photo-ionization and charge-exchange processes.

The low-FIP ACR ions are truly worthy of the name 'anomalous', since their abundances are suppressed by a factor of $\sim$50 relative to O. All of the low-FIP ions except Mg, Si, and S must be listed as upper limits since the presence of a non-GCR component in the low-energy spectra cannot be proven (see Figure 6.1). It is interesting to note that Mg:Si:S abundances are statistically consistent with the standard (photospheric or local galactic) abundances. In addition, we have S/Fe$\geq$0.7, already much larger than the coronal value, but still consistent with the standard abundance. The origin of these low-FIP ACR ions remains unclear, they might come from a small component of interstellar neutrals; any such neutrals entering the heliosphere would be *easily* photoionized. In some cases, e.g., C and Fe, they could be multiply charged ions, accelerated from the tail of the solar wind distribution function at the termination shock. It is even possible that S injected from the volcanoes of Io finds its way into the ACRs.

Finally, in Figure 9.1, we compare the GCR source abundances corrected for fragmentation in interstellar space (Lund 1989). The GCRs are where the FIP-effect was originally observed. The first realization that GCR abundances have a

dependence on ionization potential seems to come from Kristiansson (1971, 1972), although he considered the ionization cross section, rather than FIP. Kristiansson also included a Z^{α}-dependence that we might now recognize as a proxy for a Q/A dependence of the acceleration. Webber (1975) noted the similar behavior of the SEP and GCR abundances. Meyer (1985b) provided the most complete and convincing evidence of this similarity. Meyer noted that only the factor-of- $\sim$2 excesses in the abundances of C and of ^{22}Ne in the GCRs could not be reconciled with coronal and SEP abundances. He suggested that SEPs, or rather *stellar* energetic particles accelerated similarly, could be the seed population for GCR acceleration, presumably by supernova shock waves.

Recently, a controversy has grown over an alternative scenario for GCR acceleration (Meyer et al., 1997; Ellison et al., 1997). In this model, the FIP separation occurs because the low-FIP, or refractory, elements are bound in interstellar dust grains. Grains with $A/Q \sim 10^6$ are preferentially accelerated at supernova shocks, enhancing the abundances of their constituents by factors of $\sim$50 with respect to the volatile high-FIP elements. About 10% of the grain mass is then sputtered off as individual ions as the grains pass through the ambient material with a speed of $\sim$0.001c, resulting in a net enhancement of the refractory elements by a factor of $\sim$5. The sputtered refractory ions are then accelerated to high energies along with the volatiles. The model also presumes an A^{α}-dependence for the volatiles as a proxy for a Q/A dependence of their acceleration. ^{22}Ne and C must still be separately enhanced, presumably by Wolf–Rayet stars, in this as in all other GCR models. Lingenfelter et al. (1998) have modified this model to accelerate grains that have been freshly formed in a new supernova. They explain the high C/O ratio by formation of carbonaceous grains.

One problem with the idea of injecting SEPs from *solar-like* events as a seed population for GCR production is that adiabatic deceleration takes a serious toll on the spectrum; few of the particles escape the heliosphere with significant energy. However, Shapiro (1997; Shapiro and Silberberg, 1997) has suggested that magnetically active M and K dwarf stars may be $\sim 10^4$ times as active, producing numerous fast CMEs. They estimate that these stellar CMEs can produce $\sim$0.35 eV cm^{-3} in 'seed particles'. The intensity and energy actually scale as high powers of the shock speed, so there may be substantial margin for any adiabatic deceleration in these stellar systems. We have also seen that shocks will accelerate whatever seed population they find available. Therefore, if these 'stellar energetic particles' are sufficiently numerous, GCRs from this mundane source could easily dominate those from the more esoteric grain-acceleration pathway.

It seems unlikely that new evidence will be found to resolve this interesting GCR injection controversy conclusively in the immediate future.

10. Summary and Conclusions

The last decade has been a time of dynamic change in our perception of the energetic particles of the heliosphere. We have survived a shift in the paradigm for the acceleration and transport of particles in SEP events. However, no sooner had we settled on the terms 'gradual' and 'impulsive', than we began to find that time scale alone was ill suited to distinguishing the physical mechanisms of interest, though it still describes the behavior of MeV ions. It now seems possible that all flares may produce dramatic enhancements of energetic ^{3}He, regardless of time scale, and substantial enhancements of Fe/O can occur for shock-accelerated ions. The correct source distinction appears to lie between all flares and CME-driven shocks. Yet the terms 'gradual' and 'impulsive' have stuck and we are now beginning to model the two underlying processes of acceleration systematically.

We have explored new ways in which wave-particle interactions can produce the abundance enhancements in impulsive flares. In fact, this fundamental aspect of the physics of solar flares can only be studied with accelerated-particle abundances. The spectrum of waves near the ion gyrofrequencies cannot be observed directly and can only be studied by its effect on the energetic particles.

The greatest changes have come for gradual SEP events. We now discuss the *spatial* distribution of the acceleration, transport, and trapping with respect to the evolving CME and the shock wave it drives. The largest events accelerate protons to energies above 20 GeV near the Sun. For small events, power-law energy spectra are common, but for the large powerful events, streaming particles become trapped near the shock by self-generated waves, flattening the spectra of escaping particles at low-energies. While this process has been known for many years, we now recognize its effects on the time variation of ion abundances and spectra. *The profusion of resonant waves causes events to appear differently at low energies than at high. Previously, this lead to the mistaken perception that different acceleration mechanisms were at work in different energy regions*. We must now cope with the ways one event can affect the appearance of another coming close behind.

Recently, effects of intensity-dependent proton-generated waves have also been reported in the *in situ* observation of cross-field scattering in CIR-related shocks events. It should be obvious that shock acceleration is similar even in different sites. We have known for many years that protons streaming away from shocks generate waves. Yet, it seems to come as a surprise that waves might also be important at CIR-associated shocks and in the injection of pickup ions at the termination shock. Perhaps we must relearn old lessons at each new site.

We have explored the heliosphere in 3 dimensions, mapping the spatial distributions of the solar wind, of CIRs and of CMEs as Ulysses flew over the solar poles. Energetic particles accelerated at CIR shocks have been followed to latitudes far higher than that of the shocks themselves. These particles serve as probes of the magnetic topology, that can be explained by a new model for the migration of magnetic field-line footpoints across the solar corona.

The Voyager spacecraft have tracked the modulation of the spectra of ACRs out beyond 60 AU, and at 1 AU, new elements, Mg, Si, and S, with low intensities and uncertain origin have added their own anomalous spectra. The interstellar pickup ions that can eventually become ACR H, He, N, O and Ne have now been observed directly in the solar wind, long after their existence was predicted from the ACRs. New isotope measurements of ACR Ne confirm that local interstellar matter is similar to that in the Sun.

Element abundances have proven to be our most powerful tool in identifying the nature and properties of the source plasma and in probing the physics of acceleration and transport. Particle populations are *defined* by their abundances. The high abundances of Li, Be, and B defined the history of GCRs. The high relative abundance of S and O defined the volcanic source of the ions at Jupiter. The high abundances of He, N, O, and Ne defined the ACR source as pickup ions. So too, the average abundances in gradual SEP events define coronal abundances and ^{3}He/^{4}He $> 10\%$ defines the unique physics of ion acceleration in solar flares.

Our instruments have improved enormously, in sensitivity, in resolution and in high-speed on-board processing. Where we once measured event-averaged abundances and spectra, we can now probe time-dependent spectral evolution along both SEP and CIR shocks over 4–5 decades in energy. Isotope abundances extend observation of Q/A dependence and characterize interstellar matter. Ionization-state measurements over a broad energy range can define source temperatures and transport through matter, which may vary with time. Particle angular distributions identify local regions of intense scattering and wave growth, of streaming and of bidirectional flows. With these new tools, we have left the discovery phase and begun to focus on the detailed physics of particle acceleration in the heliosphere.

Yet, our most formidable tools are still those that have probed relentlessly for a solar cycle or more. The spacecraft that continue to operate for long periods of time, like the venerable IMP 8 that has provided data over 25 years, give us a complete perspective on the solar-cycle variations that underlie the physical processes we study. These observations also provide a large statistical sample of events that help to defend us from the temptation to draw premature conclusions from all-too-small a sample. May our new tools serve us as well.

Acknowledgements

I would like to thank C. K. Ng and A. J. Tylka for many helpful discussions during the preparation of this paper. I would also especially like to thank E. W. Cliver, J. T. Gosling, P. A. Isenberg, S. W. Kahler, M. A. Lee, G. M. Mason, F. B. McDonald, C. K. Ng, I. Roth, A. J. Tylka, and T. T. von Rosenvinge for serving as referees for this paper. This paper has benefited significantly from their patient and careful reading of it.

References

Adams, J. H. et al.: 1991, *Astrophys. J.* **375**, L45.

Arnaud, M. and Raymond, J.: 1992, *Astrophys. J.* **398**, 394.

Arnaud, M. and Rothenflug, R.: 1985, *Astron. Astrophys. Suppl.* **60**, 425.

Athay, R. G. and Moreton, G. E.: 1961, *Astrophys. J.* **133**, 935.

Baker, D. N., Zwickl, R. D., Krimigis, S. M., Carbary, J. F., and Acuña, M. H.: 1984, *J. Geophys. Res.* **89**, 3775.

Barnes, C. W. and Simpson, J. A.: 1976, *Astrophys. J.* **210**, L91.

Beeck, J., Mason, G. M., Hamilton, D. C., Wibberenz, G., Kunow, H., Hovestadt, D., and Klecker, B.: 1987, *Astrophys. J.* **322**, 1052.

Belcher, J. W. and Davis, L., Jr.: 1971 *J. Geophys. Res.* **76**, 3534.

Bell, A. R.: 1978, *Monthly Notices Roy. Astron. Soc.* **182**, 147.

Bertsch, D. L., Fichtel, C. E., and Reames, D. V.: 1969, *Astrophys. J.* **157**, L53.

Bieber, J. W., Matthaeus, W. H., Smith, C. W., Wanner, W., Kallenrode, M.-B., and Wibberenz, G.: 1994, *Astrophys. J.* **420**, 294.

Blake, J. B. and Friesen, L. M.: 1977, *Proc. 15th Internat. Cosmic-Ray Conf., Plovdiv* **2**, 341.

Blake, J. B., Kolasinski, W. A., Fillius, R. W., and Mullen, E. G.: 1992 *Geophys. Res. Letters* **19**, 821.

Boberg, P. R., Tylka, A. J., and Adams, J. H.: 1996, *Astrophys. J.* **471**, L65.

Bodmer, R., Bochsler, P., Geiss, J., von Steiger, R., and Gloeckler, G.: 1995, *Space Sci. Rev.* **72**, 61.

Breneman, H. H. and Stone, E. C.: 1985, *Astrophys. J.* **299**, L57.

Burlaga, L. F.: 1974, *Space Sci. Rev.* **17**, 327.

Burlaga, L. F., McDonald, F. B., Ness, N. F., Schwenn, R., Lazarus, A. J., and Miriani, F.: 1984, *J. Geophys. Res.* **89**, 6579.

Burlaga, L. F., McDonald, F. B., Goldstein, M. L., and Lazarus, A. J.: 1985, *J. Geophys. Res.* **90**, 12 027.

Cane, H. V., McGuire, R. E., and von Rosenvinge, T. T.: 1986, *Astrophys. J.* **301**, 448.

Cane, H. V., Reames, D. V., and von Rosenvinge, T. T.: 1988, *J. Geophys. Res.* **93**, 9555.

Cane, H. V., Reames, D. V., and von Rosenvinge, T. T.: 1991, *Astrophys. J.* **373**, 675.

Cane, H. V., Richardson, I. G., and von Rosenvinge, T. T.: 1996, *J. Geophys. Res.* **101**, 21 561.

Cane, H. V., Sheeley, N. R., Jr., and Howard, R. A.: 1987, *J. Geophys. Res.* **92**, 9869.

Carrington, R. C.: 1860, *Monthly Notices Roy. Astron. Soc.* **20**, 13.

Chupp, E. L.: 1984, *Ann. Revs Astron. Astrophys.* **22**, 359.

Cliver, E. W.: 1996, in R. Ramaty, N, Mandzhavidze and, X.-M. Hua (eds), *High Energy Solar Physics*, AIP Conf. Proc **374**, AIP press, Woodbury, NY, p. 45.

Cliver, E. W., Forrest, D. J., Cane, H. V., Reames, D. V., McGuire, R. E., and von Rosenvinge, T. T.: 1989, *Astrophys. J.* **343**, 953.

Cliver, E. W. and Kahler, S. W.: 1991, *Astrophys. J.* **336**, L91.

Cliver, E. W., Kahler, S. W., and McIntosh, P. S.: 1983, *Astrophys. J.* **264**, 699.

Cliver, E. W., Webb, D. F., and Howard, R. A.: 1999, *Solar Phys.*, in press.

Cohen, K. et al.: 1999, *Geophys. Res. Letters* **26**, 149.

Cooper, J. F.: 1983, *J. Geophys. Res.* **88**, 3945.

Coplan, M. A., Ogilvie, K. W., Bochsler, P., and Geiss, J.: 1985 *Solar Phys.* **93**, 415.

Cummings, A. C. and Stone, E. C.: 1996, *Space Science Rev.* **78**, 117.

Decker, R. B. and Vlahos, L.: 1986, *Astrophys. J.* **306**, 710.

Dwyer, J. R., Mason, G. M., Mazur, J. E., Jokipii, J. R., von Rosenvinge, T. T., and Lepping, R. P.: 1997a, *Astrophys. J.* **490**, L115.

Dwyer, J. R., Mason, G. M., Mazur, J. E., and von Rosenvinge, T. T.: 1997b, *Geophys. Res. Letters* **24**, 61.

Earl, J. A.: 1981, *Astrophys. J.* **251**, 739.

Earl, J. A.: 1987, *Proc. 20th Internat. Cosmic-Ray Conf., Moscow* **3**, 132.
Eichler, D.: 1981, *Astrophys. J.* **244**, 711.
Ellison, D. C., Drury, L. O'C., and Meyer, J. P.: 1997 *Astrophys. J.* **487**, 197.
Ellison, D. C., Möbius, E., and Paschmann, G.: 1990, *Astrophys. J.* **352**, 376.
Ellison, D. C., Jones, F. C., and Baring, M. G.: 1999, *Astrophys. J.*, in press.
Ellison, D., and Ramaty, R.: 1985, *Astrophys. J.* **298**, 400.
Evenson, P., Kroeger, R., Meyer, P., and Reames, D.: 1990, *Astrophys. J. Suppl.* **73**, 273.
Feldman, W. C., Asbridge, J. R., Bame, S. J., Fenimore, E. E., and Gosling, J. T.: 1981, *J. Geophys. Res.* **86**, 5408.
Fichtel, C. E. and Guss, D. E.: 1961, *Phys. Rev. Letters* **6**, 495.
Fisk, L. A.: 1978, *Astrophys. J.* **224**, 1048.
Fisk, L. A.: 1979, in E. N. Parker, C. F. Kennel, L. J. Lanzerotti (eds.), *Solar System Plasma Physics*, Vol. **1**, North Holland, Amsterdam, p. 177.
Fisk, L. A.: 1996a, *J. Geophys. Res.* **101**, 15 553.
Fisk, L. A.: 1996b, *Space Sci. Rev.* **78**, 129.
Fisk, L. A.: 1999, *Adv. Space Res.* **23** (3), 415.
Fisk, L. A., Kozlovsky, B., and Ramaty, R.: 1974, *Astrophys. J.* **190**, L35.
Fisk, L. A. and Lee, M. A.: 1980, *Astrophys. J.* **237**, 620.
Fisk, L. A., Schwadron, N. A., and Gloeckler, G.: 1997, *Geophys. Res. Letters* **24**, 93.
Fisk, L. A., Schwadron, N. A., and Zurbuchen, T. H.: 1999, *Astrophys. J.*, in press.
Forbush, S. E. 1946: *Phys. Rev.* **70**, 771.
Forman, M. A., Ramaty, R., and Zweibel, E. G.: in P. A. Sturrock (ed.), *Physics of the Sun*, D. Reidel, Dordrecht, Holland, p. 249.
Fox, N. J., Peredo, M., and Thompson, B. J.: 1998, *Geophys. Res. Letters* **25**, 2461.
Freden, S. C. and White, R. S.: 1960, *J. Geophys. Res.* **65**, 1377.
Fujii, Z. and McDonald, F. B.: 1999, *Adv. Space Res.* **23** (3), 437.
Garcia-Munoz, M., Mason, G. M., and Simpson, J. A.: 1973, *Astrophys. J.* **182**, L81.
Garcia-Munoz, M., Mason, G. M., and Simpson, J. A.: 1975, *Astrophys. J.* **202**, 265.
Gehrels, N. and Stone, E. C.: 1983, *J. Geophys. Res.* **88**, 5537.
Gehrels, N., Stone, E. C., and Trainor, J. H.: 1981, *J. Geophys. Res.* **86**, 8906.
Geiss, J., Gloeckler, G., Mall, U., von Steiger, R., Galvin, A. B., and Ogilvie, K.: 1994, *Astron. Astrophys.* **282**, 924.
Geiss, J., Gloeckler, G., and von Steiger, R.: 1995, *Space Sci. Rev.* **72**, 49.
Geiss, J., Gloeckler, G., Fisk, L. A., and von Steiger, R.: 1995, *J. Geophys. Res.* **100**, 23 373.
Ghosh, S., Matthaeus, W. H., Roberts, D. A., and Goldstein, M. L.: 1998, *J. Geophys. Res.* **103**, 23 705.
Giacalone, J., Jokipii, J. R., Decker, R. B., Krimigis, S. M., Scholer, M., and Kucharek, H.: 1997 *Astrophys. J.* **486**, 471.
Gloeckler, G. et al.: 1993, *Science* **261**, 70.
Gloeckler, G. et al.: 1999, *Geophys. Res. Letters* **26**, 157.
Gloeckler, G., Hovestadt, D., and Fisk, L. A.: 1979, *Astrophys. J.* **230**, L191.
Gloeckler, G., Schwadron, N. A., Fisk, L. A., and Geiss, J.: 1995, *Geophys. Res. Letters* **22**, 2665.
Goodrich, C. C., Lyon, J. G., Wiltberger, M., Lopez, R. E., and Papadopoulos, K.: 1998, *Geophys. Res. Letters* **25**, 2537.
Gosling, J. T.: 1993, *J. Geophys. Res.* **98**, 18 949.
Gosling, J. T., Asbridge, J. R., Bame, S. J., and Feldman, W. C.: 1979, *Particle Acceleration Mechanisms in Astrophysics*, AIP Conf. Proc. **56**, AIP Press, Woodbury, NY, p. 81.
Gosling, J. T., Asbridge, J. R., Bame, S. J., Feldman, W. C., Zwickl, R. D., Paschmann, G., Sckopke, N., and Hynds, R. J.: 1981, *J. Geophys. Res.* **86**, 547.
Gosling, J. T., Baker, D. N., Bame, S. J., Feldman, W. C., and Zwickl, R. D.: 1987, *J. Geophys. Res.* **92**, 8519.

Gosling, J. T., Bame, S. J., McComas, D. J., Phillips, J. L., Balogh, A., and Strong, K. T.: 1995a, *Space Sci. Rev.* **72**, 133.
Gosling, J. T., Bame, S. J., McComas, D. J., Phillips, J. L., Pizzo, V. J., Goldstein, B. E., and Neugebauer, M: 1995b, *Space Sci. Rev.* **72**, 99.
Gosling, J. T., Birn, J., and Hesse, M.: 1995c, *Geophys. Res. Letters* **22**, 869.
Gosling, J. T., Hundhausen, A. J., and Bame, S. J.: 1976, *J. Geophys. Res.* **81**, 2111.
Grevesse, N., Noels, A., and Sauval, A. J.: 1996, in S. Holt and G. Sonneborn (eds), *Cosmic Abundances*, A.S.P. Conf. Series **99**, p. 117.
Grevesse, N., and Sauval, A. J.: 1998, *Space Sci. Rev.* **85**, 161.
Grigarov, N. L., Kondratyeva, M. A., Panasyuk, M. I., Tretyakova, Ch. A., Adams, J. H. Jr., Blake, J. B., Schulz, M., Mewaldt, R. A., and Tylka, A. J.: 1991, *Geophys. Res. Letters* **18**, 1959.
Hamilton, D. C., Gloeckler, G., Armstrong, T. P., Axford, W. I., Bostrom, C. O., Fan, C. Y., Krimigis, S. M., and Lanzerotti, L. J.: 1979, *Proc. 16th Int. Cosmic-Ray Conf., Kyoto* **5**, 363.
Hasebe, N. et al.: 1994, *Geophys. Res Letters* **21**, 3027.
Hasebe, N. et al.: 1997, *Adv. Space Res.* **19**(5), 813.
Hefti, S., Zurbuchen, T. H., Gloeckler, G., Fisk, L. A., and Schwadron, N. A.: 1998, *EOS, Transactions AGU* **79**, No. 45, F693.
Hénoux, J.-C.: 1995, *Adv. Space Res.* **15**(7), 23.
Hénoux, J.-C.: 1998, *Space Sci. Rev*. **85**, 215.
Heras, A. M., Sanahuja, B., Sanderson, T. R., Marsden, R. G., and Wentzel, K.-P.: 1994, *J. Geophys. Res.* **99**, 43.
Heras, A. M., Sanahuja, B., Lario, D., Smith, Z. K., Detman. T.: 1995, *Astrophys. J.* **445**, 497.
Hess, W. N.: 1959, *Phys. Rev. Letters* **3**, 11.
Hoeksema, J. T.: 1995 *Space Sci. Rev.* **81**, 137.
Hoppe, M. M., Russell, C. T., Frank, L. A., Eastman, T. E., and Greenstadt, E. W.: 1981, *J. Geophys. Res.* **86**, 4471.
Hsieh, K. C. and Simpson, J. A.: 1970, *Astrophys. J.* **162**, L191.
Hudson, M. K., Elkington, S. R., Lyon, J. G., Marchenko, V. A., Roth, I., Temerin, M., Blake, J. B., Gussenhoven, M. S., and Wygant, J. R.: 1997, *J. Geophys. Res.* **102**, 14 087.
Hudson, M. K., Marchenko, V. A., Roth, I., Temerin, M., Blake, J. B., and Gussenhoven, M. S.: 1998, *Adv. Space Res.* **21**(4), 597.
Hundhausen, A. J.: 1972, *Coronal Expansion of the Solar Wind*, Springer-Verlag, New York.
Hundhausen, A. J., Gilbert, H. E., and Bame, S. J.: 1968, *J. Geophys. Res.* **73**, 5485.
Hundhausen, A. J. and Gosling, J. T.: 1976, *J. Geophys. Res.* **81**, 1436.
Hurford, G. J., Mewaldt, R. A., Stone, E. C., and Vogt, R. E.: 1975, *Astrophys. J.* **201**, L95.
Intrilligator, D. S. and Siscoe, G. L.: 1994, *Geophys. Res. Letters* **21**, 1117.
Jokipii, J. R.: 1987, *Astrophys J.* **313**, 442.
Jokipii, J. R.: 1990, in E. Grzedzielski and D. E. Page (eds), *Physics of the Outer Heliosphere*, Pergamon Press, New York, p. 169.
Jokipii, J. R.: 1996, *Astrophys J.* **466**, L43.
Jokipii, J. R., Kóta, J., Giacalone, J., Horbury, T. S., and Smith, E. J.: 1995, *Geophys. Res. Letters* **22**, 3385.
Jokipii, J. R. and Parker, E. N.: 1968, *Astrophys J.* **21**, 44.
Jokipii, J. R. and Parker, E. N.: 1970, *Astrophys J.* **160**, 735.
Jones, F. C. and Ellison, D. E.: 1991, *Space Sci. Rev.* **58**, 259.
Kahler, S. W.: 1982, *J. Geophys. Res.* **87**, 3439.
Kahler, S. W.: 1992, *Ann. Rev. Astron. Astrophys.* **30**, 113.
Kahler, S. W.: 1994, *Astrophys. J.* **428**, 837.
Kahler, S. W.: 1997, in N. Crooker, J. A. Jocelyn, and J. Feynman (eds), *Coronal Mass Ejections*, Geophys. Monograph **99**, AGU Press, New York, p. 197.

Kahler, S. W., Cliver, E. W., Cane, H. V., McGuire, R. E., Reames, D. V., Sheeley, N. R., Jr., and Howard, R. A.: 1987a, *Proc. 20th Int. Cosmic Ray Conf., Moscow* **3**, 121.
Kahler, S. W., Cliver, E. W., Cane, H. V., McGuire, R. E., Stone, R. G., and Sheeley, N. R., Jr.: 1986, *Astrophys. J.* **302**, 504.
Kahler, S. W., Hildner, E., and Van Hollebeke, M. A. I.: 1978, *Solar Phys.* **57**, 429.
Kahler, S. W., Lin, R. P., Reames, D. V., Stone, R. G., and Liggett, M.: 1987b, *Solar Phys.* **107**, 385.
Kahler, S. W. and Reames, D. V.: 1991, *J. Geophys. Res.* **96**, 9419.
Kahler, S. W., Sheeley, N. R., Jr., Howard, R. A., Koomen, M. J., Michels, D. J., McGuire R. E., von Rosenvinge, T. T., and Reames, D. V.: 1984, *J. Geophys. Res.* **89**, 9683.
Kallenbach, R. et al.: 1998, *Space Sci. Rev.* **85**, 357.
Kennel, C. F., Coroniti, F. V., Scarf, F. L., Livesey, W. A., Russel, C. T., Smith, E. J., Wenzel, K.-P., and Scholer, M.: 1986, *J. Geophys. Res.* **91**, 11 917.
Krimigis, S. M., Armstrong, T. P., Axford, W. I., Cheng, A. F., Gloeckler, G., Hamilton, D. C. Keath, E. P., Lanzerotti. L. J., and Mauk, B. H.: 1986, *Science* **233**, 97.
Krimigis, S. M. et al.: 1989, *Science* **246**, 1483.
Kristiansson, K.: 1971, *Astrophys. Space Sci.* **14**, 485.
Kristiansson, K.: 1972, *Astrophys. Space Sci.* **16**, 405.
Klecker, B.: 1995, *Space Science Rev.* **72**, 419.
Klecker, B., Oetliker, M., Blake, J. B., Hovestadt, D., Mason, G. M., Mazur, J. E., and McNab, M. C.: 1997, *Proc 25th Int. Cosmic Ray Conf, Durban* **2**, 273.
Kóta, J. and Jokipii, J. R.: 1998, *Space Sci. Rev.* **83**, 137.
Larson, D. E. et al.: 1997, *Geophys. Res. Letters*, **24**, 1911.
Lee, M. A.: 1982, *J. Geophys. Res.* **87**, 5063.
Lee, M. A.: 1983, *J. Geophys. Res.* **88**, 6109.
Lee, M. A.: 1992, in G. P. Zank and T. K. Gaisser (eds), *Particle Acceleration in Cosmic Plasmas*, AIP Conf. Proc. **264**, AIP Press, New York, p. 27.
Lee, M. A.: 1996, *Space Sci. Rev.* **78**, 109.
Lee, M. A.: 1997, in N. Crooker, J. A. Jocelyn, J. Feynman (eds), *Coronal Mass Ejections*, Geophys. Monograph **99**, AGU Press, New York, p. 227.
Lenchek, A. M. and Singer, S. F.: 1963: *Planetary Space Sci.* **11**, 1151.
Leske, R. A., Cummings, J. R., Mewaldt, R. A., Stone, E. C., and von Rosenvinge, T. T.: 1995, *Astrophys J.* **452**, L149.
Leske, R. A., Mewaldt, R. A. , Cummings, A. C., Cummings, J. R., Stone, E. C., and von Rosenvinge, T. T.: 1996, *Space Sci. Rev.* **78**, 149.
Lin, R. P. and Hudson, H. S.: 1976, *Solar Phys.* **50**, 153.
Lingenfelter, R. E.: 1963, *J. Geophys. Res.* **68**, 5633.
Lingenfelter, R. E., Ramaty, R., and Kozlovsky, B.: 1998, *Astrophys. J.* **500**, L153.
Litvinenko, Y. E.: 1996, in R. Ramaty, N. Mandzhavidze, X.-M. Hua (eds), *High Energy Solar Physics*, AIP Conf. Proc. **374**, AIP Press, Woodbury, NY, p. 498.
Lovell, J. L., Duldig, M. L., Humble, J. E.: 1998, *J. Geophys. Res.* **103**, 23 733.
Luhn, A. et al.: 1985, *Proc. 19th Internat. Cosmic-Ray Conf., La Jolla* **4**, 241.
Luhn, A., Klecker B., Hovestadt, D., Gloeckler, G., Ipavich, F. M., Scholer, M., Fan, C. Y. and Fisk, L. A.: 1984, *Adv. Space Res.* **4**, 161.
Luhn, A., Klecker, B., Hovestadt, D., and Möbius, E.: 1987, *Astrophys. J.* **317**, 951.
Lund, N.: 1989, in C. J. Waddington (ed.), *Cosmic Abundances of Matter*, A.I.P. Conf. Proc. **183**, p. 111.
Maclennan, C. G., Lanzerotti, L. J., Decker, R. B., Krimigis, S. M., Collier, M. R., and Hamilton, D. C.: 1996, *Astrophys. J.* **468**, L123.
Mandzhavidze, N., Ramaty, R., and Kozlovsky, B.: 1999, *Astrophys. J.* **518**, 918.
Marsch, E., von Steiger, R., and Bochsler, P.: 1995, *Astron. Astrophys.* **301**, 261.

Marsden, R. G., Sanderson, T. R., Tranquille, C., Wenzel, K.-P., and Smith, E. J.: 1987, *J. Geophys. Res*, **92**, 11 009.
Mason, G. M., Ng, C. K., Klecker, B., and Green, G.: 1989, *Astrophys. J.* **339**, 529.
Mason, G. M., Gloeckler, G., and Hovestadt, D.: 1984, *Astrophys. J.* **280**, 902.
Mason, G. M., Mazur, J. E., Dwyer, J. R., Reames, D. V., and von Rosenvinge, T. T.: 1997, *Astrophys. J.* **486**, L149.
Mason, G. M., Mazur, J. E., Looper, M. D., and Mewaldt, R. A.: 1995, *Astrophys. J.* **452**, 901.
Mason, G. M., Mazur, J. E., and Hamilton D. C.: 1994, *Astrophys. J.* **425**, 843.
Mason, G. M., Mazur, J. E., and von Rosenvinge, T. T.: 1996, *Geophys. Res. Letters* **23**, 1231.
Mason, G. M., Reames, D. V., Klecker, B., Hovestadt, D., and von Rosenvinge, T. T.: 1986, *Astrophys. J.* **303**, 849.
Mason, G. M., Reames, D. V., and Ng, C. K.: 1991,*Proc. 22nd Internat. Cosmic-Ray Conf., Dublin* **3**, 197.
Matthaeus, W. H., Goldstein, M. L., and Roberts, D. A.: 1990, *J. Geophys. Res.* **95**, 20 673.
Mazur, J. E., Mason, G. M., Klecker, B., and McGuire, R. E.: 1992, *Astrophys. J.* **401**, 398.
Mazur, J. E., Mason, G. M., Looper, M. D., Leske, R. A., and Mewaldt, R. A.: 1999, *Geophys. Res. Letters* **26**, 173.
McComas, D. J., Gosling, J. T., Hammond, C. M., Moldwin, M. B., and Phillips, J. L.:1994 *Geophys. Res. Letters* **21**, 1751.
McCracken, K.: 1962, *J. Geophys. Res.* **67**, 423.
McDonald, F. B., Schardt, A. W., and Trainor, J. H.: 1980, *J. Geophys. Res.* **85**, 5813.
McDonald, F. B., Teegarden, B. J., Trainor, J. H., and von Rosenvinge, T. T.: 1975, *Astrophys. J.* **203**, L149.
McDonald, F. B., Teegarden, B. J., Trainor, J. H., and Webber, W. R.: 1974, *Astrophys. J.* **187**, L105.
McGuire, R. E., von Rosenvinge, T. T., and Mc Donald, F. B.: 1978, *Astrophys. J.* **301**, 938.
McKenzie, D. L., and Feldman, U.: 1992, *Astrophys. J.* **389**, 764.
McKibben, R. B.: 1972, *J. Geophys. Res.* **77**, 3959.
Melrose, D. B.: 1980, *Plasma Astrophysics*, Vol. 1, Gordon and Breach, New York.
Mewaldt, R. A., Selesnick, R. S., Cummings, J. R., Stone, E. C., and von Rosenvinge, T. T.: 1996, *Astrophys J.* **466**, L43.
Mewaldt, R. A., Stone, E. C., and Vogt, R. E.: 1978 *Geophys. Res. Letters* **5**, 965.
Meyer, J. P.: 1985a, *Astrophys. J. Suppl.* **57**, 151.
Meyer, J. P.: 1985b, *Astrophys. J. Suppl.* **57**, 173.
Meyer, J. P.: 1993, in N. Prantzos, E. Vangioni-Flam and M. Casse (eds), *Origin and Evolution of the Elements*, Cambridge Univ. Press, p. 26.
Meyer, J. P.: 1996, in S. Holt and G. Sonneborn (eds), *Cosmic Abundances*, A.S.P. Conf. Series **99**, p. 127.
Meyer, J. P., Drury, L. O'C., and Ellison, D. C.: 1997 *Astrophys. J.* **487**, 182.
Miller, J. A.: 1997, *Astrophys. J.* **491**, 939.
Miller, J. A., Cargill, P. J., Emslie, A. G., Holman, G. D., Dennis, B. R., LaRosa, T. H., Winglee, R. M., Benka, S. G., and Tsuneta, S.: 1997, *J. Geophys. Res.* **102**, 14 631.
Miller, J. A., LaRosa, T. N., and Moore, R. L.: 1996, *Astrophys. J.* **461**, 445.
Miller, J. A. and Reames, D. V.: 1996, in R. Ramaty, N. Mandzhavidze, X.-M. Hua (eds), *High Energy Solar Physics*, AIP Conf. Proc. **374**, AIP Press, Woodbury, NY, p. 450.
Miller, J. A. and Roberts, D. A.: 1996, *Astrophys. J.* **452**, 912.
Miller, J. A. and Viñas, A. F.: 1993, *Astrophys. J.* **412**, 386.
Möbius, E., Hovestadt, D., Klecker, B., Scholer, M., Gloeckler, G., and Ipavich, F. M.: 1985, *Nature* **318**, 426.
Möbius, E. et al.: 1999, *Geophys. Res. Letters* **26**, 145.
Möbius, E., Rucinski, D., Lee, M. A., Isenberg, P. A.: 1998, *J. Geophys. Res.* **103**, 257.
Möbius, E., Scholer, M., Hovestadt, D., Klecker, B., and Gloeckler, G.: 1982, *Astrophys. J.* **259**, 397.

Moraal, H., Steinberg, C. D. and Zank, G. P.: 1999, *Adv. Space Res*. **23** (3), 425.
Moses, S. L., Coroniti, F. V., Kennel, C. F., Kurth, W. S., and Gurnett, D. A.: 1990, *Geophys. Res. Letters* **17**, 1653.
Muraki, Y. et al.: 1992, *Astrophys. J.* **400**, L75.
Murphy, R. J., Ramaty, R., Kozlovsky, B., and Reames, D. V.: 1991, *Astrophys. J.* **371**, 793.
Ng, C. K. and Reames, D. V.: 1994 *Astrophys. J.* **424**, 1032.
Ng, C. K. and Reames, D. V.: 1995 *Astrophys. J.* **453**, 890.
Ng, C. K., Reames, D. V., and Tylka, A. J.: 1999, *Geophys. Res. Letters* **26** (July 15) in press.
Northrop, T. G.: 1963, *The Adiabatic Motion of Charged Particles* (New York: Interscience).
Oetliker, M., Klecker, B., Hovestadt, D., Mason, G. M., Mazur, J. E., Leske, R. A., Mewaldt, R. A., Blake, J. B., and Looper, M. D.: 1997, *Astrophys. J.* **477**, 495.
Osherovich, V. and Burlaga, L. F.: 1997, in N. Crooker, J. A. Jocelyn, J. Feynman (eds), *Coronal Mass Ejections*, Geophys. Monograph **99**, AGU press, New York, p. 157.
Palmer, I. D., Allum, F. R., and Singer, S. F.: 1978, *J. Geophys. Res.* **83**, 75.
Palmer, I. D.: 1982. *Rev. Geophys. Space Phys.* **20**, 335.
Pallavicini, R., Serio, S. and Vaiana, G. S.: 1977, *Astrophys. J.* **216**, 108.
Parker, E. N.: 1963, *Interplanetary Dynamical Processes* Interscience Publ., New York.
Parker, E. N.: 1987, *Physics Today*, July, 1987, p. 36.
Paschmann, G., Sckopke, N., Papamastorakis, I., Asbridge, J. R., Bame, S. J., and Gosling, J. T.: 1981, *J. Geophys. Res.* **86**, 4471.
Pesses, M. E., Jokipii, J. R., and Eichler, D.: 1981, *Astrophys. J.* **246**, L85.
Pizzo, V. J.: 1991, *J. Geophys. Res.* **96**, 5405.
Pizzo, V. J.: 1994, *J. Geophys. Res.* **99**, 4173.
Ramaty, R., Kozlovsky, B., and Lingenfelter, R.: 1979, *Astrophys. J. Suppl*. **40**, 487.
Ramaty, R., Mandzhavidze, N., and Kozlovsky, B.: 1996a, in R. Ramaty, N. Mandzhavidze and X.-M. Hua (eds), *High Energy Solar Physics*, AIP Conf. Proc **374**, AIP Press, Woodbury, NY, p. 172.
Ramaty, R., Mandzhavidze, N., Kozlovsky, B., and Murphy, R.: 1996b, *Astrophys. J.* **455**, L193.
Ramaty, R., Mandzhavidze, N., Kozlovsky, B., and Skibo, J. G.: 1993, *Adv. Space Res.* **13**(9) 273.
Rao, U. R., McCracken, K. G., and Bukata, R. P.: 1967, *J. Geophys. Res.* **72**, 4325.
Reames, D. V.: 1988, *Astrophys. J.* **330**, L71.
Reames, D. V.: 1990a, *Astrophys. J.* **358**, L63.
Reames, D. V.: 1990b, *Astrophys. J. Suppl*. **73**, 235.
Reames, D. V.: 1993, *Adv. Space Res*. **13**(9), 331.
Reames, D. V.: 1995a, *Adv. Space Res*. **15**(7), 41.
Reames, D. V.: 1995b, *Revs Geophys. (Suppl.)* **33**, (U. S. National Report to the IUGG), 585.
Reames, D. V.: 1997, in N. Crooker, J. A. Jocelyn, J. Feynman (eds), *Coronal Mass Ejections*, Geophys. Monograph **99**, AGU Press, New York, p. 217.
Reames, D. V.: 1998, *Space Science Revs*. **85**, 327.
Reames, D. V.: 1999, *Astrophys. J.* **518**, 473.
Reames, D. V., Barbier, L. M., and Ng, C. K.: 1996, *Astrophys. J.* **466**, 473.
Reames, D. V., Barbier, L. M., and von Rosenvinge, T. T.: 1997a, *Adv. Space Res.* **19**(5), 809.
Reames, D. V., Barbier, L. M., von Rosenvinge, T. T., Mason, G. M., Mazur, J. E., and Dwyer, J. R.: 1997b, *Astrophys. J.* **483**, 515.
Reames, D. V., Kahler, S. W., and Ng, C. K.: 1997c, *Astrophys. J.* **491**, 414.
Reames, D. V., Ng, C. K., Mason, Dwyer, J. R., G. M., Mazur, J. E., and von Rosenvinge, T. T.: 1997d, *Geophys. Res. Letters* **24**, 2917.
Reames, D. V., Dennis, B. R. Stone, R. G., and Lin, R. P.: 1988, *Astrophys. J.* **327**, 998.
Reames, D. V., Meyer, J. P., and von Rosenvinge, T. T.: 1994, *Astrophys. J. Suppl.* **90**, 649.
Reames, D. V. and Ng, C. K.: 1998, *Astrophys. J.* **504**, 1002.
Reames, D. V., Richardson, I. G., and Barbier, L. M.: 1991, *Astrophys. J.* **382**, L43.
Reames, D. V. and Stone, R. G.: 1986, *Astrophys. J.* **308**, 902.

Reames, D. V., von Rosenvinge, T. T., and Lin, R. P.: 1985, *Astrophys. J.* **292**, 716.
Richardson, I. G.: 1997, in N. Crooker, J. A. Jocelyn, and J. Feynman (eds), *Coronal Mass Ejections*, Geophys. Monograph **99**, AGU press, New York, p. 189.
Richardson, I. G., Barbier, L. M., Reames, D. V., and von Rosenvinge, T. T.: 1993, *J. Geophys. Res.* **98**, 13.
Richardson, I. G. and Reames, D. V.: 1993, *Astrophys. J. Suppl.* **85**, 411.
Roelof, E. C. and Krimigis, S. M.: 1977, *J. Geophys. Res.* **78**, 5375.
Roelof, E. C., Simnett, G. M., Decker, R. B., Lanzerotti, L. J., Maclennan, C. G., Armstrong, T. P., and Gold, R. E.: 1997, *J. Geophys. Res.* **102**, 11 251.
Roth, I. and Temerin, M.: 1997, *Astrophys. J.* **477**, 940.
Rucinski, D., Cummings, A. C., Gloeckler, G., Lazarus, A. J., Möbius, E., and Witte, M.: 1996, *Space Science Rev.* **78**, 73.
Russell, C. T., Lepping, R. P., and Smith, C. W.: 1990, *J. Geophys. Res.* **95**, 2273.
Sarris, E. T., Krimigis, S. M., Bostrom, C. O., and Armstrong, T. P.: *J. Geophys. Res.* **83**, 4289.
Schardt, A. W. and McDonald, F. B.: 1983, *J. Geophys. Res.* **88**, 8923.
Schmelz, J. T.: 1993, *Astrophys. J.* **408**, 373.
Scholer, M.: 1992, in G. P. Zank and T. K. Gaisser (eds), *Particle Acceleration in Cosmic Plasmas*, AIP Conf. Proc. **264**, AIP Press, New York, p. 125.
Scholer, M., Hovestadt, D., Klecker, B., and Gloeckler, G.: 1979, *Astrophys. J.* **227**, 323.
Schwadron, N. A., Fisk, L. A., and Zurbuchen, T. H.: 1999, *Astrophys. J.*, in press.
Selesnick, R. S., Cummings, A. C., Cummings, J. R., Mewakdt, R. A., and Stone, E. C.: 1995, *J. Geophys. Res.* **100**, 9503.
Shapiro, M. M.: 1997, *Proc. 25th Int. Cosmic-Ray Conf., Durban* **4**, 353.
Shapiro, M. M. and Silberberg, R.: 1997, *Proc. 25th Int. Cosmic-Ray Conf., Durban* **4**, 349.
Share, G. H. and Murphy, R. J.: 1995, *Astrophys. J.* **452**, 933.
Share, G. H., and Murphy, R. J.: 1998, *Astrophys. J.* **508**, 876.
Sheeley, N. R, Jr. et al.: 1975, *Solar Phys.* **45**, 377.
Sheeley, N. R., Jr., Howard, R. A., Koomen, M. J., Michels, D. J., Schwenn, R., Mühlhäuser, K. H., and Rosenbauer, H.: 1985, *J. Geophys. Res.* **90**, 163.
Shelley, E. G.: 1995, *Rev. Geophys. Suppl.* **33**, (U. S. National Report to the IUGG), 709.
Simnett, G. M., Sayle, K. A., Tappan, S. J., and Roelof, E. C.: 1995 *Space Sci. Rev.* **72**, 327.
Simpson, J. A., Bastian, T. S., Chenette, D. L., McKibben, R. B., Pyle, K. R.: 1980, *J. Geophys. Res.* **85**, 5731.
Singer, S. F.: 1958, *Phys. Rev. Letters* **1**, 181.
Smith, E. J., Balogh, A., Neugebauer, M., and McComas, D.: 1995, *Geophys. Res. Letters* **22**, 3381.
Steinacker, J., Meyer, J. P., Steinacker, A., and Reames, D. V.: 1997 *Astrophys. J.* **476**, 403.
Stix, T. H.: 1962, *The Theory of Plasma Waves* McGraw-Hill, New York.
Stone, E. C., Cooper, J. F., Cummings, A. C., McDonald, F. B., Trainor, J. H., Lal, N., McGuire, R., and Chenette, D. J.: 1986, *Science* **233**, 93.
Stone, E. C., Cummings, A. C., Looper, M. D., Selesnick, R. S., Lal, N., McDonald, F. B., Trainor, J. H., and Chenette, D. J.: 1989, *Science* **246**, 1489.
Takashima, T. et al.: 1997, *Astrophys. J.* **477**, L111.
Tan, L. C., Mason, G. M., Gloeckler, G., and Ipavich, F. M.: 1989, *J. Geophys. Res.* **94**, 6554.
Tan, L. C. and Mason, G. M.: 1993, *Astrophys. J.* **409**, L29.
Temerin, M., and Roth, I.: 1992, *Astrophys. J.* **391**, L105.
Thompson, B. J. et al.: 1999, *Astrophys. J.*, to be published.
Toida, M. and Ohsawa, Y.: 1997, *Solar Phys.* **171**, 161.
Tsurutani, B. T. and Gonzalez, W. D.: 1987, *Planetary Space Sci.* **35**, 405.
Tu, C.-Y. and Marsch, E.: 1993, *J. Geophys. Res.*, **98**, 1257.
Tylka, A. J., Dietrich, W. F., and Boberg, P. R.: 1997, *Proc. 25th Int. Cosmic-Ray Conf., Durban* **1**, 101.

Tylka, A. J., Boberg, P. R., Adams, J. H., Jr., Beahm, L. P., Dietrich, W. F., and Kleis, T.: 1995, *Astrophys. J.* **444**, L109.
Tylka, A. J., Reames, D. V., and Ng, C. K.: 1999, *Geophys. Res. Letters* **26** (July 15) in press.
Viñas, A. F., Goldstein, M. L., and Acuña, M. H.: 1984, *J. Geophys. Res.*, **89**, 3762.
Van Allan, J. A., Randall, B. A., Baker, D. N., Goertz, C. K., Sentman, D. D., Thomsen, M. F., Flindt, H. R.: 1974, *Science* **188**, 459.
Van Hollebeke, M. A. I., McDonald, F. B., Trainor, J. H., and von Rosenvinge, T. T.: 1978, *J. Geophys. Res.* **83**, 4723.
von Steiger, R. and Geiss, J.: 1989, *Astron. Astrophys.* **225**, 222.
Wang, Y.-M. and Sheeley, N. R., Jr.: 1993, *Astrophys. J.* **414**, 916.
Webb, D. F.: 1995, *Rev. Geophys. Suppl.* **33**, (U. S. National Report to the IUGG), 577.
Webb, D. F., Cliver, E. W., Gopalswamy, N., Hudson, H. S., and St Cyr, O. C.: 1998, *Geophys. Res. Letters* **25**, 2469.
Webb, D. F. and Howard, R. A.: 1994, *J. Geophys. Res.* **99**, 4201.
Webber, W. R.: 1975, *Proc 14th Int. Cosmic Ray Conf. Munich* **3**, 1597.
Wentzel, D. G.: 1974, *Ann. Rev. Astron. Astrophys.* **12**, 71.
Wild, J. P., Smerd, S. F., and Weiss, A. A.: 1963, *Ann. Rev. Astron. Astrophys.* **1**, 291.
Williams, D. J. et al.: 1991, *Science* **253**, 1525.
Williams, D. L., Leske, R. A., Mewaldt, R. A., and Stone, E. C.: 1998, *Space Science Rev.* **85**, 379.
Yoshimori, M., Suga, K., Morimoto, K., Hiraoka, T., Sato, J., Kawabata, K., and Okhi, K.: 1994, *Astrophys. J. Suppl.* **90**, 639.
Zank, G. P. and Pauls, H. L.: 1996, *Space Sci. Rev.* **78**, 95.
Zhang, G. and Burlaga, L. F.: 1988, *J. Geophys. Res.* **93**, 2511.
Zhang, T. X.: 1995, *Astrophys. J.* **449**, 916.
Zhang, T. X. and Ohsawa, Y.: 1995, *Solar Phys.* **158**, 115.
Zurbuchen, T. H., Schwadron, N. A., and Fisk, L. A.: 1997, *J. Geophys. Res.* **102**, 24 175.
Zurbuchen, T. H., Fisk, L. A., Gloeckler, G., and Schwadron, N. A.: 1998, *Space Sci. Rev.* **85**, 397.